

Feedback between a retinoid-related nuclear receptor and the *let-7* microRNAs controls the pace and number of molting cycles in *C. elegans*.

Ruhi Patel^{1,3*}, Himani Galagali^{2*}, John K. Kim^{2†} and Alison R. Frand^{1†}

*Equal contributions

¹ Department of Biological Chemistry, David Geffen School of Medicine
University of California, Los Angeles, Los Angeles, CA 90095

² Department of Biology, Johns Hopkins University
Baltimore, MD 21218

³ Current address:
Department of Molecular Immunology and Microbiology, David Geffen School of Medicine
University of California, Los Angeles, Los Angeles, CA 90095

†To whom correspondence should be addressed:

jnkim@jhu.edu

afrand@mednet.ucla.edu

Keywords: molting cycle, gene expression oscillations, heterochronic pathway, ultradian and circadian rhythms

Abbreviations:

CCG	<u>C</u> lock <u>C</u> ontrolled <u>G</u> ene
ChIP	<u>C</u> hromatin <u>I</u> mmunoprecipitation
CRISPR	<u>C</u> lustered <u>R</u> egularly <u>I</u> nterspersed <u>S</u> hort <u>P</u> alindromic <u>R</u> epeats
crRNA	<u>C</u> RISPR <u>R</u> NA
GFP	<u>G</u> reen <u>F</u> luorescent <u>P</u> rotein
iCLIP	<u>I</u> ndividual-nucleotide resolution <u>C</u> rosslinking <u>I</u> mmunoprecipitation
LCS	<u>l</u> et-7 <u>C</u> onsensus <u>S</u> ite
let	<u>L</u> ethal
MFE	<u>M</u> inimum <u>F</u> ree <u>E</u> nergy
Mlt	<u>M</u> olting Cycle Defective
NHR	<u>N</u> uclear <u>H</u> ormone <u>R</u> eceptor
nls	nuclear localization signal
PER	<u>P</u> ERIOD gene
pri	<u>P</u> rietary
qPCR	<u>Q</u> uantitative <u>P</u> olymerase <u>C</u> hain <u>R</u> eaction
RE	<u>R</u> esponse <u>E</u> lement
RNAi	<u>R</u> NA <u>i</u> nterference
ROR	<u>R</u> etinoid-related <u>O</u> rphan <u>R</u> eceptor
RORE	<u>R</u> etinoid-related <u>O</u> rphan <u>R</u> eceptor <u>R</u> esponse <u>E</u> lement
siRNA	<u>S</u> hort- <u>i</u> nterfering <u>R</u> NA
ssODN	<u>S</u> ingle <u>S</u> tranded <u>O</u> ligo <u>D</u> NA <u>N</u> ucleotide
tdTomato	<u>T</u> andem Tomato
tracrRNA	<u>T</u> rans- <u>a</u> ctivating <u>c</u> rRNA
UTR	<u>U</u> ntranslated <u>R</u> egion

SUMMARY

Animal development requires coordination among cyclic processes, sequential cell fate specifications, and once-a-lifetime morphogenic events, but the underlying mechanisms are not well understood. *C. elegans* undergo four molts at regular 8–10 h intervals. The pace of the cycle is governed by PERIOD/*lin-42* and other as-yet unknown factors. Cessation of the cycle in young adults is controlled by the *let-7* family of microRNAs and downstream transcription factors in the heterochronic pathway. Here, we characterize a negative feedback loop between NHR-23, the worm homolog of mammalian retinoid-related orphan receptors (RORs), and the *let-7* family of microRNAs that regulates both the frequency and finite number of molts. The molting cycle is decelerated in *nhr-23* knockdowns, accelerated in *let-7(-)* mutants, and similar to wild type animals in *let-7(-) nhr-23(-)* double mutants. NHR-23 binds response elements (ROREs) in the *let-7* promoter and activates transcription. In turn, *let-7* dampens *nhr-23* expression across development via a complementary *let-7* binding site (LCS) in the *nhr-23* 3' UTR. The molecular interactions between NHR-23 and *let-7* hold true for other *let-7* family microRNAs. Either derepression of *nhr-23* transcripts by LCS deletion or high gene dosage of *nhr-23* leads to protracted behavioral quiescence and extra molts in adults. NHR-23 and *let-7* also co-regulate scores of genes required for execution of the molts, including *lin-42*. In addition, ROREs and LCSs isolated from mammalian *ROR* and *let-7* genes function in *C. elegans*, suggesting conservation of this feedback mechanism. We propose that this feedback loop unites the molting timer and the heterochronic gene regulatory network possibly by functioning as a cycle counter.

Introduction

Timekeeping is a critical component of animal development. Developmental clocks, like the somitogenesis clocks of vertebrates and segmentation clocks of insects, govern the frequency of cyclic processes (Diaz-Cuadros et al., 2021; Uriu, 2016). Heterochronic gene pathways, like the microRNA-mRNA networks in *Caenorhabditis elegans* and other organisms, regulate sequential events and orchestrate the timing of development across tissue types (Ambros and Ruvkun, 2018; Galagali and Kim, 2020). The mechanism by which developmental clocks and heterochronic pathways interact to coordinate repeated developmental processes with cell fate transitions remains unknown.

Studies of circadian rhythms have provided a framework for understanding how biological clocks schedule rhythmic processes. The circadian clock governs diurnal physiologic rhythms in animals, for example, feeding-fasting and sleep-wake cycles, and helps coordinate the underlying cellular and molecular processes to predictable 24 hour (h) changes in the environment (Takahashi, 2016). The period of developmental clocks, unlike physiologic clocks, may vary based on changes in external environmental cues, such as temperature, nutrition and growth factors. Developmental clocks that regulate morphogenic processes may also need to stop after a finite number of iterations (Rensing et al., 2001; Tsiairis and Grosshans, 2021).

The mechanistic basis for both developmental and physiological clocks are molecular-genetic oscillators. Cyclical expression of the core components of oscillators and their target genes together underlie biological rhythms. Molecular-genetic oscillators are comprised of interconnected feedback loops among the core components. Theoretical studies indicate that negative feedback loops with intrinsic delays or interdependent positive and negative feedback loops with intrinsic delays can both set up self-sustaining genetic oscillators (Johnson and Day, 2000; Novak and Tyson, 2008; Tsiairis and Grosshans, 2021). In both cases, time delays are caused in part by unequal rates of RNA versus protein synthesis and degradation. For example, during somitogenesis, the Hes7 transcription factor represses its own transcription, setting up a negative feedback loop with a delay (Bessho et al., 2003).

The key components of the mammalian circadian clock in mammals also consists of transcriptional activators and repressors interacting through interlocked feedback loops. During the day, CLOCK and BMAL1 activate the transcription of *PERIOD/PER* and other genes. During the night, PER proteins interact with CLOCK and BMAL1 and repress their own transcription (Partch et al., 2014; Takahashi, 2016; 2017). The short half-life of the PER protein, in combination with the continued transcriptional repression of *PER*, results in decrease of PER proteins late in the night. The decrease in the levels of PER is accompanied by increases in the levels of CLOCK

and BMAL1 early in the morning. CLOCK and BMAL1 also activate transcription of *REV-ERB α* and *REV-ERB β* . The competition between the transcriptional repressors, REV-ERBs, and the transcriptional activators, the Retinoid-related Orphan Receptors (RORs), for the same binding sites in the *BMAL1* promoter regulates rhythmic expression of *BMAL1* in peripheral organs and the central nervous system (Cook et al., 2015; Zhang et al., 2017).

The components of the circadian clock are also subject to post-transcriptional and post-translational regulation. The *bantam* microRNAs regulate the temporal expression of *Drosophila clock* by directly binding the *clock* 3' UTR and repressing translation (Kadener et al., 2009). In mice, the microRNAs *miR-24* and *miR-30* regulate stability of *Per2* mRNA and repress translation through interactions with the *Per2* 3' UTR (Yoo et al., 2017). A few other microRNAs regulate the expression of core clock components. However, the prevalence of microRNA-mediated post-transcriptional feedback loops among biological clocks is not well understood (Alvarez-Saavedra et al., 2011; Chen et al., 2013; Du et al., 2014).

Molting in *C. elegans* is a reiterated and periodic developmental process. Under favorable conditions, *C. elegans* develop through four larval stages, L1–L4. Larvae molt from one stage to the next at regular 8–10 h intervals and then emerge as adults. *C. elegans* enter and exit a state of behavioral quiescence, termed lethargus, during each molt (Figure 1A). Across lethargus, epithelia detach from the old cuticle and synthesize the new cuticle. The animal then escapes from the old cuticle at ecdysis. Newly emerged larvae forage and feed during the intermolt. Prior studies identified PER/LIN-42 as a key component of the underlying pacemaker (Monsalve et al., 2011, McCulloch and Rougvie, 2014).

More recent work has identified and modeled a single genetic oscillator that governs the oscillatory expression of more than 3,700 genes across *C. elegans* larval development, including 257 linked to specific aspects of molting (Hendriks et al., 2014; Kim et al., 2013; Meeuse et al., 2020). Transcript levels of these genes oscillate with the same frequency as the molting cycle, and the waveforms have a phase-locked peak once per larval stage, i.e., the genes peak at the same relative time-point within each larval stage (Meeuse et al., 2020; Tsiairis and Großhans, 2021). It is not known whether the PER-based molting cycle timer and the genetic oscillator represent the same timekeeping mechanism.

The heterochronic gene pathway regulates the timing of unidirectional cell fate transitions during the development of *C. elegans*. Key heterochronic genes include the conserved *let-7* microRNA, its paralogs, and stage-specific targets of the *let-7* family (Abbott et al., 2005; Ambros and Ruvkun, 2018; Reinhart et al., 2000) (Figure 1B). Each larval stage is marked by stereotypic divisions of the lateral epidermal stem cells, called seam cells. The *let-7* paralogs *mir-48*, *mir-84*,

and *mir-241* specify the L2 fate of the seam cells, wherein the cells undergo one symmetric and one asymmetric division (Abbott *et al.*, 2005). The *let-7* microRNA specifies later L3 and L4 fates, which include homotypic fusion of the seam cells into lateral syncytia and secretion of trilobed structures in the worm cuticle called alae (Reinhart *et al.*, 2000; Vadla *et al.*, 2012).

NHR-23, the only *C. elegans* homolog of mammalian ROR transcription factors, is repeatedly expressed in the larval epidermis during each larval stage (Frand *et al.*, 2005; Kostrouchova *et al.*, 1998). Predicted targets of NHR-23 are enriched for genes associated with molting, including cuticle collagens and enzymes necessary for synthesis and degradation of the cuticle (Kouns *et al.*, 2011). LIN-42, the *C. elegans* homolog of the core circadian clock protein and tumor suppressor PERIOD (Jeon *et al.*, 1999), sustains the 8 h intervals between molts (Monsalve *et al.*, 2011). LIN-42 and the *let-7* family mutually inhibit one another (Figure 1C) (McCulloch and Rougvie, 2014; Perales *et al.*, 2014; Reinhart *et al.*, 2000; Van Wynsberghe *et al.*, 2014). Moreover, homologs of genes involved in the maintenance of circadian rhythm in *Drosophila* interact genetically with *let-7* and regulate the L4-to-adult transition in *C. elegans* (Banerjee *et al.*, 2005).

Further evidence of crosstalk between the molting cycle timer and the heterochronic pathway comes from the observation that the levels of primary *let-7* family transcripts cycle in phase with the molts (McCulloch and Rougvie, 2014; Van Wynsberghe *et al.*, 2011). The cyclical expression profile of primary *let-7* family transcripts is consistent with temporally reiterated, as well as stage-specific, function(s). However, the transcriptional activator responsible for the oscillatory expression of *let-7* remains unknown.

Here, we show that both NHR-23 and the *let-7* family of microRNAs (the *let-7s*) are key components of a simple regulatory circuit that operates within the molecular-genetic oscillator underlying the molting cycle and also within the heterochronic gene regulatory network. Using longitudinal studies of the biorhythm of molting in relevant genetic backgrounds, molecular and cell biological analyses, and bioinformatic approaches, we show that NHR-23 transcriptionally activates the *let-7s* and, in turn, the *let-7s* post-transcriptionally repress *nhr-23* mRNA. In addition, NHR-23 positively autoregulates its own transcription. Together, NHR-23/ROR and the *let-7s* establish a transcriptional–post-transcriptional feedback loop that governs the pace and extinction of the cycle after four iterations. As both the key components and *cis*-regulatory elements comprising this feedback loop are conserved from nematodes to mammals, our findings may apply to specific developmental and circadian clocks of humans and related pathologies including birth defects, malignancies, sleep disorders, and metabolic syndromes (Oyama *et al.*, 2017; Patke *et al.*, 2017; Puram *et al.*, 2016; Roenneberg and Merrow, 2016).

RESULTS

Larval molting cycles lengthen in *nhr-23* knockdowns and shorten in *let-7* family mutants.

To determine the role of *nhr-23* and *let-7* in timing the molting cycle, we measured and compared the length of molting cycles in *nhr-23* knockdowns, *let-7* mutants, and control larvae through a series of longitudinal studies. Each experiment captured one iteration of the molting cycle. The full set captured emergence of L2s, L3s, L4s and young adults. In each experiment, we measured 1) the interval of physical activity in the target stage (defined as the time elapsed between successive episodes of lethargus); 2) the interval of lethargus associated with the molt; and 3) the wake-to-wake interval (defined as the time elapsed between two sequential transitions from lethargus to activity) (Figure 2A).

Feeding L1 stage hatchlings bacteria that express dsRNAs complementary to *nhr-23* (*nhr-23(RNAi)*) usually leads to severe molting defects and larval arrest in the L2 stage. To circumvent L2 arrest and determine how knockdown of *nhr-23* affects the timing of the L3 and L4 stages, we maintained worms on control bacteria for 6 h and 14 h, respectively, and then moved the worms to *nhr-23(RNAi)* bacteria. This strategy ensured that all test subjects emerged in the target stage superficially normal, but none of the test subjects fully shed the cuticle from the ensuing molt—signifying complete penetrance of the molting-defective (Mlt) phenotype associated with *nhr-23(RNAi)*. Age-matched, wild-type larvae fed the same bacterial strain transformed with an empty vector served as controls.

The actograms in Figure 2 display the results of these longitudinal studies. Each actogram corresponds to an isogenic cohort of animals. Therein, each column represents a single animal that emerged in the target stage (L4 in Figure 2B and L3 in Figure 2C), developed, and underwent the ensuing molt. Each animal was isolated during the preceding molt to achieve stringent synchronization at the outset. After it emerged, the worm was observed for approximately 1 min at regular 1-h intervals. At each timepoint, the worm was “active” if both pharyngeal muscle contractions (pumps) and sinusoidal locomotion were observed. Conversely, the subject was “lethargic” if neither pharyngeal pumps nor sinusoidal locomotion were observed, and its body posture resembled a hockey stick (Iwanir et al., 2013; Raizen et al., 2008). Separation of the preexisting cuticle from the body and detection of the shed cuticle on the culture plate signified the commencement and completion of ecdysis, respectively (Singh and Sulston, 1978).

As expected, the cohort of wild-type (control) animals first emerged as L4s, then entered and exited lethargus, shed the larval cuticle (ecdysed), and emerged as young adults almost

synchronously (Figure 2B and Supplemental Table 1). The cohort of *nhr-23(RNAi)* animals that emerged as L4s entered lethargus later and remained lethargic for twice as long as the control cohort. All of the *nhr-23(RNAi)* animals began to pump and locomote once again, but oftentimes at lower rates than wild-type adults. In principle, this intermittent sluggishness might result from incomplete arousal or hindrance by unshed parts of the L4-stage cuticle. Regardless, the wake-to-wake interval of the L4-stage *nhr-23(RNAi)* cohort was 13 ± 1.1 h as compared with 10.3 ± 0.4 h for the control cohort ($p \leq 0.0001$). Following this trend, the L3-stage cohort of *nhr-23(RNAi)* larvae also entered lethargus later and remained in lethargus twice as long as the age-matched wild-type cohort (Figure 2C). Similarly, the cohort of *nhr-23(RNAi)* larvae molting from L2 to L3 were in lethargus 3-fold longer than the age-matched controls (Supplemental Table 1). Thus, delayed and protracted lethargi were associated with knockdown of *nhr-23* across three larval stages.

To evaluate the role of the *let-7*s, we tracked cohorts of *let-7(n2853)*, *let-7(mg279)* and *let-7(mg279); mir-84(tm1304)* double mutants across late larval stages. Both *n2853* and *mg279* are associated with lower levels of mature *let-7*, relative to wild-type animals. However, *n2853* is a substitution in the seed sequence, whereas *mg279* is a 27 bp deletion upstream of the mature microRNA (Bracht et al., 2004; Reinhart et al., 2000). The null allele of *mir-84* enhances relevant phenotypes associated with *let-7(mg279)* (Hayes and Ruvkun, 2006). We also tracked *mir-48 mir-241(nDf51); mir-84(n4037)* triple mutants across L2, when the corresponding microRNAs are expressed but mature *let-7* is not yet detected (McCulloch and Rougvie, 2014). In contrast to animals subjected to *nhr-23(RNAi)*, *let-7(n2853)* mutants both entered and exited lethargus more quickly than wild-type animals. For example, the wake-to-wake interval for the *let-7(n2853)* cohort developing from L4s into adults was only 7.9 ± 0.6 h, an acceleration of 2.9 ± 0.7 h relative to the wild-type cohort (Figure 2B). All of the *let-7(n2853)* animals subsequently ruptured at the vulva, a hallmark of this strong loss-of-function allele (Ecsedi et al., 2015). In complementary studies, L4-stage cohorts of both *let-7(mg279)* single and *let-7(mg279); mir-84(tm1304)* double mutants also entered lethargus ahead of wild-type L4s (Supplemental Table 1). Moreover, the cohort of *let-7(n2853)* mutants observed from emergence in L3 onward passed through two consecutive lethargic phases and emerged as young adults ahead of the entire wild-type cohort (Figure 2C). As such, repetition of the L3 stage, a retarded heterochronic phenotype, cannot explain the acceleration of the L4 stage observed in *let-7(n2853)* mutants, because both the L3 and L4 stages of the mutants were shorter than those of wild-type larvae. Thus, lethargus was advanced and larval development was accelerated in three distinct mutants of the *let-7* family.

When we combined stage-specific *nhr-23(RNAi)* with *let-7(n2853)*, the altered pace of molting associated with each single mutant was partially co-suppressed (Figure 2B, C and Supplemental Table 1). Strikingly, none of the *let-7(n2853)* mutants ruptured on *nhr-23(RNAi)*, suggesting that the *let-7*-mediated suppression of *nhr-23* regulates both lethargus and the morphogenesis of the vulva. (Figure 2B). The L4-stage cohort of *nhr-23(RNAi) let-7(n2853)* double mutants entered lethargus later than *let-7(n2853)* single mutants but emerged from lethargus earlier than *nhr-23(RNAi)* single mutants. As a result, the wake-to-wake interval of the L4-stage cohort of *nhr-23(RNAi) let-7(n2853)* double mutants was 10.6 ± 0.8 h, similar to the value of the wild-type cohort ($p \geq 0.9$). Notably, *nhr-23(RNAi) let-7(n2853)* double mutants underwent aberrant ecdysis, indicating that the role of *nhr-23* in lethargus and ecdysis are genetically separable.

Partial co-suppression of the altered pace of molting was also apparent during the L2 and L3 stages. The wake-to-wake interval of the *nhr-23(RNAi) let-7(n2853)* double mutants during the L3 stage was 1.4 ± 1.4 h shorter than *nhr-23(RNAi)* alone ($p=0.0002$). Moreover, the triple knockout of the *let-7* sisters, *mir-48 mir-241(nDf51); mir-84(n4037)*, partially suppressed the prolonged lethargy associated with *nhr-23(RNAi)* across the L2/L3 molt, shortening the lethargic interval by 0.9 ± 1.0 h ($p=0.002$, Supplemental Table 1) to that of wild-type animals.

Taken together, these longitudinal data suggest a model whereby NHR-23 accelerates the molting cycle, partly by directly activating the expression of the *let-7*s, and the *let-7*s decelerate the cycle, partly by directly repressing the expression of *nhr-23*.

NHR-23 promotes oscillatory expression of primary *let-7* and its paralogs.

Based on the findings of the longitudinal studies described above, we hypothesized that NHR-23 may directly activate transcription of *let-7*. Consistent with this hypothesis, a binding peak for NHR-23 was reported within ~300 bp upstream of primary *let-7* by the ModENCODE Consortium (Figure 3A) (Celniker et al., 2009). Nuclear hormone receptors usually bind DNA response elements as homotypic or heterotypic dimers (Evans and Mangelsdorf, 2014). NHR-23 and its mammalian counterpart ROR α are among the few that bind the consensus sequence 5'-(A/G)GGTCA-3' as monomers to activate transcription of target genes (Giguere et al., 1994; Kouns et al., 2011). We identified 3 occurrences of this sequence, called the ROR response element (RORE), within the reported NHR-23 binding peak (Figure 3A). Additionally, the 300 bp region containing the ROREs is contained within a previously characterized enhancer element required for *let-7* transcription (Johnson et al, 2003, Kai et al, 2013).

To validate NHR-23 binding upstream of *let-7* during L3 and L4, we appended the coding sequence for a 3xFLAG affinity tag to the endogenous *nhr-23* gene using the CRISPR-Cas9 system (Paix et al., 2015) and performed chromatin immunoprecipitation coupled with gene-specific, quantitative polymerase chain reactions (ChIP-qPCR). The signal flanking RORE3 was enriched 4-fold during the L3 stage and 21-fold during the L4 stage in QK159[*nhr-23::3xflag*] samples as compared with wild-type (N2) samples. In contrast, signal from the promoter of *col-19*, which is not targeted by NHR-23, was not detectably enriched in either strain (Figure 3B, C). Together, the data show that NHR-23 binds one or more ROREs in the promoter of *let-7* during two sequential larval stages. Using the same combination of bioinformatic and biochemical approaches, we also found that NHR-23 occupies the promoters of three *let-7* sisters (*mir-48*, *mir-241* and *mir-84*) in both L3 and L4 larvae (Supplemental Figure 1A–D) (Johnson et al., 2003).

We next asked whether *nhr-23* promotes the temporally reiterated expression from the promoter of *let-7*. To address this question, we measured and compared the abundance of nuclear-localized GFP expressed from the *let-7* promoter (Kai et al., 2013) in stage-specific *nhr-23* knockdowns and age-matched control animals via quantitative fluorescence microscopy (Supplemental Figure 2A, B). In preliminary studies, we tracked the cycling signal associated with this particular *let-7p::nls-gfp* fusion gene and detected peaks early in the third and fourth molts. Accordingly, nuclei in the lateral epidermis were imaged within the first hour of the L3/L4 and L4/adult molts. The signal intensity in hyp7 nuclei was 2.3 ± 1.3 -fold (mean \pm sd) lower in *nhr-23(RNAi)* than control animals. Levels of GFP detected in seam nuclei were more variable during the L3-to-L4 molt than the L4-to-Adult molt, possibly due to continuation of the cell cycle. Even so, the mean signal intensity in the seam was consistently lower in *nhr-23* knockdowns than control animals (Supplemental Figure 2A, B).

To determine the extent to which *nhr-23* promotes the reiterated expression of endogenous *let-7*, we used TaqMan RT-qPCR to detect primary (pri-) *let-7* and mature *let-7* in successive samples of *nhr-23* knockdowns and mock-treated, wild-type animals developing from L2s into L4s or L3s into young adults (Figure 3D–G). Attenuation of the RNAi of *nhr-23* enabled the collection of hundreds of *nhr-23(RNAi)* animals late in larval development, as <40% of *nhr-23(RNAi)* animals exhibited molting defects by the endpoint. Under these conditions, peak levels of *nhr-23* transcripts were 4.1-fold lower in *nhr-23(RNAi)* than wild-type animals (data not shown). Levels of pri-*let-7* in control samples peaked in L3 and once again in L4 (Figure 3D and 3F). In contrast, transcript levels of pri-*let-7* detected in *nhr-23* knockdowns were 1.5-fold lower at L3 (30h) and 3-fold lower at L4 (42h) than the peak value detected in age-matched, control larvae (Figure 3D and 3F). Levels of mature *let-7* stagnated in *nhr-23(RNAi)* knockdowns but rose

continuously in control samples collected across the L3-to-L4 and larval-to-adult transitions (Figure 3E and 3G). In both L3 and L4 stages, molting-defective larvae were first observed as levels of *let-7* plateaued, consistent with the attribution of the phenotype to knockdown of *nhr-23*. The levels of the other members of the *let-7* family, *mir-48*, *mir-84* and *mir-241*, were similarly reduced in *nhr-23(RNAi)* larvae developing across the L3 stage, as compared with age-matched control larvae (Supplemental Figure 2C, D). Collectively, these findings strongly suggest that NHR-23 directly and repeatedly activates the transcription of primary *let-7* family of microRNAs.

Scrambling the ROREs reduces NHR-23 binding at *let-7* promoters and phenocopies *let-7* loss-of-function (*lf*) mutants.

To test the physiological relevance of the three consensus ROREs in the promoter of *let-7*, we used CRISPR/Cas9 mediated gene editing to scramble the ROREs in pairs (Figure 4A). The GC content of the scrambled region was the same in mutant and wild-type animals. Mutant strains were outcrossed multiple times and then subjected to molecular assays and phenotypic analyses. For technical reasons, we were only able to generate *let-7(scRORE1,2)* and *let-7(scRORE1,3)* strains.

To determine the extent to which the ROREs were necessary for NHR-23 occupancy at the promoter of *let-7*, we performed ChIP-qPCR in *let-7(xk41-scRORE1,2)*, *let-7(xk39-scRORE1,3)* and wild-type animals during the L4 stage. The level of enrichment of the wild-type *let-7* promoter in the *nhr-23::3xflag* samples was 25-fold higher, relative to control animals. In contrast, the enrichment was only ~5-fold higher in both *let-7(scRORE1,2)* and *let-7(scRORE1,3)* mutants relative to the control animals (Figure 4B, Supplemental Figure 1E). The level of enrichment of the *let-7* promoter in *let-7(scRORE1,2)* and *let-7(scRORE1,3)* mutants was still above background, suggesting that the remaining RORE not scrambled in each of the *let-7(scRORE)* mutants may contribute to some binding by NHR-23.

Next, we queried the levels of primary and mature *let-7* transcripts in *let-7(scRORE1,2)*, *let-7(scRORE1,3)* and wild-type animals immediately following the L2/L3 molt (Figure 4C, D). At the peak of expression (22 h), the levels of *pri-let-7* in *let-7(scRORE1,2)* and *let-7(scRORE1,3)* animals were decreased by 2.4-fold and 1.7-fold, respectively, relative to wild type (Figure 4C). Correspondingly, the levels of mature *let-7* at the same time points were reduced by 2.7-fold and 2.5-fold in the *let-7(scRORE1,2)* and *let-7(scRORE1,3)* animals, respectively, relative to wild type animals (Figure 4D). However, no significant difference was detected in the levels of mature *let-7* at the L4 stage in *let-7(scRORE1,2)* and *let-7(scRORE1,3)* animals compared to wild type

animals (data not shown). Thus, reduced binding of NHR-23 is accompanied by reduced transcription and slower accumulation of *let-7* in these strains.

To characterize heterochronic phenotypes associated with scrambling the ROREs, we scored the number of seam cell nuclei in the *let-7(scRORE1,2)* and *let-7(scRORE1,3)* mutants and wild-type animals. At least two independent isolates of each scrambled mutant were analyzed. As positive controls, we included two *let-7* hypomorphs, *let-7(n2853)* and *let-7(mg279)*, since these mutants have higher numbers of seam cells than wild type animals (Chan and Slack, 2009; Reinhart et al., 2000). Seam cell nuclei were identified and scored in adult animals based on the fluorescent reporter gene *Pscm::gfp*, which was crossed into each strain prior to scoring. All lines of the *let-7(scRORE1,2)* and *let-7(scRORE1,3)* strains exhibited significantly increased number of seam cells relative to wild-type adults (Figure 4E). The extent of seam cell hyperplasia detected in the *let-7(scRORE)* mutants was comparable to *let-7(mg279)*, but less severe than *let-7(n2853)* (Figure 4E).

To examine how the ROREs, and by extension, NHR-23-mediated activation of *let-7*, affect the biorhythm of molting, we conducted longitudinal behavioral studies on *let-7(scRORE1,2)*, *let-7(scRORE1,3)* and wild-type animals developing from the L3-to-L4 molt until young adulthood (Figure 4F). All four mutant strains (i.e., two independent alleles of *let-7(scRORE1,2)* and *let-7(scRORE1,3)*) were found to enter into and emerge from the L4-to-adult molt significantly earlier than wild type, similar to previous findings with *let-7(lf)* mutants. Therefore, scrambling the ROREs is sufficient to increase the speed of development, consistent with our model that NHR-23-mediated activation of the *let-7s* normally slows the pace of molting.

Thus, reduced occupancy of the *let-7* promoter by NHR-23, reduced levels of primary *let-7* transcripts, seam cell hyperplasia and quicker pace of the molting cycle are all associated with the *let-7(scRORE1,2)* and *let-7(scRORE1,3)* mutants. It is likely that the kinetics of accumulation of mature *let-7* strongly affects development of the seam and the pace of molting, consistent with prior reports on the time sensitive nature of *let-7* function (Reinhart et al., 2000).

The *nhr-23* 3' UTR contains a functional *let-7* consensus site.

To determine if NHR-23 and *let-7* constitute a feedback loop, we next asked whether the *let-7* family of microRNAs downregulates *nhr-23* transcript abundance in developing larvae. We identified a single element in the 868-bp 3' UTR of *nhr-23* (Mangone et al., 2010) that perfectly complements the 5' seed sequence of *let-7* and partially complements the remainder of the microRNA. Hereafter, this element is called the *let-7* consensus site (LCS). Three other

sequences in the 3' UTR of *nhr-23* partially complement the *let-7*s with mismatches to the seed (Figure 5A and Supplemental Table 2).

To assess the significance of the LCS, we designed and utilized a set of bicistronic reporters for post-transcriptional *cis*-regulatory elements, each housed in a distinct extrachromosomal array and unique transgenic strain (Figure 5B). Briefly, the coding sequence of tandem (td) Tomato was fused with the 3' UTR of *nhr-23*, whereas the coding sequence of GFP was fused with the 3' UTR of *unc-54*, which is not targeted by the *let-7*s. An SL2 trans-spliced leader sequence bridged the two fusion genes. The promoter of *dpy-7* drove expression of the operon in the hypodermis. The readout was the ratiometric signal of TdTomato to GFP detected in the lateral epidermis (Supplemental Figure 3). This approach controlled for potential differences in gene expression associated with particular arrays or mosaic animals rather than the test 3' UTR.

Figure 4C shows the merged and individual signals detected in transgenic animals in the L4-to-adult molt, at which time both *let-7* and *dpy-7* are highly expressed. The ratiometric signal for the *nhr-23* 3' UTR reporter was ~6 fold lower than the negative control *unc-54* 3' UTR reporter (Figure 5D). Similarly, the ratiometric signal for the positive control *lin-41* 3' UTR reporter was 3-fold lower than the negative control. It is unlikely that the 3' UTR fused to TdTomato affects the efficiency of trans-splicing or causes nonsense-mediated decay of the polycistronic pre-mRNA, because the absolute intensities of GFP of all three constructs were equivalent.

We next systematically deleted each of the four predicted *let-7* binding sites in the *nhr-23* 3' UTR and compared their reporter signals with the signal detected from the wild-type reporter for *nhr-23* 3' UTR. Excision of the LCS led to a two-fold increase in the ratio of tdTomato/GFP signals, relative to the average ratio associated with the reporter for the full-length 3' UTR of *nhr-23* (Figure 5E). In contrast, deletions of the other predicted *let-7* binding sites ($\Delta 26-42$, $\Delta 227-249$, and $\Delta 623-646$) in the *nhr-23* 3' UTR reporters did not increase the ratio of the tdTomato/GFP signals, suggesting that the LCS is the only bona fide *let-7* binding site tested in the *nhr-23* 3' UTR. Consistent with this result, a highly-sensitive, high-throughput approach to catalog targets of microRNAs identified the 3' UTR of *nhr-23* among cellular transcripts associated with ALG-1, the primary Argonaute of the worm microRNA RISC complex (Broughton et al., 2016; Grishok et al., 2001). Thus, *let-7* represses *nhr-23* by directly binding the LCS in its 3' UTR.

Both the LCS and *let-7*s contribute to dampening the expression of *nhr-23*.

We next deleted the endogenous LCS of *nhr-23* by CRISPR/CAS9 (Paix et al., 2015) to generate the *nhr-23(aaa20- Δ LCS)* strain. We then detected and compared temporal waves in the

abundance of *nhr-23* transcripts among wild-type animals and both *nhr-23(aaa20-ΔLCS)* and *let-7(n2853)* mutants developing from late L2s into young adults by TaqMan RT-qPCR. To stage each strain, we inspected and scored the behavior of ~100 worms as active or quiescent at each timepoint prior to collection of the sample. Lethargi, and by extension the molts, were identified *post-hoc* based on these measurements. Wild-type larvae developed more slowly than gain-of-function *nhr-23(aaa20-ΔLCS)* or loss-of-function *let-7(n2853)* mutants in this particular experiment. However, we captured oscillatory expression of *nhr-23* across the target stages among the time samples of each strain (Figure 6A and Supplemental Figure 4A). Additionally, we used the program Metacycle (Wu et al., 2016) to calculate the amplitude and phase of the expression curves of *nhr-23* and performed manual calculations to determine the rates of accumulation and decay of *nhr-23* transcripts (Figure 6A'). Peak levels of *nhr-23* were typically detected one-third to one-half of the way through the L2, L3 and L4 stages in wild-type time samples. However, the peak values of sequential waves dropped by a regular increment of ~1.5-fold from one life stage to the next, an indication of dampening (Figure 6A', Supplemental Table 3).

Three metrics of the expression curves for *nhr-23*, amplitude, peak value and rising slope, were consistently higher both in *nhr-23(aaa20-ΔLCS)* mutants and *let-7(n2853)* mutants, as compared with wild-type animals, across both the L3 and L4 stages in two independent biological replicates (Figure 6A, A', Supplemental Figure 4A, A', Supplemental Table 3). For instance, the peaks in *nhr-23* transcript levels that were detected early in L3 and L4 were ~1.6-fold higher in *nhr-23(aaa20-ΔLCS)* samples than in wild-type samples, despite the dampening (Figure 6A, Supplemental Table 3). Similarly, the amplitude, peak value, and slope of *nhr-23* curves in *let-7(n2853)* mutants were also both significantly higher relative to wild type during the L3 and L4 stages. The phases of the *nhr-23* waveforms differed among the three cohorts but were not consistently earlier in either mutant relative to wild-type animals, across both life stages and biological replicates (Supplemental Table 3). Interestingly, an extra pulse of *nhr-23* expression was detected in both *nhr-23(aaa20-ΔLCS)* and *let-7(n2853)* time samples collected after the fourth molt, suggesting the potential for a supernumerary molt (see arrows, Figure 6A).

We used a similar approach to determine the extent to which the *let-7*s repress the expression of *nhr-23* during the L2 stage. We compared the abundance of *nhr-23* transcripts in regular time samples of *nhr-23(aaa20-ΔLCS)* single mutants, *mir-48 mir-241(nDf51)*; *mir-84(n4037)* triple mutants, and wild-type larvae developing from late L1s into early L3s (Supplemental Figure 4B–B'). The L2 stage expression curves detected in both mutants were at least 3-fold steeper and peaked at higher levels than the those detected in wild-type larvae.

In complementary studies, we tracked the abundance of NHR-23 protein expression in epidermal nuclei as indicated by the signal associated with the NHR-23::GFP fusion protein. Protein levels also cycled from the L2 through the L4 stage. For example, the signal peaked 2 h after emergence in the L4 stage but was not detected 3 h later (Supplemental Figure 5A, B). Both the extent and kinetics of protein increase and decrease corresponded well with the expression curves for *nhr-23* transcripts detected in wild-type larvae. We next asked if the *let-7*s regulate the abundance of NHR-23 proteins by comparing the abundance of the NHR-23::GFP fusion protein in the *let-7(mg279); mir-84(tm1304)* double mutant and wild-type animals (Supplemental Figure 5C). GFP was detected in the epidermal nuclei of the *let-7(mg279); mir-84(tm1304)* mutant molting from L4s to adults but was not readily detected in wild-type molting animals. The signal from NHR-23::GFP became bright in the *let-7(mg279); mir-84(tm1304)* mutant that had emerged as adults but remained dim in wild-type adults. Interestingly, the corresponding 3.4-fold increase in fluorescence intensity matched the 3.4-fold increase in abundance of *nhr-23* transcripts detected in *let-7(n2853)* versus wild-type samples collected at a comparable timepoint. Of note, the native 3' UTR of *nhr-23* was fused to *nhr-23::gfp* in the genetic reagent used in our study, whereas the ectopic 3' UTR of *unc-54*, which is not a target of the *let-7*s, was fused to *nhr-23::gfp* in a distinct reagent used in previous research (Hayes et al., 2006; Kostrouchova et al., 1998). Thus, the current study is the first to report that the *let-7*s likely directly repress *nhr-23* through association with the LCS in the *nhr-23* 3' UTR to prevent the accumulation of *nhr-23* transcripts and proteins in wild-type adults.

To study how the LCS, and by extension, *let-7*-mediated repression of *nhr-23*, affects the biorhythm of molting, we tracked cohorts of *nhr-23(aaa20-ΔLCS)* larvae across both the L3 and L4 stages (Figure 6B, C). As a complementary approach, we also tracked larvae that expressed multiple copies of *nhr-23* from an integrated, tandem array across the same life stages (Celniker et al., 2009). The majority of *nhr-23(aaa20-ΔLCS)* L3 larvae entered lethargus and emerged as L4 larvae before most wild-type L3 larvae began to molt. The wake-to-wake interval of the *nhr-23(aaa20-ΔLCS)* L3-stage cohort was 1.5 ± 0.9 h shorter than that of wild-type L3s. Likewise, the majority of *wgls43[nhr-23⁺⁺]* larvae, which overexpress *nhr-23*, entered lethargus and emerged in the next life stage faster than age-matched, wild-type animals (Figure 6B, C). The wake-to-wake interval was 6.9 ± 0.6 h for the *wgls43[nhr-23⁺⁺]* cohort developing from L3 to L4, compared with 7.8 ± 0.6 h for the wild-type cohort ($p \leq 0.01$). Combining *wgls43[nhr-23⁺⁺]* with *let-7(n2853)* led to larval lethality and prohibited a similar analysis. Thus, both de-repression and increased dosage of *nhr-23* were associated with advanced lethargus and faster cycles, similar to our earlier findings with *let-7(lf)* mutants.

Together, these findings show that the endogenous LCS in the *nhr-23* 3' UTR is indeed a *cis*-regulatory repressive element, strongly suggesting that *let-7* and its paralogs bind this functional LCS and negatively regulate the expression of *nhr-23* transcripts and proteins, while larvae transit the molts and emerge in the subsequent life stage. Therefore, these data are consistent with a model whereby NHR-23 and the *let-7*s form a transcriptional-post transcriptional feedback loop that regulates the duration of the molt. Immediately following the molt, NHR-23 activates transcription of the *let-7*s early during the larval stage. The post transcriptional repression of *nhr-23* by the *let-7*s keeps the levels of *nhr-23* below a particular threshold, preventing early entry into the next molt.

Forced expression of *nhr-23* is sufficient to trigger supernumerary molts.

As described above, there was no detectable dampening of *nhr-23* transcript levels in *let-7(n2853)* mutants, whereas the phenomenon was obvious in wild-type animals (Figure 6A, Supplemental Figure 4A). Mutations in *let-7* were originally characterized as retarded heterochronic mutants that underwent supernumerary molts (Hayes *et al.*, 2006; Reinhart *et al.*, 2000). Considering this, we hypothesized that *let-7*-dependent dampening of the oscillatory expression of *nhr-23* effectively counts down the number of molts and ultimately extinguishes the molting cycle.

To test this idea, we tracked and compared instances of molting-associated behaviors and animal viability between wild-type adults and age-matched gain-of-function (*gf*) mutants where *nhr-23* is overexpressed: *nhr-23(aaa20-ΔLCS)* (Figure 6A, Supplemental Figure 4A) and *wgls43[nhr-23⁺⁺]* (Celniker *et al.*, 2009). At first, we inspected partially synchronized populations at regular timepoints 2–5 days after the emergence of adults. Behavioral quiescence, defined by a lack of detectable pharyngeal pumping or locomotion, was more common among both *nhr-23(aaa20-ΔLCS)* and *wgls43[nhr-23⁺⁺]* adults than wild-type animals across this interval. Moreover, the percentage of quiescent *nhr-23(gf)* adults peaked and significantly exceeded the percentage of quiescent wild-type adults during 3 to 4 successive time samples (Figure 7A). We next asked whether quiescent *nhr-23(aaa20-ΔLCS)* and *wgls43[nhr-23⁺⁺]* adults observed at those particular timepoints were in fact undergoing lethargi associated with supernumerary molts rather than transient, satiety-induced quiescence (You *et al.*, 2008). To distinguish between these two possibilities, we singled quiescent adults into 3 respective cohorts per genotype and tracked the animals within each cohort for an additional 12 h (Figure 7B). In parallel, we singled and tracked quiescent wild-type adults. The overwhelming majority of singled *nhr-23(gf)* adults were quiescent for several hours and then attempted to ecdyse, a sequence of events indicative of a

supernumerary molt. Most animals shed entire cuticles or parts thereof, but nonetheless died (Supplemental Movie 2, 3). The *nhr-23(aaa20-ΔLCS)* adult shown in Supplemental Movie 3 is one such example. The animal was quiescent for 6 h, then exhibited intermittent twitches of the grinder, a behavior that accompanies ecdysis, and ultimately bagged, likely because unshed cuticle occluded the vulva. In contrast, all quiescent wild-type adults regained activity and only one animal died during the period of observation (Figure 7B, Supplemental Movie 1). By the abovementioned criteria, 97% (n = 34) of singled *nhr-23(aaa20-ΔLCS)* adults and 91% (n = 33) of singled *wgls43[nhr-23⁺⁺]* adults underwent supernumerary molts whereas none (n = 11) of the wild-type adults did so (P < 0.0001, chi-square test). Figure 7C shows one example each of an *nhr-23(aaa20-ΔLCS)* and a *wgls43[nhr-23⁺⁺]* adult that underwent aberrant molts and became trapped in partly shed cuticles. Both animals had eggs in the uterus. However, the *nhr-23(aaa20-ΔLCS)* animal had an old cuticle attached to its tail. Also, alae were visible on both the lateral surface of the extant cuticle and the partly shed cuticle, implying that the epidermis had terminally differentiated prior to the attempted molt. These results show that forced expression of *nhr-23* is sufficient to initiate a supernumerary molt but not sufficient to properly complete the molt. Taken together, these data suggest that artificially increasing the abundance of NHR-23 relative to the *let-7s* drives additional iterations of the molting cycle.

Dynamic levels of *nhr-23* and the *let-7s* shape expression curves of many effectors of the molting cycle.

NHR-23 and *let-7* may act as core components of a molecular-genetic oscillator that regulates the onset and duration of the molts. Other biological clocks generate and sustain orderly waves in the expression of both core clock components and groups of “clock-controlled genes (CCGs)” that encode coordinated effectors of the biorhythm. Consistent with this model, genes that are depleted in *nhr-23* knockdowns are strongly enriched for oscillating genes (Tsai et al., 2021). From this perspective, we considered how the negative feedback loop between *nhr-23* and the *let-7s* might affect the expression of genes that oscillate in phase with different events linked to the molting cycle. To test this idea, we chose two oscillatory genes linked to molting: 1) *fbn-1*, which encodes a component of the sheath that encloses and protects animals during each molt (Katz et al., 2021); and 2) *mlt-10*, which encodes a component of the cuticle (Frand et al., 2005; Meli et al., 2010). We then queried the expression levels of each of the above transcripts in *nhr-23(RNAi)*, *nhr-23(aaa20-ΔLCS)* and *let-7(n2853)* mutants and control animals collected at regular intervals from late L2 through young adulthood using RT-qPCR (Figure 8A–D). As

described earlier, the amplitude and phase of each waveform were determined using Metacycle, while the slope of each waveform was calculated manually.

As expected, peak levels of *fbn-1* were detected early in the L3 and L4 stages in control animals (Figure 8 A, B). Knockdown of *nhr-23* during both stages reduced the amplitude of *fbn-1* by 4–5-fold (Figure 8A). However, the slope and phase of the *fbn-1* waveform were virtually identical in both *nhr-23(RNAi)* and mock-treated larvae (Supplemental Table 3). In contrast, both LCS deletion and *let-7* mutations increased the amplitude and peak level of *fbn-1* transcripts by ~1.5-fold in L4-stage animals as compared with age-matched controls (Figure 8B, Supplemental Table 3). The slope of the *fbn-1* expression curves was 2-fold higher in *nhr-23(aaa20-ΔLCS)* mutants and 3-fold higher in *let-7(n2853)* mutants than wild type (Supplemental Table 3). Notably, the phase of *fbn-1* expression was ~1 h earlier in both *nhr-23(aaa20-ΔLCS)* and *let-7(n2853)* mutants relative to wild type (Supplemental Table 3). This is consistent with the observation that *nhr-23(aaa20-ΔLCS)* and *let-7(n2853)* mutants molt earlier than wild-type animals. Similar findings were observed in a second, independent trial with *nhr-23(aaa20-ΔLCS)*, *let-7(n2853)* and wild-type animals (Supplemental Figure 6A).

Peak levels of *mlt-10* transcripts were detected late in each larval stage, right before animals enter the molt (Figure 8C). In L4-stage *nhr-23(RNAi)* larvae, the peak level of *mlt-10* was reduced by 2-fold, relative to control animals, even though the amplitude and phase remained similar in both backgrounds. Additionally, knockdown of *nhr-23* reduced the slope of the *mlt-10* expression curve to 0.1, compared with 0.4 in control animals, suggesting that *nhr-23* likely affects the rate of accumulation of *mlt-10* transcripts (Supplemental Table 3). In *nhr-23(aaa20-ΔLCS)* and *let-7(n2853)* mutants, both the amplitude and peak value of *mlt-10* expression were about ~2-fold higher than wild type. Consistent with earlier findings on *fbn-1*, the slope of the *mlt-10* expression curve was ~4-fold higher and the phase was ~1 h earlier than wild type. Supplemental Figure 6B shows similar results that were obtained in an additional independent experiment. Thus, the cyclical expression profiles of *fbn-1* and *nhr-23* are altered in *nhr-23* knockdowns, and in *nhr-23(gf)* and *let-7(lf)* mutants. As we describe below, both genes have *cis*-regulatory elements for NHR-23 and the *let-7s* in their promoters and 3' UTRs, respectively, suggesting direct transcriptional activation by NHR-23 and direct repression by the *let-7s*. The feedback loop likely sculpts the temporal expression profiles of *fbn-1* and *mlt-10*, as well as other genes linked to molting.

To determine whether joint regulation by NHR-23 and *let-7s* was a signature of oscillatory genes that are linked to molting, we used a bioinformatics approach. We selected a set of potential target genes of the molting timer based on two criteria: 1) expression of the gene oscillates with

a period of 8–10 h across larval development (Hendriks et al., 2014; Kim et al., 2013); and 2) activity of the gene affects one of the many distinct but interdependent steps within the molting cycle. We consider these genes as “clock-controlled genes (CCGs)”. Collectively, the 67 selected CCGs encode transcription factors, signaling molecules, enzymes and matrix proteins that are involved in the synthesis and removal of cuticles, and neuropeptides that regulate quiescence and arousal (Supplemental Table 4). Next, we systematically and independently evaluated each CCG as a probable target of NHR-23 or *let-7s* through meta-analyses of published datasets mentioned below and original bioinformatic approaches. A CCG classified as a direct target of NHR-23 met at least two of the following criteria: 1) NHR-23 occupied the 5' regulatory region of the gene *in vivo*, as annotated in a ChIP-Seq dataset (Celniker et al., 2009); 2) the same regulatory region contained more ROREs than expected by chance; and 3) knock down of *nhr-23* resulted in lower transcript levels (Kouns et al., 2011). A CCG classified as a target of the *let-7s* met two criteria: 1) ALG-1 bound the 3' UTR of the respective mRNA *in vivo*, as reported in an ALG-1 iCLIP dataset (Broughton et al., 2016); and 2) the 3' UTR contained more LCSs than expected by chance.

By these rubrics, 57% of CCGs were classified as shared targets of both NHR-23 and the *let-7s* (including *fhn-1* and *mlt-10*); 24% as targets of only NHR-23; 10% as targets of only *let-7s*; and 13% as targets of neither factor (Figure 8E, Supplemental Table 4). Notably, multiple response elements for NHR-23 were identified in the promoters of almost all CCGs classified as *let-7* targets and vice versa, even though NHR-23 or ALG-1 were not enriched at those genomic locations in the abovementioned ChIP-Seq or iCLIP datasets. Therefore, 57% may be an underestimate and more outputs of the molting timer may ultimately be recognized as dual targets of both NHR-23 and the *let-7s*. Only 10% of twenty randomly selected genes that are not known to cycle in expression were classified as shared targets of both NHR-23 and *let-7s*, suggesting that NHR-23 and the *let-7s* together may specifically regulate the expression of oscillatory genes that drive molting. These findings suggest that partly interdependent waves in the abundance of NHR-23 and the *let-7s* sculpt the temporal expression profiles of *fhn-1*, *mlt-10* and possibly many additional effectors of the molting timer.

NHR-23 and *let-7s* govern the temporal expression profile of other key clock genes

The bioinformatics analysis described above provided more evidence for regulatory interactions among other key components of the oscillator. Our analysis suggested that NHR-23 promotes the expression of both *lin-42/PER* and the *let-7s*, whereas *let-7s* repress the expression of both *lin-42/PER* and *nhr-23* transcripts. Three major isoforms of *lin-42* are recognized

regulators of the molting cycle and components of the heterochronic pathway (Edelman et al., 2016; Jeon *et al.*, 1999; Monsalve *et al.*, 2011). We identified three ROREs in the unique promoter of *lin-42a* and three additional ROREs in the shared promoter of *lin-42b* and *lin-42c* (Supplemental Figure 7A). The ROREs in both promoters correspond to sites of NHR-23 enrichment detected by ChIP-Seq and annotated by the modENCODE Consortium (Celniker *et al.*, 2009). Consistent with the data from the modENCODE consortium, NHR-23 ChIP-qPCR analysis during L3 showed that the *lin-42a* promoter was enriched by 5-fold and the *lin-42b* promoter was enriched 7-fold in the *nhr-23::3xflag* samples, relative to background (Figure 9A). To further characterize the extent to which NHR-23 activates the pulsatile expression of *lin-42*, we measured and compared the levels of *lin-42* transcripts across the L4 stage in attenuated *nhr-23* knockdowns and control animals (Figure 9B). As expected, levels of *lin-42* in control samples peaked in L3 and once again in L4. No such peak was detected in *nhr-23(RNAi)* at the L4 stage. The transcript levels of *lin-42* detected in *nhr-23* knockdowns at the L4 stage (42 h) were 2.6-fold lower than the peak value detected in age-matched, control larvae. Likewise, the amplitude and slope of *lin-42* expression were 3-fold and 6-fold lower, respectively, in L4-stage *nhr-23(RNAi)* larvae, relative to age-matched controls. Moreover, we identified a single RORE site 827–833 bp upstream of the start codon of human *PER2*, suggesting that NHR-23/ROR-mediated transcriptional activation of *lin-42/Per* may be conserved in mammals.

We identified four LCSs, including one with perfect complementarity to the *let-7* seed region, in the shared 3' UTR of *lin-42a* and *b*, suggesting that the *let-7s* directly repress both *lin-42* isoforms (Supplemental Figure 7D). Although *lin-42* was previously described as containing sites complementary to the *let-7s*, the specific *cis*-regulatory elements were not well defined (Reinhart *et al.*, 2000). No LCSs were detected in the 3' UTR of *lin-42c*, which is modeled as a dominant negative (Monsalve *et al.*, 2011). To determine how *let-7* affects the expression of *lin-42*, we measured the levels of *lin-42* transcripts in *let-7(n2853)* and wild-type animals (Figure 9C). We also included samples from *nhr-23(aaa20-ΔLCS)* mutants in the analysis. Both the amplitude and peak level of *lin-42* expression were 1.5-fold higher in *let-7(n2853)* mutants relative to the control. The phase was advanced by ~1 h in *let-7(n2853)* larvae (Supplemental Table 3). Similar results were observed in *nhr-23(aaa20-ΔLCS)* mutants, as well as in a second biological replicate (Supplemental Figure 7C). Going further, we identified two LCSs perfectly complementary to the *let-7* seed in the 3' UTR of human *Per2* transcripts (Supplemental Figure 7D), suggesting that the regulatory interactions between LIN-42 and the *let-7s* may be conserved in humans.

The bioinformatics analysis also provided evidence of potential positive autoregulation of *nhr-23*. We found eight ROREs within the upstream regulatory region of *nhr-23*. Two of these

ROREs were occupied by NHR-23 *in vivo*, as indicated by ChIP-Seq data from the modENCODE Consortium (Supplemental Figure 7B). NHR-23 ChIP-qPCR during L3 showed that the promoter of the *nhr-23* gene was enriched in *nhr-23::3xflag* samples, further substantiating the hypothesis of autoregulation. To test whether NHR-23 promotes its own expression, we used a fusion gene wherein the last two and a half exons of *nhr-23* were replaced with *gfp* fused to the 3' UTR of *unc-54* (Figure 9D). We compared the expression of this fusion gene in the lateral epidermis of *nhr-23* knockdown and control animals during the mid-L4 stage (Figure 9E, F). In this assay, the dsRNAs used to downregulate *nhr-23* expression specifically target the last two and half exons and thus, in theory, should affect expression of only endogenous *nhr-23* and not the *nhr-23::gfp::unc-54* transgenic reporter. Fluorescence signal was easily detectable in the epidermis of control animals, but not in *nhr-23(RNAi)* larvae (Figure 9E). The intensity of GFP detected in hyp7 of *nhr-23(RNAi)* animals was ~2-fold lower than mock-treated animals (Figure 9F). The intensity of GFP in the seam was similarly lowered upon knockdown of *nhr-23*. These data suggest that NHR-23 activates its own expression. Together, these data show that the positive autoregulation of *nhr-23*, in combination with the previously characterized NHR-23-*let-7* negative feedback loop, may contribute to a self-sustaining molecular-genetic oscillator. Key components of the molting cycle timer, including *lin-42* and CCGs, may be regulated by both NHR-23 and *let-7s*.

Reciprocal regulatory elements may be conserved in mammalian *ROR* and *let-7* genes.

We next asked whether the feedback loop between NHR-23/ROR and the *let-7s* may be conserved between nematodes and vertebrates. Using bioinformatic approaches, we searched for ROREs upstream of the homologs of *let-7* in the fully sequenced and annotated genomes of humans, mice, and zebrafish. We inspected the genomic region 3 kb upstream of the precursor *let-7* microRNA and identified 1 to 5 distinct ROREs in all homologs (Supplemental Figure 8A). Figure 10A depicts the ROREs found upstream of selected homologs of *let-7*. In each example, more ROREs were found than predicted by chance.

To determine the extent to which NHR-23/ROR could promote the expression of mammalian homologs of *let-7*, we fused the promoter of *M. musculus let-7a-1* with *gfp* and used fluorescence microscopy to detect and compare the expression of the reporter gene in *nhr-23(RNAi)* and control animals undergoing the L4-to-adult molt (Figure 10B, C). Fluorescence signal of this heterologous reporter in control animals was bright in the pharynx, a tissue where *nhr-23* is normally expressed (Figure 10B; Kostrouchova et al, 1998). In contrast, negligible signal was detected in the pharynx of *nhr-23(RNAi)* animals. Quantitative analyses of the GFP

fluorescence signal show that the intensity in *nhr-23(RNAi)* animals was ~3-fold lower, on average, than control animals (Figure 10C). Thus, these findings show that NHR-23 regulates the expression of the promoter of *M. musculus let-7a-1* in *C. elegans*, suggesting that the positive arm of the NHR-23-*let-7* feedback loop may be conserved to mammals.

Next, we searched for LCSs in the 3' UTRs of all 13 homologs of *nhr-23/ROR* annotated in the reference genomes of flies, frogs, zebrafish, chickens, mice and humans (Figure 10D, Supplemental Table 2). We first aligned and compared the nucleotide sequence of the query 3' UTR with the sequences of corresponding ESTs. In two cases – zebrafish ROR β and ROR γ – multiple ESTs supported longer 3' UTRs than those presently annotated on the UCSC Genome Browser (see Key Resources Table). We found 1–3 LCSs perfectly complementary to the seed sequence of *let-7* within 3' UTRs of 10 of the *nhr-23/ROR* homologs. We also found one or two more LCSs with a single mismatch to the seed sequence of *let-7* in 6 of the corresponding 3' UTRs. For example, we identified one perfectly complementary LCS in the center of the validated 3' UTR of human ROR β , flanked by two more sites with respective single nucleotide mismatches to the seed of *let-7* (Figure 10D). Similar LCSs with at most a single mismatch to the seed sequences of the *let-7*s were found in the 3' UTRs for each of the remaining four homologs (Supplemental Table 2).

To test the significance of the LCSs detected in the mammalian ROR 3' UTRs, we focused on the 3' UTRs of *H. sapiens* ROR β and *M. musculus* ROR α . Each 3' UTR has two LCSs that perfectly match the seed region of *let-7*: sequences starting at nt 3576 and 4055 in *H. sapiens* ROR β , and nt 2055 and 2184 in *M. musculus* ROR α (Figure 10D). We selected a 590 bp fragment of the *H. sapiens* ROR β 3' UTR, spanning the two LCSs (Figure 10D, boxed region). Similarly, we chose a 281 bp fragment of the *M. musculus* ROR α 3' UTR also spanning the two LCSs (Figure 10D, boxed region). We fused each fragment, as well as variants thereof that lack both LCSs, to *tdTomato* in the bicistronic reporter system described in Figure 5B. We then used fluorescence microscopy to measure the intensity of tdTomato and GFP signals in the lateral epidermis of animals undergoing the L4-to-adult molt. When the *H. sapiens* ROR β 3' UTR was fused to *tdTomato*, the intensity of tdTomato signal was barely detectable in the epidermis, whereas the intensity of GFP signal in the same animal was conspicuous (Figure 10E, Supplemental Figure 8B). Deletion of both LCSs from the *H. sapiens* ROR β 3' UTR increased the intensity of TdTomato signal by ~30-fold relative to the wild-type constructs (Figure 10F). Similar findings were made with the bicistronic reporter constructs that housed the *M. musculus* ROR α 3' UTR (Figure 10G, H, Supplemental Figure 8C). These data suggest that *C. elegans let-7* can repress the expression of specific mammalian ROR 3' UTRs. Taken together, these findings imply

that the feedback loop between NHR-23/ROR and *let-7*s may be conserved and may regulate the cyclical expression of target genes in mammalian tissues.

DISCUSSION

The principal findings of this study unite two distinct time keeping mechanisms mutually dependent on a transcriptional-post-transcriptional feedback loop between NHR-23 and the *let-7*s: the heterochronic genetic pathway that controls the singular switch from larval to adult fates and the genetic oscillator that controls the biorhythm of the molting cycle.

NHR-23 transcriptionally activates *let-7* and *let-7* post-transcriptionally represses *nhr-23* to form a molecular-genetic oscillator.

In *C. elegans*, the primary transcripts of the *let-7* family of microRNAs (*mir-48*, *mir-84*, *mir-241* and *let-7*) oscillate in abundance and peak once in every larval stage (McCulloch and Rougvie, 2014; Van Wynsberghe et al., 2011). This oscillatory gene expression pattern is regulated at the transcriptional level (Kai et al., 2013). A few negative and positive regulators of *let-7* transcription have been identified previously, although none completely account for the oscillatory expression of the primary *let-7*s. The transcription factor HBL-1 negatively regulates the transcription of *let-7* in the hypodermis until the L3 stage (Roush and Slack, 2009). Similarly, the transcription factor LIN-14 restricts the transcription of *mir-48*, *mir-84* and *mir-241* until the L2-to-L3 transition (Tsialikas et al., 2017). The Period protein homolog LIN-42 binds the promoter of *let-7* and dampens the amplitude of primary *let-7* oscillations to prevent early accumulation of mature *let-7* (McCulloch and Rougvie, 2014; Perales et al., 2014; Van Wynsberghe et al., 2014). LIN-42 also dampens oscillations of primary *mir-48* transcripts and prevents the early accumulation of *mir-48*. However, *lin-42* is not required for the oscillatory expression pattern of the primary *let-7* transcripts (McCulloch and Rougvie, 2014). The transcription factor DAF-12 is involved in a complex regulatory network that couples environmental and developmental signals to regulate *let-7* family transcription. During unfavorable conditions, unliganded DAF-12 represses the expression of the *let-7*s. However, during favorable conditions, and in the presence of its ligand, DAF-12 binds the promoters of *mir-84* and *mir-241* and mildly upregulates transcription (Bethke et al., 2009; Hammell et al., 2009). The GATA transcription factor ELT-1 binds upstream of *let-7* and promotes transcription during the L4 stage. ELT-1 also acts redundantly with DAF-12 to positively regulate the levels of *mir-48*, *mir-84* and *mir-241* (Cohen et al., 2015). However, both *daf-12* and *elt-1* are expressed at nearly constant levels during post embryonic development

(Hendriks et al., 2014; Kim et al., 2013) and hence, cannot completely explain the oscillatory expression pattern of the primary transcripts of the *let-7* family.

We have shown that NHR-23 binds upstream of *let-7*, *mir-48*, *mir-84* and *mir-241* during L3 and L4 stages (Figure 3B, 3C, Supplemental Figure 1C, 1D) and is required for the transcriptional activation of these microRNAs (Figure 3D-G, Supplemental Figure 2). Importantly, we show that NHR-23 is necessary for the cyclical expression profile of primary *let-7*, *mir-48* and *mir-84*, as the oscillations in the primary transcript levels of these microRNAs are almost undetectable upon knockdown of *nhr-23* (Figure 3D, 3F, Supplemental Figure 2C). We demonstrate that scrambling the RORE sites in the *let-7* promoter results in decreased binding by NHR-23 (Figure 4B, Supplemental Figure 1E), decreased primary *let-7* levels (Figure 4C) and slower accumulation of mature *let-7* (Figure 4D). The increased number of seam cells (Figure 4E) and the quicker pace of development of *let-7(scRORE1,2)* and *let-7(scRORE1,3)* animals (Figure 4F) also supports our conclusion that NHR-23 binding at the RORE sites is necessary for physiologically sufficient transcriptional activation of *let-7*.

A previous study proposed that the *let-7* family of microRNAs negatively regulated *nhr-23* by an indirect mechanism, independent of the 3' UTR of *nhr-23* (Hayes et al., 2006). Here, we show that *let-7* directly represses *nhr-23* in a manner dependent on a *let-7* complementary sequence (LCS) in the *nhr-23* 3' UTR (Figure 5, 6A, 6A', Supplemental Figure 4A, 4A'). However, our data do not rule out the possibility of additional regulatory pathways that are dependent on *let-7* but independent of the *nhr-23* 3' UTR. During the adult stage, the level of inappropriately expressed *nhr-23* in *let-7(n2853)* was higher than the level of *nhr-23* in the *nhr-23(aaa20-ΔLCS)* strain, suggesting the involvement of more than one pathway in the repression of *nhr-23* by *let-7* (Figure 6A, Supplemental Figure 4A). During the juvenile-to-adult transition, *let-7* represses the RNA binding protein *lin-41* and this allows the translation of the LIN-41 target, *lin-29* (Reinhart et al., 2000; Slack et al., 2000). Mutants of *lin-29* exhibit increased expression of NHR-23 during adulthood, suggesting that LIN-29 represses transcription of *nhr-23* (Harris and Horvitz, 2011). Therefore, the *lin-29*-mediated inhibition may be the 3' UTR independent pathway by which *let-7* represses *nhr-23*.

Thus, NHR-23 and *let-7* form a transcriptional-post-transcriptional negative feedback loop. Within a given larval stage, NHR-23 promotes the expression of the *let-7*s and the *let-7*s repress *nhr-23*. The expression levels of *let-7* peak ~1.6 hours after *nhr-23*, resulting in an intrinsic delay between the accumulation of *nhr-23* and that of *let-7* (Figure 3D, 3F, 6A). Across development, the *let-7*s dampen the relative amplitude of *nhr-23* expression from one larval stage to the next (Figure 6A, Supplemental Figure 4A). Furthermore, NHR-23 autoregulates its own expression

(Figure 9A, 9D-F). Together, these interconnected feedback loops set up a self-sustained molecular-genetic oscillator that is extinguished in adulthood.

Negative feedback between NHR-23 and *let-7s* sets the pace of the molting cycle.

The feedback loop between NHR-23 and the *let-7s* functions in an oscillator-based mechanism to regulate the duration of the molting cycle, in part by driving waves in expression of both key clock components, as well as output/target genes. We have shown that the Period homolog *lin-42* is a transcriptional target of NHR-23 (Figure 9A-C, Supplemental Figure 7C). The *let-7* family also post-transcriptionally represses *lin-42*. (McCulloch and Rougvie, 2014; Perales *et al.*, 2014; Van Wynsberghe *et al.*, 2014). Similarly, other genes necessary for molting, including *fbn-1* and *mlt-10*, are shared targets of NHR-23 and *let-7* (Figure 8, Supplemental Table 4). The transcription factor NHR-25, which is required for molting, may also be a shared target of NHR-23 and *let-7* (Supplemental Table 4) (Hayes *et al.*, 2006). We propose that the NHR-23-*let-7* feedback loop acts within the LIN-42/PER-based molting cycle timer, alongside other as-yet unidentified components.

Based on our findings, we propose a model to explain how the feedback loop between NHR-23 and the *let-7s* controls the speed of the molting cycle. Early in each larval stage, as animals commit to a forthcoming molt, NHR-23 first reaches a functional concentration at the promoters of genes with relatively higher numbers of ROREs, such as *fbn-1* and *noah-1*, and initiates the gene expression programs leading to the biogenesis of the sheath. The sheath is a temporary exoskeleton that encapsulates molting animals and is thought to protect the body of the worm from imploding while the old cuticle is released and a new one is synthesized (Katz *et al.*, 2021). At the same time, NHR-23 also promotes accumulation of the repressor *let-7*. As NHR-23 continues to accumulate, it begins to activate the expression of genes with relatively fewer ROREs such as *mlt-10* and *osm-11*, which respectively encode components of the cuticle and lethargus-promoting peptides (Meli *et al.*, 2010; Singh *et al.*, 2011). In this manner, NHR-23 might schedule the start of cuticle biogenesis and onset of lethargus. Then, *let-7*-mediated repression of the same CCGs and *nhr-23* likely signals both the end of cuticle remodeling and lethargus. Repression of *nhr-23* delays accumulation of the protein in the next life stage and the onset of any subsequent molt (Figure 6, Figure 7 and Supplemental Figure 4A). Thus, negative feedback between NHR-23 and the *let-7s* regulates the pace of the molting cycle in part by controlling the rate at which *nhr-23* transcripts accumulate and the amplitude of *nhr-23* expression. This model is consistent with the earlier onset of lethargus and accelerated development observed in both *nhr-23(aaa20-ΔLCS)* and *let-7(n2853)* mutants (Figure 2B and

6B). Both mutants have steeper curves and higher amplitude of *nhr-23* expression (Figure 6A and Supplemental Figure 4A). In contrast, delayed and protracted lethargus are observed in *nhr-23(RNAi)* animals (Figure 2B), which have shallower curves and lower amplitude of *nhr-23* expression. Thus, in theory, the intrinsic rates of ascent of *nhr-23* and the *let-7s* transcripts, and the ~1.6 h time difference between the accumulation of NHR-23 and accumulation of the *let-7s* together likely impact the amplitudes of the expression curves of multiple CCGs and, by extension, the temporal organization of critical phases of the molting cycle such as cuticle synthesis, lethargus and ecdysis. To determine whether the pace of the molting cycle is regulated by the amplitude of *nhr-23* expression versus the rate of accumulation of *nhr-23* transcripts will require future experiments wherein the two factors are manipulated independently of one another.

***let-7* mediated dampening of *nhr-23* levels sets the number of oscillations.**

All nematodes molt four and only four times. This represents striking and specific uniformity across some 25,000 different species, including numerous parasites of humans. In contrast, intra- and interspecies variation in the number of molts both before and after reproductive maturity occurs in animals of other phyla in the Ecdysozoan clade (Aguinaldo et al., 1997). Therein, the total number of molts varies in response to intrinsic and extrinsic factors, including the salinity and temperature of aquatic habitats, the availability of blood meals and other food sources, and the photoperiod (Esperk et al., 2007). The fundamental basis of this seemingly invariant limitation among nematodes is not known, despite the long-standing recognition of supernumerary molts associated with loss-of-function mutations in *let-7* and other heterochronic genes.

We propose that the balance between the activity of NHR-23 and the activity of the *let-7s* controls the finite number of molts. In our model, NHR-23 is a positive effector and the *let-7s* are negative regulators of molting. Consistent with this model, both *nhr-23(gf)* and *let-7(lf)* mutants undergo extra molts. As larvae develop from one stage to the next, the amplitude of NHR-23 expression gradually declines, while the levels of the *let-7s* gradually increase, culminating in the extinction of the cycle in adulthood. We have shown that *let-7*-mediated repression is at least partially responsible for the dampening of *nhr-23* expression (Figure 7A, Supplemental Figure 4A). Gradual reduction of positive autoregulation by NHR-23 through successive larval stages may be a second factor that could contribute to the dampening of *nhr-23* expression.

NHR-23 and *let-7* act together with other feedback loops, by a possibly conserved mechanism, to regulate developmental timing.

We have shown that NHR-23 and *let-7* are key components of a biological clock that regulates the pace of molting. Previous studies have characterized ~3700 genes that exhibit oscillatory patterns of gene expression coupled to the molting cycle (Hendriks *et al.*, 2014; Kim *et al.*, 2013; Meeuse *et al.*, 2020). These ~3700 genes have been proposed to form a massive genetic oscillator that could act as a developmental clock during *C. elegans* development (Meeuse *et al.*, 2020; Tsiairis and Grosshans, 2021). The interdependence of the molting cycle and the proposed developmental clock remain unknown (Tsiairis and Grosshans, 2021). The extent to which the pace of the molting cycle timer sets the pace of the theoretical developmental clock, and vice versa, is unclear. However, given the significant coupling of the molting cycle and the proposed developmental clock, the NHR-23-*let-7* genetic oscillator may contribute to the pace of the *C. elegans* developmental clock.

Using transgenic reporters, we showed that the transcriptional activation of *let-7* by NHR-23 and the post-transcriptional inhibition of *nhr-23* by *let-7* may be conserved in the context of mammalian homologs (Figure 10). RORs and mammalian *let-7* both regulate the expression of key clock components in the hepatic circadian clock. Specifically, RORs promote the expression of the clock components *Bmal1* and *Cry1*, as well as clock-controlled genes *Elovl3* and *Cyp8b1*, in both the livers of mice and cultured human liver cell lines (Takeda *et al.*, 2012; Zhang *et al.*, 2017). Liver-specific genetic disruption of only ROR γ , or in combination with ROR α , alters the levels of serum cholesterol, HDL and LDL, and liver triglycerides relative to wild-type mice (Takeda *et al.*, 2014; Zhang *et al.*, 2017). Thus, our work on the molting cycle timer may have implications for mammalian circadian clocks and related disorders of sleep and metabolism.

Our findings are consistent with the emerging concept that microRNA-mediated feedback loops increase the robustness of numerous gene regulatory networks and related outcomes, including cell fate decisions, stress responses, and developmental trajectories. The NHR-23-*let-7* genetic oscillator integrates the molting cycle timer with the heterochronic pathway in *C. elegans*, representing an elegant and possibly conserved mechanism of regulating developmental timing.

ACKNOWLEDGEMENTS

The American Cancer Society (RSG-12-149-01-DDC to ARF), the National Science Foundation (IOS1258218 to ARF), and the National Institutes of Health (R01 GM129301 awarded to JKK) supported this research. Some strains were provided by the *Caenorhabditis* Genetics Center (CGC), which is funded by the NIH Office of Research Infrastructure Programs (P40 OD010440).

FIGURE LEGENDS

Figure 1. Animal development requires coordination between reiterated processes and successive transitions in cell fate. **A)** Stages of the molting cycle of *C. elegans*, emphasizing the regular intervals of lethargus (yellow), ecdysis (orange) and physical activity (blue). Upon hatching, the embryo grows and develops through four larval stages that are punctuated by molts. **B)** Successive transitions in the fate of the lateral epidermal stem cells, called seam cells (red nuclei), in developing worms. The microRNAs *mir-48*, *mir-84*, *mir-241* are paralogs of *let-7* that promote transitions in the fate of the seam that are specific to the L2 stage. The microRNA *let-7* promotes fate transitions that are associated with the L3 and L4 stages. The adult stage is characterized by the presence of cuticular structures called alae. **C)** Schematic depicting interactions between ROR/*nhr-23*, *let-7* microRNAs and PER/*lin-42* in *C. elegans*. Arrowheads and bars signify positive and negative regulation, respectively. Question marks distinguish regulatory events evaluated in this study from those previously established.

Figure 2. Opposite and codependent effects of *nhr-23* and *let-7* on molting biorhythms. **A)** Stages of the life cycle (left) and the molting cycle (right) of *C. elegans*. **B)** Actograms depict the behavior, life stage and phenotype of worms observed at 1 h intervals from emergence in L4 onward. Each chart combines records from two independent trials. The records within each column correspond to a single worm. In addition, the molting-defective phenotype is labelled only when first detected. The wake-to-wake interval (W-W) has been indicated. Relevant scoring rubrics are fully defined in the Results and Methods. **** $p \leq 0.0001$; Ordinary One-Way ANOVA with Bonferroni's correction for multiple comparisons. **C)** The same as B, except that the actograms depict animals observed from the emergence in the L3 onward. **** $p \leq 0.0001$, * $p \leq 0.05$; Ordinary One-Way ANOVA with Bonferroni's correction for multiple comparisons. Supplemental Table 1 includes the active, lethargic, and w-w intervals of these eight cohorts and additional cohorts of both *let-7s(-)* mutants and *nhr-23* knockdowns.

Figure 3. NHR-23 promotes transcription of primary *let-7*. **A)** Schematic of the *let-7* locus in *C. elegans* (top) and corresponding NHR-23 ChIP peaks (bottom). Top: Magenta labels mature *let-7*; black labels *pri-let-7*; dark gray labels upstream DNA present in the *let-7p::gfp* transcriptional reporter (Kai et al, 2013); light gray labels the minimal seam-specific enhancer (MP) (Johnson et al, 2003); brown labels the consensus ROREs. TSS indicates the major transcriptional start site for *pri-let-7* (Kai et al, 2013). Dotted line represents the amplicon quantified by ChIP-qPCR.

Bottom: The NHR-23 ChIP-seq peaks reported by the modENCODE consortium are indicated. **B-C)** ChIP-qPCR analysis of NHR-23 enrichment at the *let-7* promoter in L3 and L4 stage wild type (untagged NHR-23) and *nhr-23::3xflag* larvae. The promoter of *col-19*, which had no NHR-23 ChIP-seq peak, was used as a negative control. Values represent the mean \pm sem of three independent trials, each of which included three technical replicates. Values for the amplicon of interest in QK159 [*nhr-23::3xflag*] and N2 were first normalized to the respective input. The average fold-enrichment in QK159 samples was then normalized to the average fold-enrichment in N2 samples within each trial. ** $p \leq 0.01$, *** $p \leq 0.001$; Two-way ANOVA with Bonferroni's correction for multiple comparisons. **D)** Levels of primary *let-7* transcript determined by TaqMan RT-qPCR in *nhr-23(RNAi)* and mock-treated larvae developing from the late L2 stage until the L3-to-L4 molt. Each value was normalized to *ama-1* transcript levels in the same sample. Values were then normalized to the average of all control time samples. Symbols represent the mean and range from two biological replicates. The x-axis indicates time elapsed (h) on food. The underlying bar depicts developmental stages; gray boxes therein signify lethargi. The times of initial exposure to *nhr-23* siRNAs and the appearance of molting-defective *nhr-23(RNAi)* larvae are indicated. **** $p \leq 0.0001$, ** $p \leq 0.01$; Two-way ANOVA with Bonferroni's correction for multiple comparisons. **E)** Same as D, except the levels of mature *let-7* transcripts, normalized to levels of the snoRNA U18, are shown. **** $p \leq 0.0001$, *** $p \leq 0.001$; Two-way ANOVA with Bonferroni's correction for multiple comparisons. **F-G)** Same as D and E respectively, except the larvae were collected from the early L3 stage until the L4-to-adult stage. ** $p \leq 0.01$, * $p \leq 0.05$; Two-way ANOVA with Bonferroni's correction for multiple comparisons.

Figure 4. Scrambling the ROREs in the *let-7* promoter reduces NHR-23 occupancy and phenocopies *let-7(lf)* mutants. **A)** The RORE sites upstream of the endogenous pri-*let-7* were scrambled in pairs using CRISPR/Cas9 mediated genome editing. The dotted line represents the amplicon quantified by ChIP-qPCR. **B)** ChIP-qPCR analysis of NHR-23 binding to the *let-7* promoter in *nhr-23::3xflag*; *let-7(xk41-scRORE1,2)* and *nhr-23::3xflag*; *let-7(xk39-scRORE1,3)*. The promoter of *col-19*, which had no NHR-23 ChIP-seq peak, was used as a negative control. One biological replicate of ChIP-qPCR from L4 animals is shown. The bar graph represents the mean of the 2 technical replicates. The error bars represent mean \pm standard deviation. Values for the amplicon of interest were first normalized to the respective input. The average fold-enrichment for each genotype was then normalized to the average fold-enrichment in N2 samples. n.s. not significant, * $p < 0.05$; Two tailed Student's unpaired t-test. A second biological replicate is shown in Supplemental Figure 1E. **C)** Levels of primary *let-7* transcript determined by RT-qPCR

in *let-7(xk41-scRORE1,2)* and *let-7(xk39-scRORE1,3)* immediately after the L2/L3 molt. Three biological replicates, with 2 technical replicates each are shown. The bar graph represents the mean of the 6 values first normalized to the levels of *eft-2* and then normalized to the value of the N2 sample at 20 h. The error bars represent mean \pm standard deviation. * $p \leq 0.05$, ** $p \leq 0.01$, *** $p < 0.001$; Two tailed Student's paired t-test. **D)** Same as C, except levels of mature *let-7* determined using Taqman RT-qPCR were first normalized to U18 snoRNA and then normalized to the value of the N2 sample at 20h. * $p \leq 0.05$, ** $p \leq 0.01$, *** $p < 0.001$; two tailed Student's paired t-test. **E)** Number of seam cell nuclei in *let-7(RORE-1,2)* and *let-7(RORE-1,3)* at 25°C. *let-7(n2853)* and *let-7(mg279)* were scored as controls. All scoring was done in the background of JR672 (*Pscm::GFP*). Mean \pm standard deviation has been shown. ($n \geq 100$) *** $p < 0.001$; One-way ANOVA. **F)** Left: Actograms depict the behavior and life stage of single wild type or mutant animals observed at regular 1 h intervals, as described in Figure 2B. Here, high activity (H) refers to continuous pharyngeal pumping, whereas low activity (L) refers to intermittent pharyngeal pumping at the time of observation. Right: Table with wake-to-wake intervals for multiple independent isolates. **** $p \leq 0.0001$, *** $p \leq 0.001$, ** $p \leq 0.01$; Mann-Whitney Test.

Figure 5. The 3' UTR of *nhr-23* contains a functional *let-7* consensus site (LCS). **A)** Predicted base-pairing between the LCS in the *nhr-23* 3' UTR and mature *let-7*. Schematic also shows three other predicted *let-7* binding sites. Stop codon is shown as a black box. **B)** Design of bicistronic reporters for 3' UTR-mediated gene regulation. **C)** Rows of representative fluorescence images show merged and individual signals from tdTomato and GFP co-expressed in the lateral epidermis of the same worm. Labels indicate the 3' UTR fused to tdTomato in the corresponding reporter. Arrowheads point to hyp-7 nuclei. Scale bar = 10 μ m. All images were captured with an exposure time of 10 milliseconds. **D)** Quantitation of the ratiometric signal (tdTomato/GFP) associated with each 3' UTR reporter detected. Each symbol represents the average value of three ROIs per worm. N indicates the cumulative sample size from two independent experiments. Bars signify the mean \pm sd for the cumulative sample. **** $p \leq 0.0001$, *** $p \leq 0.001$, Ordinary One-Way ANOVA with Tukey's correction for multiple comparisons. **E)** As above, except that ratiometric values were normalized to same-day controls. The full-length *nhr-23* construct is depicted in blue; deletion constructs in brown.

Figure 6. Steeper waveforms of *nhr-23* expression and an increased pace of development are both associated with deletion of the LCS from the 3' UTR of *nhr-23* and genetic inactivation of *let-7*. **A)** Levels of *nhr-23* transcripts detected by TaqMan RT-qPCR in regular time samples of

wild-type, *nhr-23(aaa20-ΔLCS)* and *let-7(n2853)* animals collected from late L2 through early adulthood. Rectangles beneath the x-axis signify lethargi (shaded by genotype, as per the legend); white rectangles signify intervals of physical activity. Values for *nhr-23* were first normalized to *ama-1* transcripts within each same time sample. The resulting values were further normalized to the mean of all wild-type time samples, represented by the dashed y-axis gridline. Dots and error bars represent the mean and range from three technical replicates. As the rates of development of the three genotypes differ from one another, the waveforms for the wild-type samples were shifted to the left by 4 h in both charts, to align the mutant and wild-type samples by developmental stage. The *p* values shown are for comparisons between wild-type and mutant values at the indicated time points. *****p*≤0.0001, ****p*≤0.001, ***p*≤0.01, Two-Way ANOVA with Tukey's correction for multiple comparisons. Supplemental Figure 4 shows the results of an independent biological replicate. Arrows point to the supernumerary peaks in *nhr-23* transcript levels detected in both *nhr-23(aaa20-ΔLCS)* and *let-7(n2853)* animals. Wild-type animals were sampled 24–50 h after release from L1 diapause; both mutant animals, 22–48 h. **A)** Metrics used to compare the sequential waves of *nhr-23* expression associated with each of the indicated genotypes. The amplitude of the waveforms was calculated using Metacycle. The rising slope refers to the rate at which transcript levels ascend from the trough detected before or during the preceding molt to the peak detected within the specified stage. **B-C)** Actograms depict the behavior and life stage of single animals observed at regular 1 h intervals, as described in Figure 2. In this case, high or low activity refers to continuous or sporadic pharyngeal pumping observed during the time sample. As previously described, Supplemental Table 1 has the active, lethargic, and w-w intervals of the cohorts in these studies. *****p*≤0.0001, ***p*≤0.01, Ordinary One-Way ANOVA with Bonferroni's correction for multiple comparisons.

Figure 7. Both derepression and overexpression of *nhr-23* trigger additional molts in reproductively mature animals. **A)** The percentage of wild-type, *nhr-23(aaa20-ΔLCS)*, and *wgls43[nhr-23++]* adults that appeared quiescent at regular timepoints 54–120 h after release from diapause and cultivation with food. Values represent the mean ± standard deviation from 2 independent trials, with cumulative sample sizes of 300 to 400 animals per timepoint. The values for the wild-type cohort were repeated in both graphs for ease of comparison. Significant peaks in the prevalence of quiescent animals are marked by asterisks. The corresponding values significantly exceeded the values for age-matched, wild-type animals (*p*<0.0001, chi-square test, χ^2 ranged from 39 to 223). **B)** Actograms depict the behavior and fate of quiescent adults singled at each timepoint marked by an arrow and then observed at regular 2 h intervals. Records within

each row correspond to a single worm. The behavior of a worm at a particular timepoint was scored as active, lethargic, or ecdysing as described in the Methods section. Aberrant molts and death were also recorded (see Methods). **C)** DIC micrographs show examples of adults that attempted to molt. Arrows point to former cuticles dislodged from the tail or head; arrowheads, to alae on both the passing and emergent cuticles. The letter “e” denotes fertilized embryos within the uterus. Scale bars = 10 μ m.

Figure 8. Most genes regulated by the molting clock are shared targets of both NHR-23 and *let-7s*. **A)** Levels of *fhn-1* transcripts detected by TaqMan RT-qPCR in regular time samples of mock-treated and *nhr-23(RNAi)* animals collected from the late L2 through young adulthood. The data were collected from distinct experiments: one set, which comprised two independent trials, covered the late L2 stage until the L3-to-L4 molt; and the other set, which also comprised two independent trials, covered the late L3 stage until the L4-to-adult molt. Rectangles beneath the x-axis signify lethargus; white rectangles signify intervals of physical activity. Values for *fhn-1* were first normalized to *ama-1* transcripts within each same time sample. The resulting values were further normalized to the mean of all wild-type time samples, represented by the dashed y-axis gridline. Dots and error bars represent the mean and range from two biological replicates. The table beneath the chart lists the amplitude and rising slope for the waveforms for the L4 stage, calculated as described earlier. **** $p \leq 0.0001$, * $p < 0.05$, Two-way ANOVA with Bonferroni’s correction for multiple comparisons. **B)** Same as A, except that the levels of *fhn-1* transcripts were measured in wild-type, *nhr-23(aaa20- Δ LCS)* and *let-7(n2853)* animals collected from late L2 through early adulthood. Additionally, the rectangles beneath the x-axis that depict the molts are shaded by genotype, as per the legend. **** $p \leq 0.0001$, Two-way ANOVA with Bonferroni’s correction for multiple comparisons. Wild-type animals were sampled 24–50 h after release from L1 diapause; both mutant animals, 22–48 h. **C-D)** Same as B and C, respectively, except the levels of *mlt-10* transcripts were measured using Taqman RT-qPCR. **** $p \leq 0.0001$, ** $p < 0.01$, Two-way ANOVA with Bonferroni’s correction for multiple comparisons. **E)** Venn diagram summarizes the classification of 67 clock-controlled genes (CCGs) as direct targets of NHR-23, *let-7s*, both or neither based on original bioinformatic approaches and meta-analyses of published ChIP-Seq, comparative microarray, and ALG-1-iCLIP data sets (Broughton *et al.*, 2016). Supplemental Table 4 provides the detailed information used to classify each gene of interest. Relevant scoring rubrics are fully described in the results and methods. The flowchart beneath the Venn diagram shows examples of prospective components of the molting timer and effectors of specific subroutines of the molting cycle that emerged as dual targets from the meta-analysis.

Figure 9. NHR-23 and *let-7s* govern the temporal expression profile of other key clock genes. **A)** CHIP-qPCR for NHR-23 enrichment at *lin-42* and *nhr-23* promoters in N2 (untagged NHR-23) or *nhr-23::3xflag* L3 stage larvae. Values represent the mean \pm sem of three independent trials, each of which included two technical replicates. Values for the amplicon of interest in each sample was first normalized to the respective input and then the average values for QK159 [*nhr-23::3xflag*] were normalized to the average value of the amplicon in N2 within each trial. **** $p \leq 0.0001$, ** $p \leq 0.01$; Two-way ANOVA with Bonferroni's correction for multiple comparisons. **B)** Levels of *lin-42* transcripts detected by TaqMan RT-qPCR in regular time samples of mock-treated and *nhr-23(RNAi)* animals collected from the late L2 through young adulthood, as described in Figure 8A. *** $p \leq 0.001$, * $p < 0.05$; Two-way ANOVA with Bonferroni's correction for multiple comparisons. **C)** Levels of *lin-42* transcripts detected by TaqMan RT-qPCR in regular time samples of wild-type, *nhr-23(aaa20-ΔLCS)* and *let-7(n2853)* animals collected from late L2 through early adulthood, as described in Figure 8B. **** $p \leq 0.0001$, *** $p \leq 0.001$; Two-way ANOVA with Bonferroni's correction for multiple comparisons. **D)** Schematic of the *nhr-23* genomic locus and the *nhr-23::gfp* fusion gene that was used to determine the extent to which NHR-23 regulates the expression of itself. The light teal rectangle depicts the region 2.5 kb upstream of the start codon of *nhr-23* Isoform A, the dark teal rectangles depict exons in *nhr-23* and the light grey rectangle represents the *nhr-23* 3' UTR. The last two and half exons of *nhr-23* were replaced by the coding sequence for *gfp*, as shown by a green rectangle. The 3' UTR of *nhr-23* was replaced by the *unc-54* 3' UTR, which is depicted in dark grey. The ROREs are shown as brown boxes. The dotted line represents the region complementary to the dsRNA used to knockdown endogenous *nhr-23*. While the dotted line is shown spanning the introns, the dsRNA only targets the exonic regions. **E)** Fluorescence and DIC micrographs show the signal from GFP detected in the lateral epidermis of mid-L4 stage animals that express the *nhr-23::gfp::unc-54* reporter. Micrographs on the left show a representative mock-treated animal and those on the right show a representative *nhr-23(RNAi)* animal. **F)** Related signal intensities in E were measured and are depicted. Therein, circles represent the average of three separate nuclei within the same worm, and error bars indicate the mean and standard deviation. Scale bar = 15 μ m and exposure time = 25 ms. **** $p \leq 0.0001$, *** $p \leq 0.001$; One-way ANOVA with Bonferroni's correction for multiple comparisons.

Figure 10. Reciprocal regulatory elements may be conserved in mammalian *ROR* and *let-7* genes. **A)** Each schematic depicts the 3 kb region upstream of selected homologs of *let-7*. Brown boxes show the multiple ROREs identified upstream of mature *let-7* (magenta) in the annotated

genomes of the indicated species and are numbered relative to the first nucleotide of the mature microRNA. Black arrows are aesthetic landmarks for probable, but not experimentally verified, transcriptional start sites. **B-C)** A transgenic strain containing the 3 kb fragment upstream of *M. musculus let-7* fused to the coding sequence for *gfp* was used to determine the extent to which *C. elegans nhr-23* regulates the expression of *M. musculus let-7*. Fluorescence and DIC micrographs show expression of the *M. musculus let-7a-1* promoter in the pharynx of mock-treated and *nhr-23(RNAi)* animals undergoing the L4-to-adult molt. Quantification of fluorescence intensity is shown in the graph in C. Each dot represents the mean of three ROIs measured within the pharynx and error bars depict the mean and standard deviation in measurements across the entire sample. The yellow asterisk represents the GFP signal in the neurons attributed to the *ttx-3::gfp* coinjection marker. Scale bar = 15 μ m; Exposure time = 200 milliseconds. ** $p \leq 0.01$; One-way ANOVA with Bonferroni's correction for multiple comparisons. **D)** Schematic shows the LCSs (gold), 3' UTR (blue), and stop codons (black) of six annotated homologs of *nhr-23/ROR*. Gradients and bold labels distinguish sites perfectly complementary to the seed of *let-7s*. The dotted boxes indicate regions tested in Figures E-H. Each 3' UTR was retrieved from the UCSC genome browser; verified by comparison with curated ESTs; and LCSs identified using RNAhybrid. Supplemental Table 2 provides additional information about the prospective duplexes between each of these LCSs and *let-7*. Accession numbers for the related ESTs and genomic sequences are included in the Key Resources Table. **E-H)** Representative images and quantitation of the ratiometric signal (tdTomato/GFP) associated with fragments of the 3' UTRs of *H. sapiens ROR β* and *M. musculus ROR α* and variants thereof that lack both LCSs. Each symbol represents the average value of three ROIs per worm. N indicates the total sample size from two independent experiments. Bars signify the mean \pm sd for the sample. **** $p \leq 0.0001$; Ordinary One-Way ANOVA with Bonferroni's correction for multiple comparisons. Representative images from multiple independent isolates are shown in Supplemental Figure 8.

METHOD DETAILS

Working with *C. elegans*

Unique strains of the model nematode *Caenorhabditis elegans* (*C. elegans*) generated by and applied to this research are described in the Key Resources Table. *C. elegans* were cultivated, preserved, observed, and transformed using standard methods (Stiernagle, 2006). Strains were cultivated at 25°C unless otherwise specified. Newly-hatched worms were developmentally synchronized by passage through starvation-induced, L1-stage diapause. Briefly, eggs were isolated by lysis of gravid hermaphrodites in sodium hypochlorite, suspended in M9 buffer supplemented with 5 µg/mL cholesterol, and incubated for 16 to 24 h with rotational aeration. Hatchlings were then plated on solid nematode growth medium (NGM) seeded with *Escherichia coli* (*E. coli*) strain OP50-1, HT115(DE3) or HB101, as indicated. One to two hundred hatchlings were routinely plated on 6 cm NGM plates; ten to fifteen thousand hatchlings, on 10 cm NGM plates seeded with 10-fold concentrated bacteria; twenty five thousand hatchlings on 15cm NGM plates seeded with 10-fold concentrated bacteria.

Bacterial-mediated RNA-interference (RNAi)

Relevant clones of *E. coli* HT115(DE3) were cultured, plated on solid NGM supplemented with 8 mM isopropyl β-D-1-thiogalactopyranoside (IPTG, Laguna Scientific), and incubated for 16 to 24 h at 25° C, allowing for IPTG-induced expression of dsRNAs. Worms used as controls were fed bacteria transformed with the empty vector pPD129.36 (a gift from Andy Fire, Stanford University). Alternatively, worms were fed bacteria transformed with a derivative of the same vector with an inserted *nhr-23* sequence. The latter clone matched I-3F11 (Source BioScience) but was isolated directly from the Ahringer *C. elegans* Genome RNAi library (Kamath and Ahringer, 2003). Because the insert corresponds to three constitutive exons at the 3' end of the *nhr-23*, the dsRNA made by this clone targets all 6 isoforms of *nhr-23* annotated in WS273.

To knockdown *nhr-23* during a specific larval stage and circumvent predominant arrest during a preceding molt, hatchlings were fed control bacteria for a certain interval as elaborated below, harvested, washed thrice in M9 buffer, and then divided into two samples. Next, larvae in the test sample were fed bacteria that expressed *nhr-23* dsRNAs; larvae in the control sample were once again fed bacteria that expressed only short, dsRNAs dissimilar from any worm gene (Kamath and Ahringer, 2003). Hatchlings destined to become test subjects in longitudinal studies of newly-emerged L2s, L3s, and L4s were initially fed control bacteria for 0, 6, and 14 h, respectively. To further attenuate the efficacy of RNAi, as needed to collect large time samples of

synchronized L2s, L3s and L4s for RT-qPCR experiments, hatchlings were initially fed control bacteria for 16 h and then split into test and control samples, as above. For L3s, L4s and young adults, as in Figure 3F and 3G, hatchlings were initially fed control bacteria for 24 h and then split into test and control samples, as above.

Longitudinal studies of molting-associated biorhythms

This section provides additional information about the collection, analysis, and presentation of data in Figure 2, Figure 4, Figure 6 and Supplemental Table 1. Cohorts of larvae molting to the stage of interest were isolated from synchronized populations; singled in 12-well NGM-RNAi plates; and observed for 5 to 60 s at regular 1 h intervals, using a Zeiss M²BioDiscovery microscope. L4s and older worms were observed at 300-fold magnification; L3s and younger worms, at 600-fold magnification. At each time sample, each subject was classified as active or lethargic based on the observation of defined target behaviors. Molting-defective (Mlt) and ruptured through the vulva (Rup) worms were identified by conventional criteria (Reinhart *et al.*, 2000).

The longitudinal studies represented in Figure 2 included videotaping the head of the worm using a Sony HDR-XR500V or Nikon D500 camera attached to the microscope. Later, the number of pharyngeal contractions (pumps) in a 15 s recorded interval was counted while the film was viewed at 4-fold reduced speed using iMovie version 10.11.2. Pumping rates (Hz) determined by three independent counts of selected films fell within 95% of the mean, validating this method. High, medium and low levels of activity were then graded *post-hoc* on a one-way standard scale defined by the standard deviations and mean pumping rate of all age-matched, wild-type time samples. As an example, wild-type young adults pumped at 3.9 ± 1.1 Hz (mean \pm sd). The activity levels of nearly all worms that reawakened from lethargi associated with the L4/A molt were therefore graded as high, medium, or low if the worm pumped at greater than, or equal to, 2.8 Hz; between 2.8 and 1.7 Hz; or less than 1.7 Hz, respectively. A reasonable exception to this system was made if sinusoidal locomotion was obvious but no pharyngeal pumps were captured on video. In this scenario, the worm was scored as active at a low level. This exception applied to only 8 out of 56 time samples of *nhr-23* single knockdowns and 14 out of 84 time samples of *nhr-23(RNAi) let-7(n2853)* double mutants. Among animals that reawakened from lethargi associated with the L3/L4 molt, the same exception applied to 20 out of 120 time samples of *nhr-23* single knockdowns and 20 out of 180 time samples of *nhr-23(RNAi) let-7(n2853)* double mutants. The longitudinal studies represented in Figure 3 and Figure 6 did not involve video-recordings. Instead, high versus low levels of activity were assigned based on the direct observation of

continuous versus sporadic pharyngeal pumps during the time sample.

Detection and characterization of supernumerary lethargi and molts

To score quiescence among populations of young adults, synchronized hatchlings were released from starvation-induced diapause by plating on 10-fold concentrated lawns of *E. coli* OP50-1 at a density of 200-400 worms per 10 cm NGM plate. For each strain of interest, six distinct clutches were plated at 12 h intervals, facilitating the later evaluation of time samples covering a 72-h interval. As described, worms were observed by light microscopy and scored as quiescent or active at regular 3 h intervals, 54 to 120 h post-release from diapause. For related longitudinal studies, quiescent adults were selected and singled in 12-well NGM plates seeded with thin lawns of bacteria. Each cohort of animals was then either observed at regular 2 h intervals (Figure 7), or video-recorded for 15-30 s, at regular 2 h intervals, with a Nikon D500 camera. All the previously described scoring rubrics were applied. In addition, ecdysis was recognized by the execution of one or more of the following idiosyncratic movements: rotation on the long axis (flipping), bilateral contraction and relaxation on the long axis, and elevation plus semi-circular rotation of the head. Aberrant molts were scored based on the observation of puckered sections of cuticle along the body, or the adherence of partly shed cuticle fragments to the body. If a particular animal had passed through lethargus, then the following behaviors were also considered evidence of an aberrant molt: pharyngeal spasms, incomplete pumps wherein the grinder failed to close, and incomplete flips that resulted in twists or kinks along the body. Detection of a shed cuticle, or parts thereof, on the culture plate was recorded separately. The latter categories were not mutually exclusive. An inactive or decrepit worm unresponsive to adverse stimuli was pronounced dead. Absence of a supernumerary molt was inferred if the animal was active and superficially normal at the endpoint.

Construction of fusion genes and transgenic strains

The sequences of all oligonucleotides used in this study are specified in Supplemental Table 5. All DNA nucleotides were synthesized by and purchased from Integrated DNA Technologies (IDT). The bicistronic reporters used to detect regulatory elements within 3' UTRs were constructed by Gibson Assembly (NEB) and standard methods. Phusion High-Fidelity DNA Polymerase (NEB) was used to amplify DNA molecules. The resulting plasmids contained the pBR322 backbone of Fire Lab vectors; the *dpy-7* promoter, which corresponds to nucleotides 7,537,914-7,538,219 of *C. elegans* Chr. X (NC_003284); the synthetic intron embedded in primer HM01; the coding sequence for *tandem (td) tomato*, which was isolated from Addgene plasmid

#30530 (a gift from Gerhart Ryffel); one of the test 3' UTRs described below; and an *SL2::gfp::unc-54* 3' UTR cassette. The gene-specific 3' UTRs from *C. elegans* comprised nucleotides amplified from Chr. I (NC_003279) as follows: *nhr-23*, 7,220,953-7,221,820; *unc-54*, 14,855,909-14,856,180; *lin-41*, 9,334,850-9,335,964. Deletions within the *nhr-23* 3' UTR reporter (cloned in pHR017) were created using a Q5 Site-Directed Mutagenesis Kit (NEB) and verified by Sanger Sequencing (Genewiz Inc.). Additionally, a 565-bp fragment of the 3' UTR of *H. sapiens* *RORβ* (chr9:74689171-74689705; GRCh38/hg38), a 256-bp fragment of the 3' UTR of *M. musculus* *RORα* (chr9:69380941-69381196 GRCm39/mm39), as well as derivatives lacking both LCSs, were ordered as gBlocks Gene Fragments from IDT and fused to *tdTomato*. To generate distinct extrachromosomal arrays harboring each bicistronic reporter, mixtures of the corresponding plasmid (1 ng/μl), the co-transformation marker *ttx-3::gfp* (40 ng/μl), and filler DNA pRS316 (59 ng/μl) were microinjected into the gonads of wild-type hermaphrodites. Transgenic progeny and unique descendent strains were isolated by standard methods.

A transcriptional reporter for *M. musculus* *Mirlet7a-1* was generated by using fusion PCR to combine the 3000-bp region upstream of the mature *let-7-a-1* miRNA (chr13:48538273-48541272; GRCm38/mm10) with *gfp* (pPD95.75). The resulting PCR product was first cloned into the topo vector pCR-Blunt-II-Topo (ThermoFisher Scientific) to generate pRA46. The strain ARF431 was generated by co-injecting pRA46 (1 ng/μl), *ttx-3::gfp* (40 ng/μl), and pRS316 (59 ng/μl) into wild-type hermaphrodites.

The strain ARF422 was made by first crossing *wgls43* hermaphrodites with *let-7(mg279)* *mir-84(tm1304)* males. After singling F2's from the crosses, we screened for *wgls43* homozygotes among the F3 generation. Only the strains that were homozygous for *wgls43* were selected and screened for *let-7(mg279)*; *mir-84(tm1304)* homozygotes. The transgene *wgls43* was obtained from OP43 and *let-7(mg279)*; *mir-84(tm1304)* was obtained from ARF249.

The strain ARF432 was generated by injecting construct 4271 (Kostrouchova et al, 1998) at a concentration of 5 ng/μl, together with the co-injection marker *ttx-3::gfp* (40 ng/ μg/μl), and pRS316 (45 ng/μl) into wild-type hermaphrodites. Transgenic lines were isolated by standard methods.

CRISPR/Cas9-mediated editing of *C. elegans* genes

The CRISPR/Cas9 system was used essentially as described (Paix et al., 2015) to delete the endogenous LCS from the 3' UTR of *nhr-23*, generating the allele *nhr-23(aaa20)*. Briefly, wild-type hermaphrodites were microinjected with a mixture containing the following: *nhr-23* crRNA (400ng/μL), tracrRNA (1μg/μL), *dpy-10* crRNA (160 ng/μL, GE Dharmacon), *dpy-10* ssODN

(13.75 ng/μL, IDT), and CAS9 protein (500 ng/μL, PNA Bio) in HEPES buffer pH 7.5 (Sigma-Aldrich) supplemented with 0.025 μM KCL (Sigma-Aldrich). Injected hermaphrodites (P0s) were singled and screened for Dumpy (Dpy) or Roller (Rol) offspring (F1s), both phenotypes associated with mutations in *dpy-10*. One hundred F1s were singled from a selected P0. Genotyping the F1s and their descendants (F2s) identified two strains homozygous for identical chromosomal deletions of precisely the 21 nucleotides comprising the LCS. One *nhr-23(aaa20-ΔLCS)* strain was backcrossed to N2 thrice prior to phenotypic analysis. No edits in the *dpy-10* gene were found in the backcrossed strain (ARF414).

To construct *xk22*, wild-type hermaphrodites were injected with *nhr-23* crRNA oHG202 (40μM, IDT Alt-R CRISPR crRNA), *nhr-23::3xflag* repair template (120ng/μL, IDT Ultramer DNA oligo), *dpy-10* crRNA (5.6 μM, IDT Alt-R CRISPR crRNA), *dpy-10* repair template (12 ng/μL, IDT Ultramer DNA oligo), tracrRNA (40 μM, IDT Alt-R CRISPR-Cas9 tracrRNA) and Cas9 (15.5 μM, stock at 40 μM in 20 mM HEPES-KOH pH 7.5, 150 mM KCl, 10% glycerol, 1 mM DTT from Berkeley QB3 MacroLab). All reagents were diluted in IDT duplex buffer. The crRNA and repair template both target the C-terminus of NHR-23, which is common to all predicted isoforms. Injected hermaphrodites were singled and F1 offspring were screened for the same phenotypes described above. One hundred and twenty F1s were singled from plates that had a high penetrance of Dpy and Rol phenotypes. Genotyping the F1s identified 3 lines that had *3xflag* inserted precisely before the stop codon of the *nhr-23* gene. One *nhr-23(xk22)* line was backcrossed to N2 five times to generate QK159. No edits in the *dpy-10* gene were found in QK159.

To construct the *let-7(scRORE1,2)* and *let-7(scRORE1,3)* strains, the ROREs were serially scrambled. *let-7(scRORE1)* was first made by injecting wild type hermaphrodites with crRNA oHG287(40μM, IDT Alt-R CRISPR crRNA), repair template oHG293(120ng/μL, IDT Ultramer DNA oligo), and other components as described above. Injected hermaphrodites were singled and F1 offspring were screened for the same phenotypes described above. Genotyping the F1s identified several lines that had RORE1 scrambled in the *let-7* promoter. The *dpy-10* mutation was outcrossed from 1 line. To construct *let-7(scRORE1,2)*, this line was then injected with crRNA oHG282(40μM, IDT Alt-R CRISPR crRNA), repair template oHG367(120ng/μL, IDT Ultramer DNA oligo), and other components as described above. Injected hermaphrodites were singled and F1 offspring were screened for the same phenotypes described above. Genotyping the F1s identified 3 lines that had RORE1 and RORE2 scrambled in the *let-7* promoter. These lines were backcrossed to N2 three times to generate QK201, Q202 and QK203. To construct *let-7(scRORE1,3)*, *let-7(scRORE1)* was injected with crRNA oHG278(40μM, IDT Alt-R CRISPR

crRNA), repair template oHG291(120ng/μL, IDT Ultramer DNA oligo), and other components as described above. Injected hermaphrodites were singled and F1 offspring were screened for the same phenotypes described above. Genotyping the F1s identified 2 lines that had RORE1 and RORE3 scrambled in the *let-7* promoter. These lines were backcrossed to N2 three times to generate QK198 and QK199.

Quantitative fluorescence microscopy

C. elegans were anesthetized with 2.5% NaN₃ (v/v) in M9 buffer, mounted on 2% agarose pads, and observed using a Zeiss Axioplan compound microscope with an attached Hamamatsu Orca ER CCD camera. The image acquisition and analysis software package Volocity 6.3 (Perkin Elmer) was used to control the microscope and digital camera and also to measure average fluorescence intensities within selected regions of interest (ROIs). In particular experiments, transgenic animals were staged partly by DIC microscopy and imaged during the L3/L4 or L4/Adult molts. Molting animals were identified by occlusion of the buccal cavity (Monsalve *et al.*, 2011). Stereotypical rearrangements of vulva precursor cells (VPCs) demarcated early versus late sub-stages of the L3-to-L4 molt. The presence of a lumen in the incipient vulva demarcated early versus late sub-stages of the L4/Adult molt (Gupta *et al.*, 2012; Van Buskirk and Sternberg, 2007).

To measure GFP signals associated with the both the *C. elegans let-7p::nls-gfp* transcriptional reporter (Kai *et al.*, 2013) and the *M. musculus let-7p::gfp* reporter, worms were imaged at 400X total magnification. For the *C. elegans let-7* transcriptional reporter, both DIC and fluorescence images of the lateral epidermis were acquired – the latter with an exposure time of 25 ms. Three nuclei in hyp7 and three in the seam were traced from the DIC image of each worm. The average fluorescence intensity within each nucleus was then measured and corrected for background signal. The average values for both hyp7 and seam nuclei (per worm) were used in further statistical analysis. For the *M. musculus let-7* transcriptional reporter, the pharynx was imaged in both the DIC and fluorescence channels. An exposure time of 200 ms was used to capture the GFP signal. Three ROIs in the pharynx were traced from the DIC image of each worm. As stated above, the average fluorescence intensity within each traced ROI was measured, corrected for background signal and used in further statistical analysis.

Signals associated with tdTomato and GFP expressed from bicistronic reporters for regulatory elements within 3' UTRs were measured using similar approaches. In this case, three distinct ROIs with areas of 40–70 μm² were manually selected per worm; each ROI included approximately equal areas of the nucleus and cytoplasm. In addition, multiple images of tdTomato

and GFP were automatically captured over a range of exposure times. The average fluorescence intensity of each ROI was measured and plotted versus the exposure time. Values within the linear range of the assay were then used to determine the ratiometric signal (tdTomato/GFP) for each ROI. The average ratiometric value of all three ROIs per worm was used for subsequent statistical analysis. Notably, the morphology of the vulva was abnormal in a subset ($\leq 10\%$) of animals that expressed any bicistronic reporter. Because the phenotype precluded staging by the abovementioned criteria, this subset of animals was excluded from the analysis.

Measurement and analysis of the GFP signal from the NHR-23::GFP reporter was done exactly as described for the *C. elegans let-7::nls-gfp* reporter above, except that an exposure time of 200 ms was used to capture the fluorescence signal.

Chromatin immunoprecipitation coupled with quantitative PCR (ChIP-qPCR)

Animals grown at 25°C were collected as a ~500 μ L packed pellet in M9. The animals were nutated for 30min at room temperature in 12mL of 2.6% (v/v) formaldehyde in autoclaved DI water for live crosslinking. To quench the reaction, 600 μ L of 2.5 M glycine was added and the worms incubated on the nutator for another 5 min. The samples were then washed thrice in water and flash-frozen. Frozen pellets were ground twice, for 1 min each, in a Retsch MM400 CryoMill at 30 Hz in liquid nitrogen-chilled stainless steel cryomill chambers, producing a frozen powder of partially lysed worms. The powder was resuspended and further lysed in 2 mL of RIPA buffer (1x PBS, 1% (v/v) NP40, 0.5% sodium deoxycholate, and 0.1% SDS), supplemented with the HALT Protease and Phosphatase Inhibitor Cocktail (ThermoFisher Scientific), for 10 min at 4° C. To shear the chromatin, samples were sonicated in a Bioruptor Pico (Diagenode) for 3 min (30 s ON/30 s OFF cycles), three times, at 4° C. A 20 μ L aliquot of the sample was treated with Proteinase K for 10 min and then cleaned by phenol chloroform extraction, as described below. The concentration of the aliquot was determined using a Qubit Fluorometer 3.0 (Invitrogen). Based on the initial concentration of the aliquot, the chromatin sample was diluted to 20-30 ng/ μ L. To check the extent of shearing, the same aliquot was run on an agarose gel. The sample was processed and analyzed further provided the DNA smear centered at 200 bp. Of the total amount of chromatin that remained, 10% was used as the input sample – i.e. stored at 4° C – and 90% was subject to immunoprecipitation. Every 10 μ g of chromatin was incubated with 2 μ g of mouse M2 anti-FLAG monoclonal antibodies (Sigma-Aldrich) overnight at 4° C on a nutator. Next, samples were incubated with 1.5 mg of affinity-purified sheep anti-mouse IgG antibodies covalently attached to superparamagnetic Dynabeads M-280 (Invitrogen) for 2 h, at 4° C.

Thereafter, complexes bound to the beads were separated thrice from the supernatant and washed in 800 μ L LiCl buffer (100 mM Tris-HCL pH 7.5, 500 mM LiCl, 1% (v/v) NP40, and 1% sodium deoxycholate). The resulting immunoprecipitates were de-crosslinked by incubation with 80 μ g of Proteinase K in 400 μ L of worm lysis buffer (100 mM Tris-HCL pH 7.5, 100 mM NaCl, 50 mM EDTA, and 1% SDS) at 65° C for 4 h—the input samples also underwent the same treatment in parallel. Residual proteins were removed from both IP and Input samples by phenol-chloroform extraction. Briefly, 400 μ L of phenol-chloroform-isoamyl alcohol pH 8.0 (Sigma-Aldrich) was added to each sample. The sample was vortexed vigorously and centrifuged at 15,000 x g for 5 min at 4° C. The top layer was transferred to a new tube and DNA was precipitated by incubating with 1 mL of 0.3 M ammonium acetate (Sigma-Aldrich) in ethanol for 1 h at 30° C. The resulting DNA pellet was washed twice in 100% ethanol and re-suspended in Tris-EDTA, pH 8.0. Prior to use as a template for qPCR, the entire DNA sample was treated with RNase A for 1 h at 37° C.

Quantitative PCR for promoter regions of interest was performed with Absolute Blue SYBR Green (Thermo Scientific) using a CFX96 Real Time System Thermocycler (BioRad) as per the manufacturers' instructions, with custom primers described in Supplementary Table 5. The Ct value for each IP sample was first normalized to the Ct value for the respective input sample. The log 2 transformed fold-change values for samples derived from QK159[*nhr-23::3xflag*] were then normalized to the respective N2 sample. Three biological replicates, each with two technical replicates, were completed for each amplicon of interest, as specified in corresponding figure legends. Pairwise statistical comparisons of the fold enrichment of a given amplicon in samples from QK159[*nhr-23::3xflag*] versus N2 were made by Two-way ANOVA with Bonferroni's correction for multiple comparisons.

For L3 ChIP-qPCR samples, hypochlorite prepped embryos were directly plated on HB101 and animals were collected after 29 hours at 25°C as a semisynchronous population. For L4 ChIP-qPCR samples in Figure 3C and Supplementary Figure 1D, hypochlorite prepped embryos were nutated in M9 buffer for 24 hours. L1 diapause worms were plated on HB101 and collected after 32 hours at 25°C as a synchronous population of mid-L4 worms. For L4 ChIP-qPCR samples in Figure 4B, hypochlorite prepped embryos were directly plated on HB101 and collected after 35 hours at 25°C as a semi-synchronous population.

Isolation of RNA

RNA was extracted from developmentally synchronized *C. elegans* as described (McCulloch and Rougvie, 2014). Samples of ~1,500 worms were collected at regular 2 h intervals. Because the strains seemed to develop at different rates, light microscopy was used to count the

fraction of pumping (active) versus non-pumping (lethargic) animals in each sample prior to collection (n = 50-100). Lethargic phases were empirically identified *post hoc* by troughs in the proportion of pumping animals. Related graphs in Figure 6A, Figure 8B, Figure 8C and Supplemental Figure 4 include 14 time samples encompassing three lethargic and two active phases per strain. Pellets containing worms (~100 μ L) were re-suspended in 4 volumes of TRIzol (ThermoFisher Scientific) and 1 volume of glass beads 400-625 μ m in diameter (Sigma). The suspensions were vortexed, flash frozen, and thawed thrice. Samples were then mixed with 0.17 volumes of 24:1 chloroform: isoamyl alcohol (OmniPur) and centrifuged. The aqueous layer was collected, mixed with an equal volume of 5:1 acid phenol: chloroform (ThermoFisher Scientific), and centrifuged again. After collection of the top layer, RNA was extracted by precipitation with ice-cold isopropanol (Sigma) and GlycoBlue (ThermoFisher Scientific). The concentration of RNA in each time sample was measured using a NanoDrop 2000 (ThermoFisher Scientific). Thereafter, 5 μ g of total RNA per sample was treated with 2U of TURBO DNase (ThermoFisher Scientific) for 1 h.

Quantitative RT-PCR

The sequences of gene-specific RT primers and identifiers for TaqMan assays used in this research are provided in Supplemental Table 5. To quantify levels of primary *let-7* and *ama-1* transcripts in the abovementioned extracts, we processed 50ng of RNA using a High-Capacity cDNA Reverse Transcription Kit (ThermoFisher Scientific). Reaction mixtures of 15 μ L included random primers, dNTPs, RNaseOUT, and reverse transcriptase, per the manufacturer's guidelines. To quantify levels of mature *let-7* and the U18 small nucleolar (sno) RNA, we processed RNA with the same kit but used gene-specific rather than random primers. Three volumes of nuclease-free water were added to completed RT reactions. Next, we set-up TaqMan assays (ThermoFisher Scientific) in 96-well plates, in triplicate. Per the manufacturer's instructions, each reaction included TaqMan Universal PCR Master Mix, no AmpErase UNG, gene-specific primers, and 1.3 μ L of the preceding RT product in a volume of 20 μ L. Reactions ran on a Stratagene MX3000P (Agilent Genomics). To measure levels of protein-coding transcripts, 1 μ g of RNA was reverse transcribed using the enzyme Transcriptor (Roche). Each reaction mixture (20 μ L) also included hexadeoxynucleotide primers (Promega), dNTPs and RNasin (Promega). Four volumes of nuclease-free water were added to completed RT reactions. TaqMan assays were performed as described using 2 μ L of the RT product as template in a volume of 10 μ L.

The amount of template used in each TaqMan assay gave Ct values in the linear range of

21 to 36. In nearly all cases, technical replicates gave Ct values within 95% of the mean and the mean Ct value was used in subsequent analyses. Separate TaqMan reactions using templates made in the absence of reverse transcriptase produced no detectable PCR products, confirming the amplification of RNA rather than genomic DNA. As described, the levels of transcripts of interest were normalized to the levels of *ama-1* mRNAs or U18 snoRNAs within each sample, which were quantified in parallel TaqMan assays. For studies of gene expression over several developmental stages, the normalized values for each time sample were further standardized to the mean of all time samples derived from mock-treated or wild-type animals.

RNA extraction and RT-qPCR for *let-7(scRORE)* mutants

Hypochlorite prepped embryos were synchronized and plated on HB101. Development was tracked by monitoring pharyngeal pumping as described before. Samples of ~8000 worms were collected every 2 hours, starting at 18 hours after plating at 25°C in TRIzol (ThermoFisher Scientific). Following 3 freeze-thaw cycles, 1-bromo-3-chloropropane was added and the RNA in the resulting aqueous phase was precipitated by incubating with isopropanol for 2 hours at -30°C. Samples were then spun at 21,000g for 30 minutes at 4°C to pellet the RNA. The pellet was washed with 75% ethanol thrice and then resuspended in water.

cDNA synthesis for primary *let-7* was done using SuperScript III Reverse Transcriptase (Invitrogen). 250ng of RNA was used for cDNA synthesis in the Eppendorf Mastercycler Pro S6325. Quantitative PCR for *pri-let-7* and *eft-2* were performed with Absolute Blue SYBR Green (Thermo Scientific) on the CFX63 Real Time System Thermocyclers (Biorad) using custom primers as listed in Supplemental Table 5. The cycle numbers for *pri-let-7* were normalized to respective cycle numbers for *eft-2*. 2 biological replicates with 2 technical replicates were done. The values were all normalized to the average of the 4 readings for the N2 sample. Two-tailed Student's t-test was done to evaluate p-values. RT-qPCR for *mlt-10* was used to validate the age matched synchronous populations across the genotypes.

TaqMan synthesis for mature *let-7* was done using probes synthesized by Applied Biosystems. 100ng of RNA was used for TaqMan Synthesis using High capacity cDNA Reverse Transcription Kit (ThermoFisher Scientific). Quantitative PCR for *let-7* and *U18* were performed using TaqMan Universal Master Mix, No AmpErase UNG (ThermoFisher Scientific) on the CFX63 Real Time System Thermocyclers (Biorad). The cycle numbers for *let-7* were normalized to respective cycle numbers for U18. 2 biological replicates with 2 technical replicates were done. The values were all normalized to the average of the 4 readings for the N2 sample. Two-tailed Student's t-test was done to evaluate p-values.

Counting seam cell nuclei

Hypochlorite prepped embryos were nutated and hatched over 24 hours in M9 buffer. L1 diapause worms were plated on HB101 at 25°C. Animals were scored between 40 and 44 hours after plating. Worms were immobilized in 50 mg/mL levamisole on a 2% agarose pad on a slide. The number of Pscm::GFP expressing cells in each worm were counted under the Zeiss Axio Zoom V16 Fluorescence Stereo Scope.

MetaCycle analysis of gene expression curves

The MetaCycle 1.2.0 package was used to calculate the amplitude and phase of expression of the genes listed in Figure 6, Figure 8, Figure 9, Supplemental Figure 4, Supplemental Figure 6, Supplemental Figure 7 and Supplemental Table 3. The normalized levels of transcripts of each gene, derived from the analysis described above were provided to MetaCycle. For each gene, the expression curves recorded from the L2-L3 molt until the L3-L4 molt, were considered as corresponding to the L3 stage. Similarly, expression curves recorded from the L3-L4 molt until the L4-A molt were considered as corresponding to the L4 stage. Gene expression curves recorded in the L3 stage were analyzed separately from those recorded during the L4 stage. Additionally, expected periods of 8 h and 10 h were used for analysis of the L3 and L4 stage data, respectively.

Identification of conserved *cis*-regulatory elements in homologous genes

DNA sequences corresponding to the upstream regulatory region, first intron and 3' UTR for each nematode gene of interest were retrieved from WormBase (WS) v.264 and saved as SnapGene v.4 (GSL Biotech) files. The upstream sequences extracted from WS included all nucleotides between the transcriptional start site of the gene of interest and the nearest protein-coding gene. Particular sequences were extended or shortened based on gene models, ESTs and transcriptional start sites archived in WS264. If the gene of interest lacked an annotated 3'UTR, then we initially retrieved 1 kb of sequence downstream of the stop codon. Particular 3' UTR sequences were revised based on ESTs and poly-AAA sites that are archived in WS264 but not yet incorporated in current gene models.

Both the upstream regulatory regions of vertebrate homologs of *let-7* and the 3' UTRs of vertebrate homologs of *nhr-23/RORs* were retrieved from the UCSC genome browser. Three human genes, two mouse genes, and six zebrafish genes encode mature miRNAs identical in sequence to *C. elegans let-7*. We extracted 3 kb of sequence upstream of each *let-7* homolog,

except in the case of *H. sapiens let-7a-3*, wherein the promoter has been experimentally delimited to 1 kb of upstream sequence (Wang et al., 2012). For a given gene, the longest 3' UTR was selected if multiple 3' UTRs existed. The 3' UTR sequences were individually and systematically validated by comparison with EST; only those genes with annotated 3' UTRs supported by ESTs were included in further analyses.

Finding clock-controlled genes regulated by NHR-23 and *let-7s*

Genes were determined to be “involved in molting” based on the literature. For example, if mutations in a particular gene caused a molting defective phenotype, the gene was considered to be involved in molting (Frandsen et al., 2005). Similarly, if inactivation of the gene had an effect on lethargus, the gene was also considered to be involved in the molting cycle. Genes were annotated as “oscillatory” based on published RNA-Seq studies (Hendriks et al., 2014; Kim et al., 2013); therein, genes whose expression at 8-10 h intervals was significantly correlated ($P < 0.05$) were considered to be cycling in expression.

To identify ROR response elements that might function as transcriptional enhancers of miRNAs or protein-coding genes of interest, we searched the upstream regulatory sequences and/or first introns for instances of the consensus response element 5'-(A/G)GGTCA-3' on both the coding and anti-coding strands of DNA. Figures 1A, 8A and Supplemental Figure 1A depict the results of these computational searches. To accurately calculate the probability of an RORE occurring by chance, we first used the k-mer counting software program DSK (Rizk G. et al, 2013) to find that the reference genome of *C. elegans*, which comprises 100.2 mega bases, includes 41,203 distinct instances of the consensus RORE. For non-nematodes, the expected frequency was the chance of either six-nucleotide sequence appearing in a longer oligonucleotide; this frequency is approximately one per 1 kb.

Regions of *C. elegans* chromosomal DNA occupied by NHR-23 *in vivo* were identified on the modEncode *C. elegans* Genome Browser (v. 2.48). The two relevant datasets archived therein were ChIP-Seq of strain OP43 cultivated at 20° C and harvested during the L2 or L3 stage. Most genomic regions where NHR-23 was significantly enriched were detected in the dataset collected from L3 stage larvae, however, we do not discriminate between the two stages in our analysis. The upstream regulatory sequences and/or first intron for each gene of interest were viewed in this browser. Regions of significant enrichment (“peaks”) were identified by Z-scores ≥ 2 (Celniker et al., 2009). Sequences extracted and aligned with the upstream regulatory regions and/or first intron as above, adjusting for differences in the related chromosomal coordinates between WS220 and WS264.

Evidence of direct or indirect regulation of transcript levels by NHR-23 – i.e expression of the gene was at least 1.2-fold reduced in *nhr-23(RNAi)* versus control larvae – was either detected by Affymetrix microarrays (Kouns *et al.*, 2011), or shown in prior publications (*lin-42a/b*, *nas-36*).

Targets of NHR-23 followed 2 out of the 3 following criteria: 1) The upstream regulatory region and/or first intron contained Chip-Seq NHR-23 peaks (Celniker *et al.*, 2009); 2) the same region contained more ROREs than predicted by chance alone; and 3) Expression was 1.2-fold lower in *nhr-23* knockdowns than mock-treated larvae.

The software RNAhybrid (Rehmsmeier *et al.*, 2004) was used to detect sequences partially complementary to the 21-nt. mature *let-7* in the 3' UTRs of annotated homologs of *nhr-23* in the genomes of *H. sapiens*, *M. musculus*, *D. rerio* and *C. briggsae*. Mature *C. elegans let-7*, which is identical to human *let-7a*, was used as the query sequence. No more than 1 mismatched nucleotide within the *let-7* seed sequence was tolerated for the prediction of LCSs in this report.

Targets of *let-7* fulfilled both of the following criteria: 1) LCSs, with up to one mismatch in the seed region, were detected in the 3' UTR more often than, or equal to, the number predicted by chance alone (Rehmsmeier *et al.*, 2004); and 2) ALG-1 co-IP the 3' UTR, on the coding strand of the gene by iCLIP-Seq (Broughton *et al.*, 2016).

Quantification and statistical analyses

The software package Volocity 6.3 (Perkin Elmer) was used to both acquire fluorescence micrographs and measure the signal intensity of selected ROIs. The software package GraphPad Prism v6.0h was used for all statistical tests except for those done on data from ChIP-qPCR experiments. Statistical tests for the ChIP-qPCR experiments were done using R Studio version 1.1.463 and R version 3.5.2. The software package MetaCycle 1.2.0 was used to calculate the amplitude and phase of expression for the cycling genes. Samples sizes for all experiments, statistical analyses, and outcomes thereof are included within each figure and its legend.

SUPPLEMENTAL MATERIAL LEGENDS

Supplemental Figure 1. NHR-23 interacts with ROREs upstream of *let-7* and its paralogs.

A-B) Three analogous schematics show the alignment of ROREs identified in verified or predicted upstream regulatory regions (gray shading) of *mir-48*, *mir-241* and *mir-84* with NHR-23 occupancy of the respective chromosomal regions (brown shading) as captured in mid-L3s by ChIP-Seq by the modENCODE consortium (Celniker *et al.*, 2009). Beige shading with a teal liner indicates regions of significant enrichment. Magenta labels mature microRNA; dark gray labels upstream DNA. Coordinates refer to *C. elegans* Chr. V (NC_003283.11) and Chr. X (NC_003284.9) as indicated. Dotted lines mark the location of qPCR primers used in C and D. **C)** Detection and quantitation of the indicated 100 bp fragments upstream of *mir-48*, *mir-241* and *mir-84* by ChIP-qPCR in L3 stage larvae, as described in Figure 3B. Error bars represent the mean \pm sem from six distinct samples: two technical replicates per three biological replicates. **** $p \leq 0.0001$, Two-way ANOVA with Bonferroni's correction for multiple comparisons. For a particular gene-specific amplicon, the value for each QK159 or N2 sample was first normalized to the respective input. The average fold-enrichment in QK159 samples was then normalized to the average fold-enrichment in N2 samples. **D)** Same as C, except L4 stage larvae were used in the analysis. **** $p \leq 0.0001$, *** $p \leq 0.001$, ** $p \leq 0.01$, Two-way ANOVA with Bonferroni's correction for multiple comparisons. **E)** Second biological replicate of ChIP-qPCR for NHR-23 enrichment at the *let-7* promoter in *nhr-23::3xflag*; *let-7(xk41-RORE-1,2)* and *nhr-23::3xflag*; *let-7(xk39-RORE-1,3)* L4 animals. The bar graph represents the mean of the 2 technical replicates. The error bars represent mean \pm standard deviation. Values for the amplicon of interest was first normalized to the respective input. The average fold-enrichment for each genotype was then normalized to the average fold-enrichment in N2 samples. n.s. not significant, * $p < 0.05$; Two tailed Student's t-test

Supplemental Figure 2. NHR-23 regulates the expression of the *let-7* family during the L3 stage.

A-B) Representative pairs of fluorescence images and respective overlays (GFP/DIC) show nuclear-localized GFP expressed from the promoter of *let-7* in the lateral epidermis. Arrows point to nuclei in hyp7 syncytia; arrowheads, seam nuclei. Scale bars = 20 μ m. Adjacent scatter plots show aggregated values from two independent trials. Bars signify the mean and sd. **** $p \leq 0.0001$, ** $p \leq 0.01$, Ordinary One-Way ANOVA with Bonferroni's correction for multiple comparisons. **C)** Levels of primary *mir-48*, primary *mir-241*, or primary *mir-84*, determined by TaqMan qRT-PCR in *nhr-23(RNAi)* and mock-treated larvae developing from the late L2 stage until the L3-to-L4 molt. As described for Figure 3D, each value was normalized to *ama-1* transcript levels in the same

sample. Values were then normalized to the average of all control time samples. Symbols represent the mean and range from two biological replicates. The x-axis indicates time elapsed (h) on food. The underlying bar depicts developmental stages; gray boxes therein signify observed intervals of behavioral quiescence. The times of initial exposure to *nhr-23* siRNAs and the appearance of molting-defective *nhr-23(RNAi)* larvae are indicated. ** $p \leq 0.01$; Two-way ANOVA with Bonferroni's correction for multiple comparisons. **D)** Same as above, for levels of mature *mir-48*, mature *mir-241*, or mature *mir-84*, each normalized to U18. **** $p \leq 0.0001$, * $p < 0.05$; Two-way ANOVA with Bonferroni's correction for multiple comparisons. N2 was used for this analysis.

Supplemental Figure 3. Molecular mechanisms relevant to the design and performance of bicistronic reporters for *cis*-regulatory elements in 3' UTRs of interest.

Schematic depicts the following series of anticipated events: 1) transcription of the bicistronic reporter under control of the *dpy-7* promoter; 2) trans-splicing of the resulting pre-mRNA, which generates distinct *tdTomato::test 3' UTR* and *gfp::unc54 3' UTR* mRNAs; and 3) standalone translation of the latter messages into fluorescent proteins.

Supplemental Figure 4. Both the functional LCS in the 3' UTR of *nhr-23* and *let-7*-family miRNAs limit the abundance of *nhr-23* transcripts across larval development. **A)** An independent replicate of the experiment described in Figure 6A. Briefly, the values represent normalized levels of *nhr-23* transcripts detected in regular 2 h time samples of wild-type, *nhr-23(aaa20-ΔLCS)* and *let-7(n2853)* larvae and newly emerged adults. As previously described, wild-type samples were shifted to the left by 2 h to account for the apparent difference in the pace of development of this cohort relative to the mutant cohorts. Also, *p* values are for comparisons between wild-type and mutant values at the indicated time points. **** $p \leq 0.0001$, Two-Way ANOVA with Tukey's correction for multiple comparisons. The samples in this trial were collected after hatchlings were cultivated on food for 24-50 h. **A')** Metrics used to compare sequential waves of *nhr-23* expression, also as described in Figure 5. **B)** Normalized *nhr-23* transcript levels detected in wild-type larvae, *nhr-23(aaa20-ΔLCS)* single mutants, and *mir-48(Δ) mir-241(Δ); mir-84(n4037)* triple mutants sampled across the L2 stage. In this chart, time samples for *nhr-23(aaa20-ΔLCS)* were shifted to the left by 2 h because the pace of development of this strain differed from the others used in this experiment. **** $p \leq 0.0001$, Two-Way ANOVA with Tukey's correction for multiple comparisons. Both wild-type and *let-7s* triple mutant larvae were collected after cultivation with

food for 14–26 h; *nhr-23(aaa20-ΔLCS)* larvae, after 16–28 h. **B')** Charts show the amplitude and rising slope of the *nhr-23* curve during the L2 stage, calculated as described earlier.

Supplemental Figure 5. The abundance of NHR-23 cycles across larval development and is elevated in *let-7(lf)* mutants relative to wild type. **A)** Representative images show NHR-23::GFP fusion proteins detected in the lateral epidermis of OP43 [*wgls43[nhr-23::gfp]*] larvae at the indicated stages. Fluorescence images were all captured with an exposure time of 300 milliseconds. In the image of an early L4, the arrowhead points to a nucleus in the seam; the arrow, to a nucleus in hyp7. Scale bars = 10 μm. **B)** Quantification of the NHR-23::GFP signal detected in cohorts of larvae collected at regular 1 h intervals across the entirety of the L4 stage. Gray and white rectangles drawn above the x-axis approximate phases of lethargus and activity, respectively. Values represent the mean ± sd derived from samples of 6-10 worms per timepoint. Within each worm, signals detected in 3 hyp7 nuclei and 3 seam nuclei were measured and the average value applied to further analysis. **C)** Pairs of fluorescence and merged GFP/DIC micrographs show NHR-23::GFP fusion proteins detected in the lateral epidermis of *wgls43[nhr-23::gfp⁺⁺]* and *wgls43; let-7(mg279) mir-84(tm1304)* animals at the indicated stages. Arrowheads point to nuclei in the syncytial hypodermis. The arrow points to a seam (s) nucleus. The letter g underscores signal detected in several germline nuclei. Scale bar = 10 μm.

Supplemental Figure 6. The genes *fhn-1* and *mlt-10* are shared targets of NHR-23 and *let-7s*. **A)** An independent replicate of the experiment described in Figure 8B. The values represent levels of *fhn-1* transcripts, normalized to *ama-1*, detected in regular 2 h time samples of wild-type, *nhr-23(aaa20-ΔLCS)* and *let-7(n2853)* larvae and newly emerged adults. These particular samples were collected after hatchlings were cultivated on food for 24-50 h. The accompanying table shows metrics that were calculated as described earlier. **B)** Same as A, except the levels of *mlt-10* transcripts are shown. ****p≤0.0001, **p≤0.01; *p≤0.05. Two-way ANOVA with Bonferroni's correction for multiple comparisons.

Supplemental Figure 7. NHR-23 and *let-7s* govern the temporal expression profile of other key clock genes. **A)** Schematics showing the alignment of the major isoforms of *lin-42* with NHR-23 occupancy of the respective chromosomal regions (brown shading) as captured in mid-L3s by ChIP-Seq, analyzed and contributed by the modENCODE consortium (Celniker *et al.*, 2009). Beige shading with a teal liner indicates regions of significant enrichment in the NHR-23 ChIP-seq. Purple rectangles depict coding sequences in the exons; grey rectangles depict UTRs in the

exons; dotted line represents the putative promoter regions; brown rectangles depict ROREs; red rectangles depict the position of the ChIP-qPCR amplicons from Figure 9A. Coordinates refer to reverse complement of *C. elegans* Chr II (NC_003280.10) **B**) Schematic similar to A, except depicting isoforms of *nhr-23*. Coordinates refer to reverse complement of *C. elegans* Chr I (NC_003279.8) as indicated. **C**) Levels of *lin-42* transcripts detected by TaqMan RT-qPCR in regular time samples of wild type wild-type, *nhr-23(aaa20-ΔLCS)* and *let-7(n2853)* animals collected from late L2 through early adulthood, as described in Figure 9C. **** $p \leq 0.0001$; Two-way ANOVA with Bonferroni's correction for multiple comparisons. **D**) Schematic depicting LCSs (gold) in the 3' UTR (blue) of *C. elegans lin-42a/b* and *H. sapiens PER2*. Gradients and bold labels distinguish sites perfectly complementary to the seed of *let-7s*. Each 3' UTR was retrieved from the UCSC genome browser; verified by comparison with curated ESTs; and LCSs identified using RNAhybrid.


Supplemental Figure 8. Reciprocal regulatory elements may be conserved in mammalian RORs and *let-7*. **A**) The 3 kb region upstream of selected homologs of *let-7*. Brown boxes label ROREs; magenta labels mature *let-7*. ROREs are numbered relative to the first nucleotide of the mature microRNA. Black arrows are landmarks for probable, but not experimentally verified, transcriptional start sites. **B-C**). Similar to Figure 10E, 10G, representative images show the tdTomato and GFP signal associated with fragments of the 3' UTRs of **B**) *H. sapiens RORβ* and **C**) *M. musculus RORα* and variants thereof that lack both LCSs.

Supplemental Table 1. Metrics of the molting biorhythm associated with specific genotypes. The active, lethargic, and wake-to-wake intervals are defined in the text. The values derived from longitudinal studies of stage-specific cohorts of singled, isogenic worms. The top row of each section corresponds to the same-day cohort of singled, wild-type worms. Dashes (–) beneath 'RNAi' indicate continuous cultivation of the worms on *E. coli* HT115(DE3). "N" is the cumulative sample size from two independent trials. All *p* values were generated by pairwise comparisons between individual metrics tabulated for a specific cohort of test subjects and also for the same-day, age-matched cohort of control subjects: **** $p \leq 0.0001$, *** $p \leq 0.001$, * $p \leq 0.05$; Ordinary One-Way ANOVA with Bonferroni's correction for multiple comparisons. Entries in the top row of each subsection correspond to six distinct cohorts of control subjects. By order of first appearance in the table, the strains tested were N2, QK509 [*let-7(n2853)*], GR1395, GR1436, ARF249, QK201, QK203, QK198, QK199, OP43, ARF414 and VT1066. Notably, both QK509 [*let-7(n2853)*] and the ancestral strain MT7626 [*let-7(n2853)*] developed at an accelerated pace: 71% of QK059

hatchlings and 79% of MT7626 hatchlings transited the larval stages and emerged as young adults within 42 h of cultivation with food, as compared with 12% of N2 hatchlings (N=100, $p \leq 0.0001$, chi-square test).

Supplemental Table 2. LCSs found in selected nematode and vertebrate homologs of *ROR*. Entries correspond to sites shown in Figure 10D. The number of nt. between the 3' end of each LCS and the stop codon is specified. The thermostability of every RNA duplex between a prospective LCS and mature *let-7*, as predicted by RNAhybrid, was lower than the predicted thermostability (-29 kcal/mol) of duplexes between the functional LCS in the 3' UTR of *lin-41* and *let-7* (Rehmsmeier *et al.*, 2004). The 3' UTRs were supported by ESTs archived in WBcel235/ce11, WBPS9, GRCh38/hg38, GRCm38/mm10, and GRCz10/danRer10.

Supplemental Table 3. Metrics of the expression curves of core clock components and clock-controlled genes in the indicated genetic backgrounds. As described in the section on Method Details, Metacycle was used to calculate the amplitude and phase of expression of the waveforms. The peak values and the slope of rise and decay were obtained by manual calculation.

Supplemental Table 4. Evaluation and classification of clock-controlled genes as direct targets of NHR-23, *let-7*s, neither or both. The bioinformatic approaches and criteria for assignment of queries to categories are described in the Method Details. The name and WormBase accession number of each gene is listed. The shorthand “# Obs./# Exp.” stands for the number of observed DNA or RNA response elements divided by the number of elements predicted by chance alone. The “↓” symbol denotes down-regulation of the query transcript in *nhr-23(RNAi)* animals as compared with wild-type controls. The “+” symbol in column 12 denotes association of the 3' UTR with ALG-1 *in vivo*. The symbol “” indicates that expression of the gene oscillates across larval development. Relevant datasets are identified in the text, Method Details and Key Resources Table.

Supplemental Table 5. Oligonucleotides used in this study. The unique identifier for each DNA or RNA molecules appears in the first column. Suppliers of specific oligonucleotides are identified in the Method Details. For those primers used to construct a particular bicistronic reporter for *cis*-regulatory elements in a 3' UTR of interest, the resulting plasmid and corresponding

extrachromosomal array are identified in the “application” column. All seven reporters and respective transgenic strains of *C. elegans* are further described in The Key Resources Table.

Supplemental Movie 1. Behavior and fate of a quiescent wild-type adult. Movie shows the behavior and fate of a wild-type adult, video recorded for 15 s every 2 h, that was quiescent at the initial time point of observation. The wild-type adult was still alive 8 h after the initial incidence of behavioral quiescence.

Supplemental Movie 2. Behavior and fate of a quiescent *nhr-23(aaa20-ΔLCS)* adult. As above, video recordings were done for 15 s at 2 h intervals from the initial detection of quiescence. Quiescence was detected at every time sample, and bits of loose cuticle were found along the head and at the vulva. The animal ultimately bagged.

Supplemental Movie 3. Behavior and fate of a quiescent *wg/s43[nhr-23⁺⁺]* adult. Video recording was done as described for Supplemental Movies 1 and 2. The animal was quiescent at the first three time samples. At 8 h after the initial detection of quiescence, the grinder of the animal was observed to twitch several times, a behavior that normally accompanies ecdysis. At the 10 h time point, the animal resumed pumping, albeit at a visibly lower rate than wild-type adults. At this time, loose cuticle could also be detected at the tail. The animal eventually bagged.

REFERENCES

- Abbott, A.L., Alvarez-Saavedra, E., Miska, E.A., Lau, N.C., Bartel, D.P., Horvitz, H.R., and Ambros, V. (2005). The let-7 MicroRNA family members mir-48, mir-84, and mir-241 function together to regulate developmental timing in *Caenorhabditis elegans*. *Dev Cell* 9, 403-414. 10.1016/j.devcel.2005.07.009.
- Aguinaldo, A.M., Turbeville, J.M., Linford, L.S., Rivera, M.C., Garey, J.R., Raff, R.A., and Lake, J.A. (1997). Evidence for a clade of nematodes, arthropods and other moulting animals. *Nature* 387, 489-493. 10.1038/387489a0.
- Alvarez-Saavedra, M., Antoun, G., Yanagiya, A., Oliva-Hernandez, R., Cornejo-Palma, D., Perez-Iratxeta, C., Sonenberg, N., and Cheng, H.Y. (2011). miRNA-132 orchestrates chromatin remodeling and translational control of the circadian clock. *Hum Mol Genet* 20, 731-751. 10.1093/hmg/ddq519.
- Ambros, V., and Ruvkun, G. (2018). Recent Molecular Genetic Explorations of *Caenorhabditis elegans* MicroRNAs. *Genetics* 209, 651-673. 10.1534/genetics.118.300291.
- Banerjee, D., Kwok, A., Lin, S.Y., and Slack, F.J. (2005). Developmental timing in *C. elegans* is regulated by kin-20 and tim-1, homologs of core circadian clock genes. *Dev Cell* 8, 287-295. 10.1016/j.devcel.2004.12.006.
- Bessho, Y., Hirata, H., Masamizu, Y., and Kageyama, R. (2003). Periodic repression by the bHLH factor Hes7 is an essential mechanism for the somite segmentation clock. *Genes Dev* 17, 1451-1456. 10.1101/gad.1092303.
- Bethke, A., Fielenbach, N., Wang, Z., Mangelsdorf, D.J., and Antebi, A. (2009). Nuclear hormone receptor regulation of microRNAs controls developmental progression. *Science* 324, 95-98. 10.1126/science.1164899.
- Bracht, J., Hunter, S., Eachus, R., Weeks, P., and Pasquinelli, A.E. (2004). Trans-splicing and polyadenylation of let-7 microRNA primary transcripts. *RNA* 10, 1586-1594. 10.1261/rna.7122604.
- Broughton, J.P., Lovci, M.T., Huang, J.L., Yeo, G.W., and Pasquinelli, A.E. (2016). Pairing beyond the Seed Supports MicroRNA Targeting Specificity. *Mol Cell* 64, 320-333. 10.1016/j.molcel.2016.09.004.
- Celniker, S.E., Dillon, L.A., Gerstein, M.B., Gunsalus, K.C., Henikoff, S., Karpen, G.H., Kellis, M., Lai, E.C., Lieb, J.D., MacAlpine, D.M., et al. (2009). Unlocking the secrets of the genome. *Nature* 459, 927-930. 10.1038/459927a.
- Chen, R., D'Alessandro, M., and Lee, C. (2013). miRNAs are required for generating a time delay critical for the circadian oscillator. *Curr Biol* 23, 1959-1968. 10.1016/j.cub.2013.08.005.
- Cohen, M.L., Kim, S., Morita, K., Kim, S.H., and Han, M. (2015). The GATA factor elt-1 regulates *C. elegans* developmental timing by promoting expression of the let-7 family microRNAs. *PLoS Genet* 11, e1005099. 10.1371/journal.pgen.1005099.
- Cook, D.N., Kang, H.S., and Jetten, A.M. (2015). Retinoic Acid-Related Orphan Receptors (RORs): Regulatory Functions in Immunity, Development, Circadian Rhythm, and Metabolism. *Nucl Receptor Res* 2. 10.11131/2015/101185.
- Diaz-Cuadros, M., Pourquie, O., and El-Sherif, E. (2021). Patterning with clocks and genetic cascades: Segmentation and regionalization of vertebrate versus insect body plans. *PLoS Genet* 17, e1009812. 10.1371/journal.pgen.1009812.

Du, N.H., Arpat, A.B., De Matos, M., and Gattfield, D. (2014). MicroRNAs shape circadian hepatic gene expression on a transcriptome-wide scale. *Elife* 3, e02510. 10.7554/eLife.02510.

Ecsedi, M., Rausch, M., and Grosshans, H. (2015). The let-7 microRNA directs vulval development through a single target. *Dev Cell* 32, 335-344. 10.1016/j.devcel.2014.12.018.

Edelman, T.L., McCulloch, K.A., Barr, A., Frokjaer-Jensen, C., Jorgensen, E.M., and Rougvie, A.E. (2016). Analysis of a lin-42/Period Null Allele Implicates All Three Isoforms in Regulation of *Caenorhabditis elegans* Molting and Developmental Timing. *G3* (Bethesda). 10.1534/g3.116.034165.

Esperk, T., Tammaru, T., and Nylin, S. (2007). Intraspecific variability in number of larval instars in insects. *J Econ Entomol* 100, 627-645. 10.1603/0022-0493(2007)100[627:ivinol]2.0.co;2.

Evans, R.M., and Mangelsdorf, D.J. (2014). Nuclear Receptors, RXR, and the Big Bang. *Cell* 157, 255-266. 10.1016/j.cell.2014.03.012.

Frand, A.R., Russel, S., and Ruvkun, G. (2005). Functional genomic analysis of *C. elegans* molting. *PLoS Biol* 3, e312. 10.1371/journal.pbio.0030312.

Galagali, H., and Kim, J.K. (2020). The multifaceted roles of microRNAs in differentiation. *Curr Opin Cell Biol* 67, 118-140. 10.1016/j.ceb.2020.08.015.

Giguere, V., Tini, M., Flock, G., Ong, E., Evans, R.M., and Otulakowski, G. (1994). Isoform-specific amino-terminal domains dictate DNA-binding properties of ROR alpha, a novel family of orphan hormone nuclear receptors. *Genes Dev* 8, 538-553.

Grishok, A., Pasquinelli, A.E., Conte, D., Li, N., Parrish, S., Ha, I., Baillie, D.L., Fire, A., Ruvkun, G., and Mello, C.C. (2001). Genes and mechanisms related to RNA interference regulate expression of the small temporal RNAs that control *C. elegans* developmental timing. *Cell* 106, 23-34. 10.1016/s0092-8674(01)00431-7.

Gupta, B.P., Hanna-Rose, W., and Sternberg, P.W. (2012). Morphogenesis of the vulva and the vulval-uterine connection. *WormBook*, 1-20. 10.1895/wormbook.1.152.1.

Hammell, C.M., Karp, X., and Ambros, V. (2009). A feedback circuit involving let-7-family miRNAs and DAF-12 integrates environmental signals and developmental timing in *Caenorhabditis elegans*. *Proc Natl Acad Sci U S A* 106, 18668-18673. 10.1073/pnas.0908131106.

Harris, D.T., and Horvitz, H.R. (2011). MAB-10/NAB acts with LIN-29/EGR to regulate terminal differentiation and the transition from larva to adult in *C. elegans*. *Development* 138, 4051-4062. 10.1242/dev.065417.

Hayes, G.D., Frand, A.R., and Ruvkun, G. (2006). The mir-84 and let-7 paralogous microRNA genes of *Caenorhabditis elegans* direct the cessation of molting via the conserved nuclear hormone receptors NHR-23 and NHR-25. *Development* 133, 4631-4641. 10.1242/dev.02655.

Hayes, G.D., and Ruvkun, G. (2006). Misexpression of the *Caenorhabditis elegans* miRNA let-7 is sufficient to drive developmental programs. *Cold Spring Harb Symp Quant Biol* 71, 21-27. 10.1101/sqb.2006.71.018.

Hendriks, G.J., Gaidatzis, D., Aeschmann, F., and Grosshans, H. (2014). Extensive oscillatory gene expression during *C. elegans* larval development. *Mol Cell* 53, 380-392. 10.1016/j.molcel.2013.12.013.

Iwanir, S., Tramm, N., Nagy, S., Wright, C., Ish, D., and Biron, D. (2013). The microarchitecture of *C. elegans* behavior during lethargus: homeostatic bout dynamics, a typical body posture, and regulation by a central neuron. *Sleep* 36, 385-395. 10.5665/sleep.2456.

Jeon, M., Gardner, H.F., Miller, E.A., Deshler, J., and Rougvie, A.E. (1999). Similarity of the *C. elegans* developmental timing protein LIN-42 to circadian rhythm proteins. *Science* 286, 1141-1146.

Johnson, M.H., and Day, M.L. (2000). Egg timers: how is developmental time measured in the early vertebrate embryo? *Bioessays* 22, 57-63. 10.1002/(SICI)1521-1878(200001)22:1<57::AID-BIES10>3.0.CO;2-L.

Johnson, S.M., Lin, S.Y., and Slack, F.J. (2003). The time of appearance of the *C. elegans* let-7 microRNA is transcriptionally controlled utilizing a temporal regulatory element in its promoter. *Dev Biol* 259, 364-379.

Kadener, S., Menet, J.S., Sugino, K., Horwich, M.D., Weissbein, U., Nawathean, P., Vagin, V.V., Zamore, P.D., Nelson, S.B., and Rosbash, M. (2009). A role for microRNAs in the *Drosophila* circadian clock. *Genes Dev* 23, 2179-2191. 10.1101/gad.1819509.

Kai, Z.S., Finnegan, E.F., Huang, S., and Pasquinelli, A.E. (2013). Multiple cis-elements and trans-acting factors regulate dynamic spatio-temporal transcription of let-7 in *Caenorhabditis elegans*. *Dev Biol* 374, 223-233. 10.1016/j.ydbio.2012.11.021.

Kamath, R.S., and Ahringer, J. (2003). Genome-wide RNAi screening in *Caenorhabditis elegans*. *Methods* 30, 313-321.

Katz, S.S., Barker, T.J., Maul-Newby, H.M., Sparacio, A.P., Nguyen, K.C.Q., Maybrun, C.L., Belfi, A., Cohen, J.D., Hall, D.H., Sundaram, M.V., and Frand, A.R. (2021). A transient apical extracellular matrix relays cytoskeletal patterns to shape permanent acellular ridges on the surface of adult *C. elegans*. *bioRxiv*, 2021.2012.2028.474392. 10.1101/2021.12.28.474392.

Kim, D., Grun, D., and van Oudenaarden, A. (2013). Dampening of expression oscillations by synchronous regulation of a microRNA and its target. *Nat Genet* 45, 1337-1344. 10.1038/ng.2763.

Kostrouchova, M., Krause, M., Kostrouch, Z., and Rall, J.E. (1998). CHR3: a *Caenorhabditis elegans* orphan nuclear hormone receptor required for proper epidermal development and molting. *Development* 125, 1617-1626.

Kouns, N.A., Nakielna, J., Behensky, F., Krause, M.W., Kostrouch, Z., and Kostrouchova, M. (2011). NHR-23 dependent collagen and hedgehog-related genes required for molting. *Biochem Biophys Res Commun* 413, 515-520. 10.1016/j.bbrc.2011.08.124.

Mangone, M., Manoharan, A.P., Thierry-Mieg, D., Thierry-Mieg, J., Han, T., Mackowiak, S.D., Mis, E., Zegar, C., Gutwein, M.R., Khivansara, V., et al. (2010). The landscape of *C. elegans* 3'UTRs. *Science* 329, 432-435. 10.1126/science.1191244.

McCulloch, K.A., and Rougvie, A.E. (2014). *Caenorhabditis elegans* period homolog lin-42 regulates the timing of heterochronic miRNA expression. *Proc Natl Acad Sci U S A* 111, 15450-15455. 10.1073/pnas.1414856111.

Meeuse, M.W., Hauser, Y.P., Morales Moya, L.J., Hendriks, G.J., Eglinger, J., Bogaarts, G., Tsiairis, C., and Grosshans, H. (2020). Developmental function and state transitions of a gene expression oscillator in *Caenorhabditis elegans*. *Mol Syst Biol* 16, e9975. 10.15252/msb.209975.

Meli, V.S., Osuna, B., Ruvkun, G., and Frand, A.R. (2010). MLT-10 defines a family of DUF644 and proline-rich repeat proteins involved in the molting cycle of *Caenorhabditis elegans*. *Mol Biol Cell* *21*, 1648-1661. 10.1091/mbc.E08-07-0708.

Monsalve, G.C., Van Buskirk, C., and Frand, A.R. (2011). LIN-42/PERIOD controls cyclical and developmental progression of *C. elegans* molts. *Curr Biol* *21*, 2033-2045. 10.1016/j.cub.2011.10.054.

Novak, B., and Tyson, J.J. (2008). Design principles of biochemical oscillators. *Nat Rev Mol Cell Biol* *9*, 981-991. 10.1038/nrm2530.

Oyama, Y., Bartman, C.M., Gile, J., and Eckle, T. (2017). Circadian MicroRNAs in Cardioprotection. *Curr Pharm Des* *23*, 3723-3730. 10.2174/1381612823666170707165319.

Paix, A., Folkmann, A., Rasoloson, D., and Seydoux, G. (2015). High Efficiency, Homology-Directed Genome Editing in *Caenorhabditis elegans* Using CRISPR-Cas9 Ribonucleoprotein Complexes. *Genetics* *201*, 47-54. 10.1534/genetics.115.179382.

Partch, C.L., Green, C.B., and Takahashi, J.S. (2014). Molecular architecture of the mammalian circadian clock. *Trends Cell Biol* *24*, 90-99. 10.1016/j.tcb.2013.07.002.

Patke, A., Murphy, P.J., Onat, O.E., Krieger, A.C., Ozcelik, T., Campbell, S.S., and Young, M.W. (2017). Mutation of the Human Circadian Clock Gene CRY1 in Familial Delayed Sleep Phase Disorder. *Cell* *169*, 203-215 e213. 10.1016/j.cell.2017.03.027.

Perales, R., King, D.M., Aguirre-Chen, C., and Hammell, C.M. (2014). LIN-42, the *Caenorhabditis elegans* PERIOD homolog, negatively regulates microRNA transcription. *PLoS Genet* *10*, e1004486. 10.1371/journal.pgen.1004486.

Puram, R.V., Kowalczyk, M.S., de Boer, C.G., Schneider, R.K., Miller, P.G., McConkey, M., Tothova, Z., Tejero, H., Heckl, D., Jaras, M., et al. (2016). Core Circadian Clock Genes Regulate Leukemia Stem Cells in AML. *Cell* *165*, 303-316. 10.1016/j.cell.2016.03.015.

Raizen, D.M., Zimmerman, J.E., Maycock, M.H., Ta, U.D., You, Y.J., Sundaram, M.V., and Pack, A.I. (2008). Lethargus is a *Caenorhabditis elegans* sleep-like state. *Nature* *451*, 569-572. 10.1038/nature06535.

Rehmsmeier, M., Steffen, P., Hochsmann, M., and Giegerich, R. (2004). Fast and effective prediction of microRNA/target duplexes. *RNA* *10*, 1507-1517. 10.1261/rna.5248604.

Reinhart, B.J., Slack, F.J., Basson, M., Pasquinelli, A.E., Bettinger, J.C., Rougvie, A.E., Horvitz, H.R., and Ruvkun, G. (2000). The 21-nucleotide let-7 RNA regulates developmental timing in *Caenorhabditis elegans*. *Nature* *403*, 901-906. 10.1038/35002607.

Rensing, L., Meyer-Grahe, U., and Ruoff, P. (2001). Biological timing and the clock metaphor: oscillatory and hourglass mechanisms. *Chronobiol Int* *18*, 329-369. 10.1081/cbi-100103961.

Roenneberg, T., and Mrosovsky, M. (2016). The Circadian Clock and Human Health. *Curr Biol* *26*, R432-443. 10.1016/j.cub.2016.04.011.

Roush, S.F., and Slack, F.J. (2009). Transcription of the *C. elegans* let-7 microRNA is temporally regulated by one of its targets, hbl-1. *Dev Biol* *334*, 523-534. 10.1016/j.ydbio.2009.07.012.

Singh, K., Chao, M.Y., Somers, G.A., Komatsu, H., Corkins, M.E., Larkins-Ford, J., Tucey, T., Dionne, H.M., Walsh, M.B., Beaumont, E.K., et al. (2011). *C. elegans* Notch

signaling regulates adult chemosensory response and larval molting quiescence. *Curr Biol* 21, 825-834. 10.1016/j.cub.2011.04.010.

Singh, R.N., and Sulston, J.E. (1978). Some observations on moulting in *Caenorhabditis elegans*. *Nematologica* 24, 63-71.

Slack, F.J., Basson, M., Liu, Z., Ambros, V., Horvitz, H.R., and Ruvkun, G. (2000). The *lin-41* RBCC gene acts in the *C. elegans* heterochronic pathway between the *let-7* regulatory RNA and the LIN-29 transcription factor. *Mol Cell* 5, 659-669.

Stiernagle, T. (2006). Maintenance of *C. elegans*. *WormBook*, 1-11. 10.1895/wormbook.1.101.1.

Takahashi, J.S. (2016). Molecular Architecture of the Circadian Clock in Mammals. In *A Time for Metabolism and Hormones*, P. Sassone-Corsi, and Y. Christen, eds. pp. 13-24. 10.1007/978-3-319-27069-2_2.

Takahashi, J.S. (2017). Transcriptional architecture of the mammalian circadian clock. *Nat Rev Genet* 18, 164-179. 10.1038/nrg.2016.150.

Takeda, Y., Jothi, R., Birault, V., and Jetten, A.M. (2012). RORgamma directly regulates the circadian expression of clock genes and downstream targets in vivo. *Nucleic Acids Res* 40, 8519-8535. 10.1093/nar/gks630.

Takeda, Y., Kang, H.S., Freudenberg, J., DeGraff, L.M., Jothi, R., and Jetten, A.M. (2014). Retinoic acid-related orphan receptor gamma (RORgamma): a novel participant in the diurnal regulation of hepatic gluconeogenesis and insulin sensitivity. *PLoS Genet* 10, e1004331. 10.1371/journal.pgen.1004331.

Tsiarlis, C., and Grosshans, H. (2021). Gene expression oscillations in *C. elegans* underlie a new developmental clock. *Curr Top Dev Biol* 144, 19-43. 10.1016/bs.ctdb.2020.11.001.

Tsialikas, J., Romens, M.A., Abbott, A., and Moss, E.G. (2017). Stage-Specific Timing of the microRNA Regulation of *lin-28* by the Heterochronic Gene *lin-14* in *Caenorhabditis elegans*. *Genetics* 205, 251-262. 10.1534/genetics.116.195040.

Uriu, K. (2016). Genetic oscillators in development. *Dev Growth Differ* 58, 16-30. 10.1111/dgd.12262.

Vadla, B., Kemper, K., Alaimo, J., Heine, C., and Moss, E.G. (2012). *lin-28* controls the succession of cell fate choices via two distinct activities. *PLoS Genet* 8, e1002588. 10.1371/journal.pgen.1002588.

Van Buskirk, C., and Sternberg, P.W. (2007). Epidermal growth factor signaling induces behavioral quiescence in *Caenorhabditis elegans*. *Nat Neurosci* 10, 1300-1307. 10.1038/nn1981.

Van Wynsberghe, P.M., Finnegan, E.F., Stark, T., Angelus, E.P., Homan, K.E., Yeo, G.W., and Pasquinelli, A.E. (2014). The Period protein homolog LIN-42 negatively regulates microRNA biogenesis in *C. elegans*. *Dev Biol* 390, 126-135. 10.1016/j.ydbio.2014.03.017.

Van Wynsberghe, P.M., Kai, Z.S., Massirer, K.B., Burton, V.H., Yeo, G.W., and Pasquinelli, A.E. (2011). LIN-28 co-transcriptionally binds primary *let-7* to regulate miRNA maturation in *Caenorhabditis elegans*. *Nat Struct Mol Biol* 18, 302-308. 10.1038/nsmb.1986.

Wang, D.J., Legesse-Miller, A., Johnson, E.L., and Collier, H.A. (2012). Regulation of the *let-7a-3* promoter by NF-kappaB. *PLoS One* 7, e31240. 10.1371/journal.pone.0031240.

Wu, G., Anafi, R.C., Hughes, M.E., Kornacker, K., and Hogenesch, J.B. (2016). MetaCycle: an integrated R package to evaluate periodicity in large scale data. *Bioinformatics* 32, 3351-3353. 10.1093/bioinformatics/btw405.

Yoo, S.H., Kojima, S., Shimomura, K., Koike, N., Buhr, E.D., Furukawa, T., Ko, C.H., Gloston, G., Ayoub, C., Nohara, K., et al. (2017). Period2 3'-UTR and microRNA-24 regulate circadian rhythms by repressing PERIOD2 protein accumulation. *Proc Natl Acad Sci U S A* 114, E8855-E8864. 10.1073/pnas.1706611114.

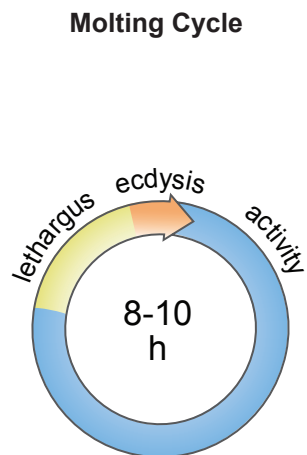
You, Y.J., Kim, J., Raizen, D.M., and Avery, L. (2008). Insulin, cGMP, and TGF-beta signals regulate food intake and quiescence in *C. elegans*: a model for satiety. *Cell Metab* 7, 249-257. 10.1016/j.cmet.2008.01.005.

Zhang, Y., Papazyan, R., Damle, M., Fang, B., Jager, J., Feng, D., Peed, L.C., Guan, D., Sun, Z., and Lazar, M.A. (2017). The hepatic circadian clock fine-tunes the lipogenic response to feeding through RORalpha/gamma. *Genes Dev.* 10.1101/gad.302323.117.

Figure 1

Patel, Galagali et al.

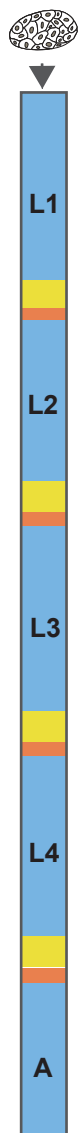
A



B

Heterochronic Pathway

embryo



miR-48
miR-84
miR-241



let-7



let-7



C

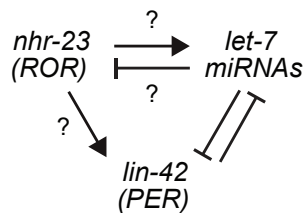
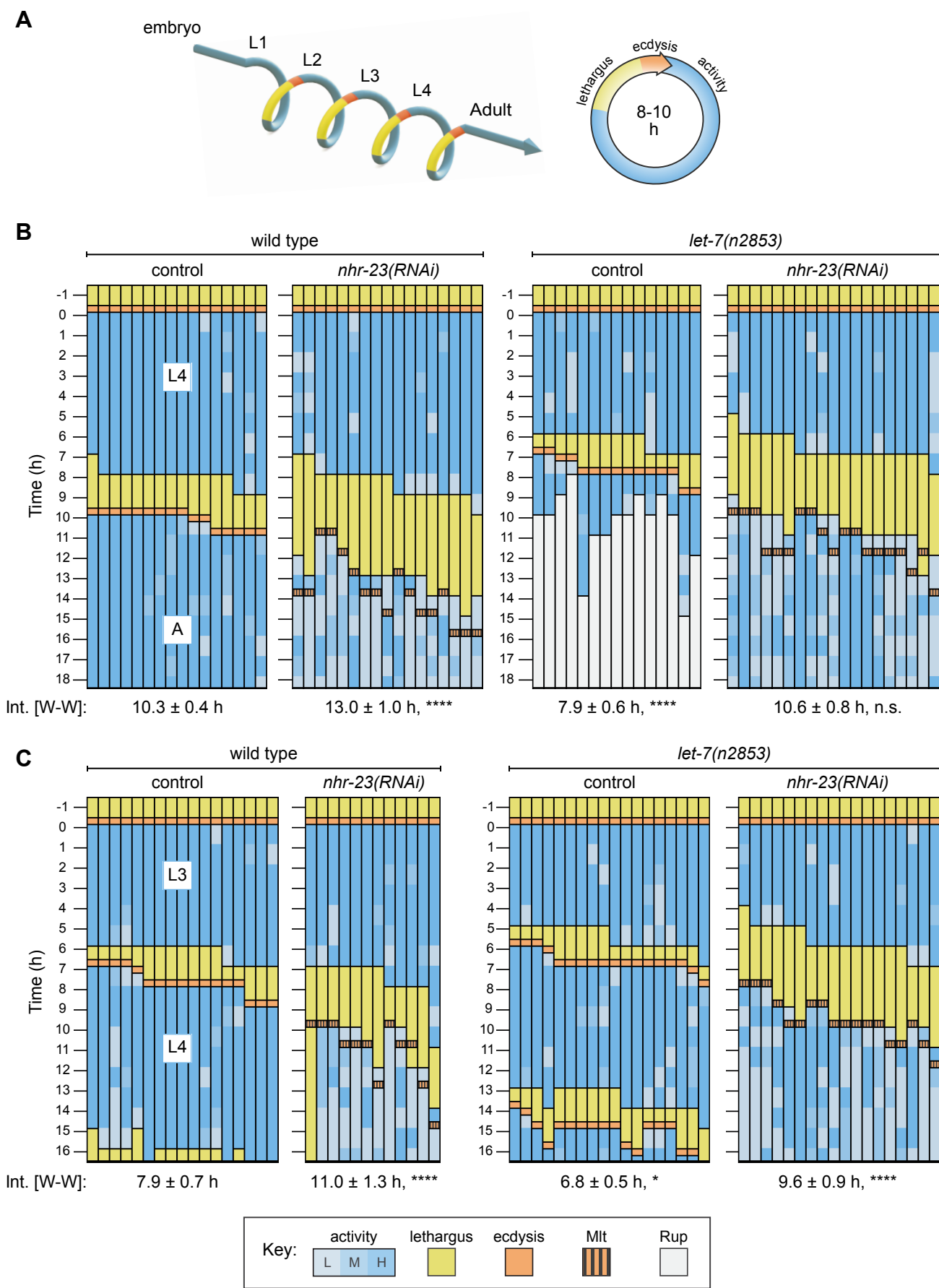
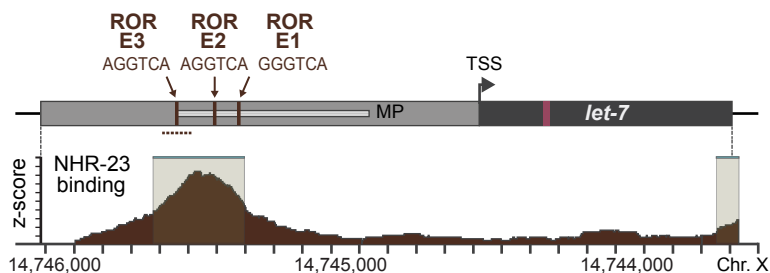
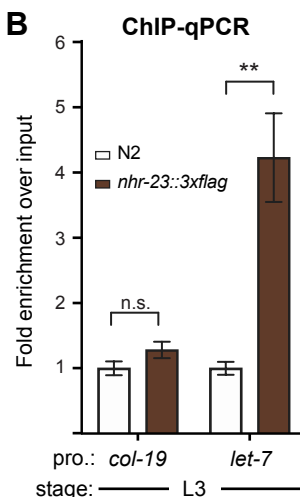
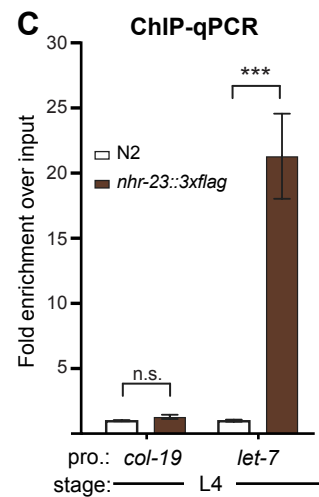
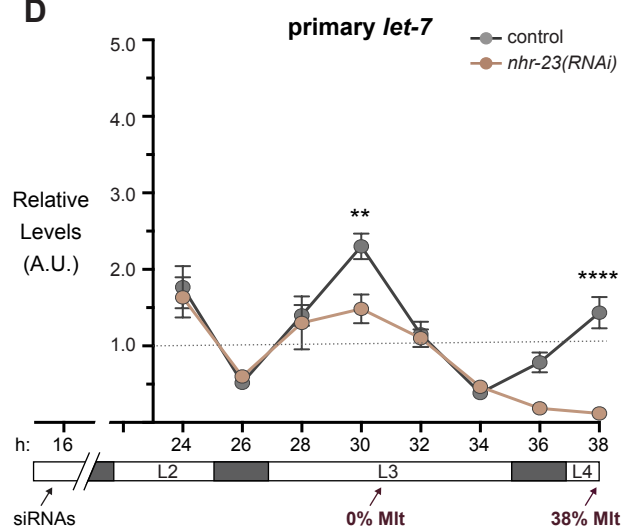
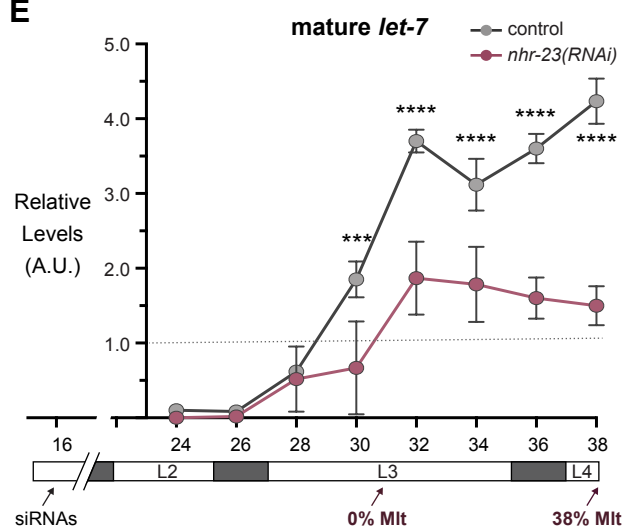
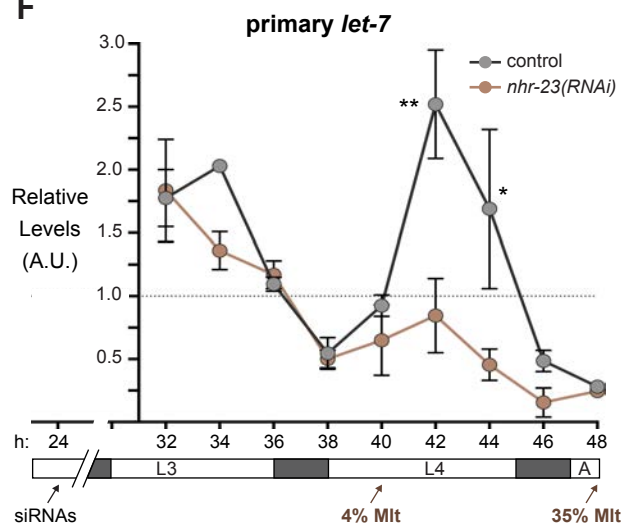
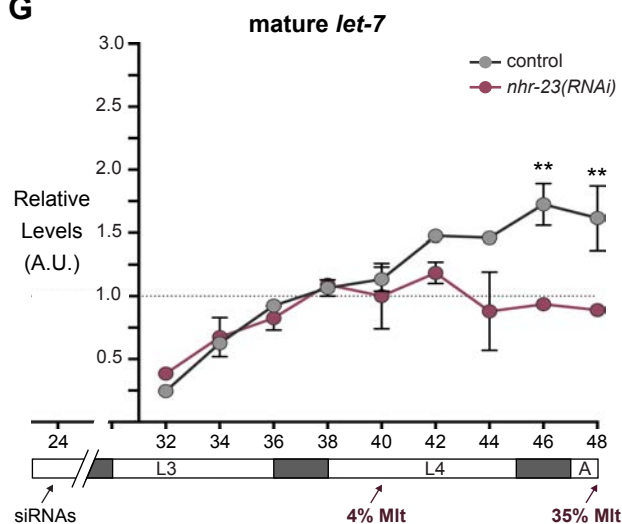
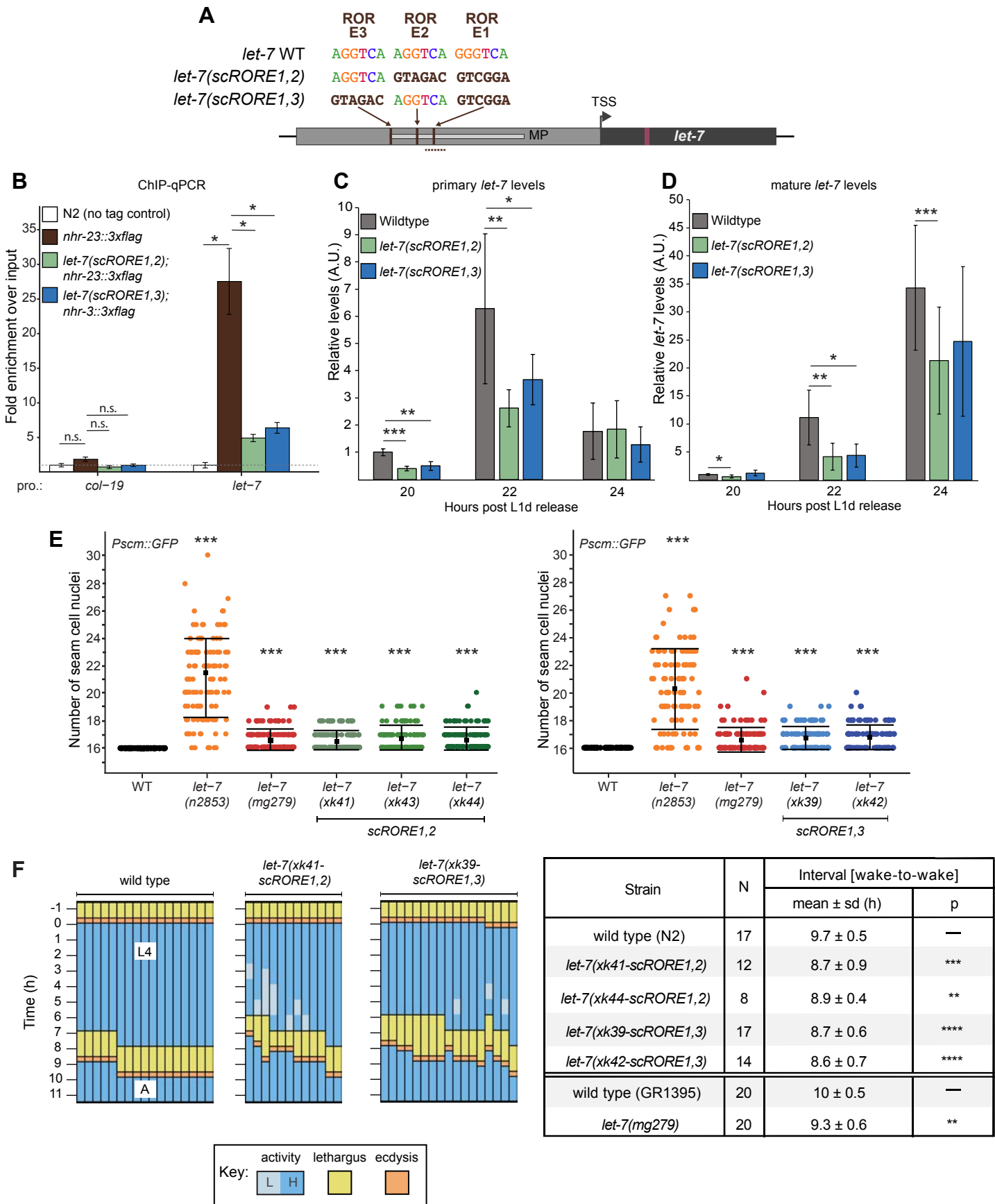


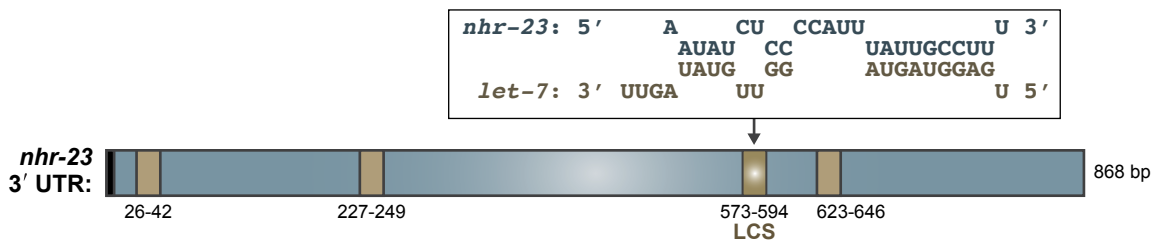
Figure 2



A**B****C****D****E****F****G**



A

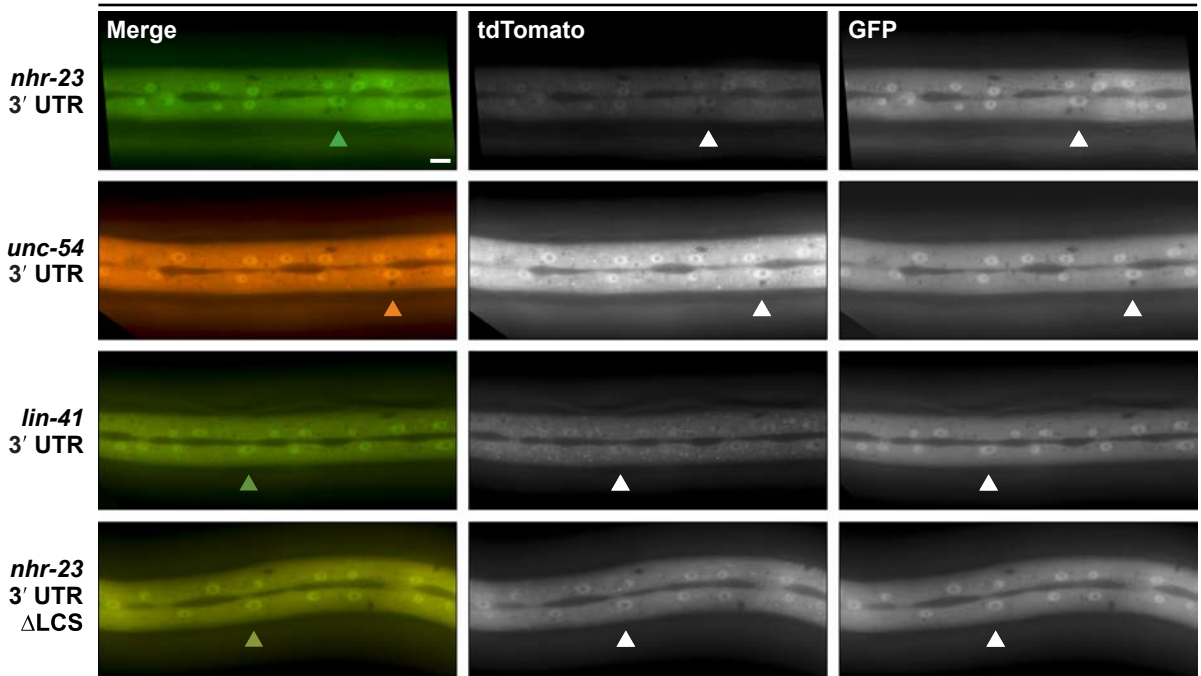


B

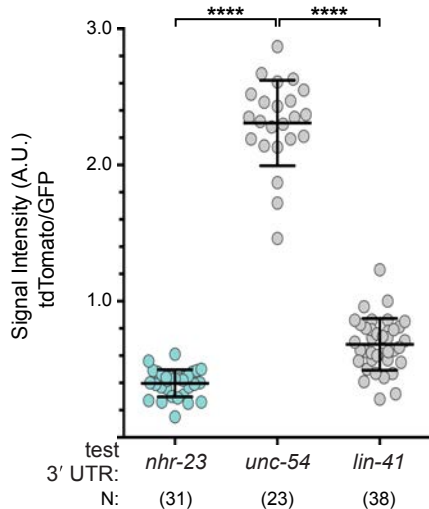


C

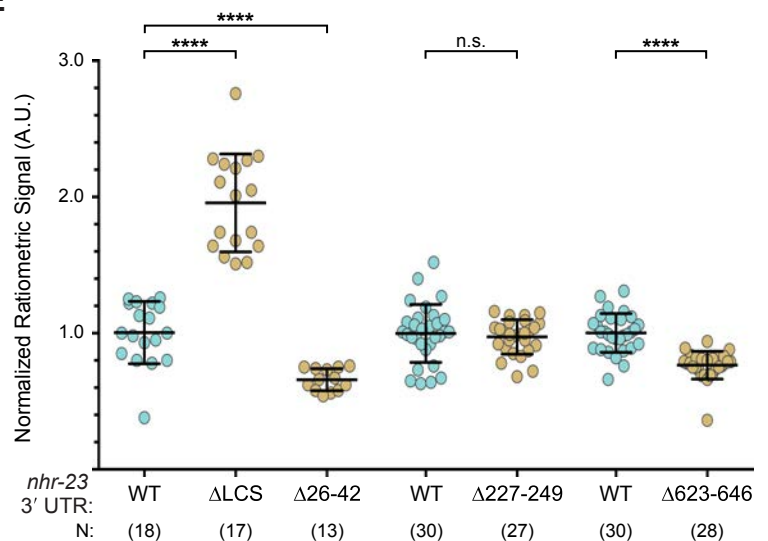
L4/Adult Molt

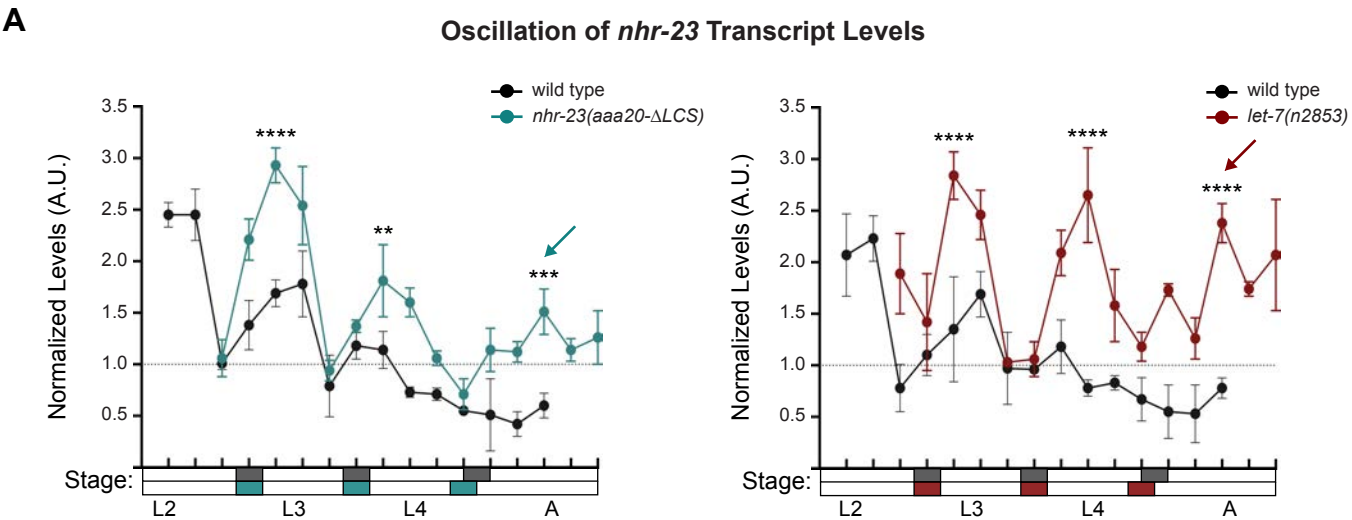


D



E





A'

Stage	L3				L4			
Genotype	wild type	<i>nhr-23(aaa20)</i>	wild type	<i>let-7(n2853)</i>	wild type	<i>nhr-23(aaa20)</i>	wild type	<i>let-7(n2853)</i>
Amplitude	0.4	1.1	0.5	0.9	0.3	0.4	0.1	0.8
Rising Slope	0.19	0.46	0.15	0.71	0.19	0.21	0.11	0.26

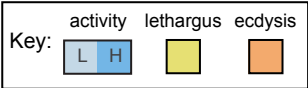
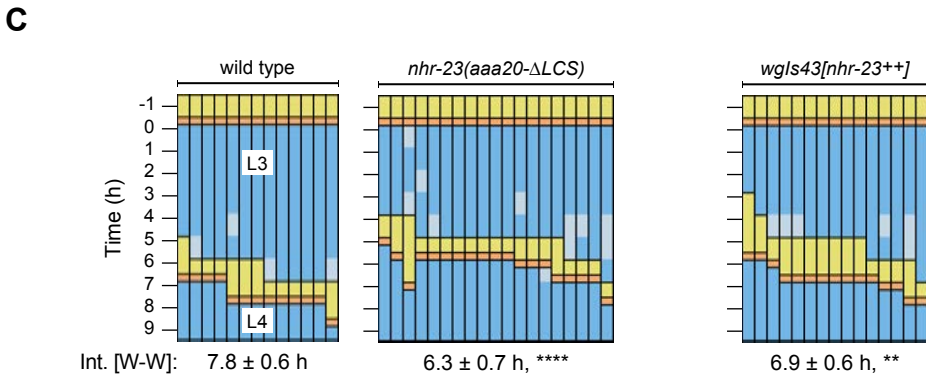
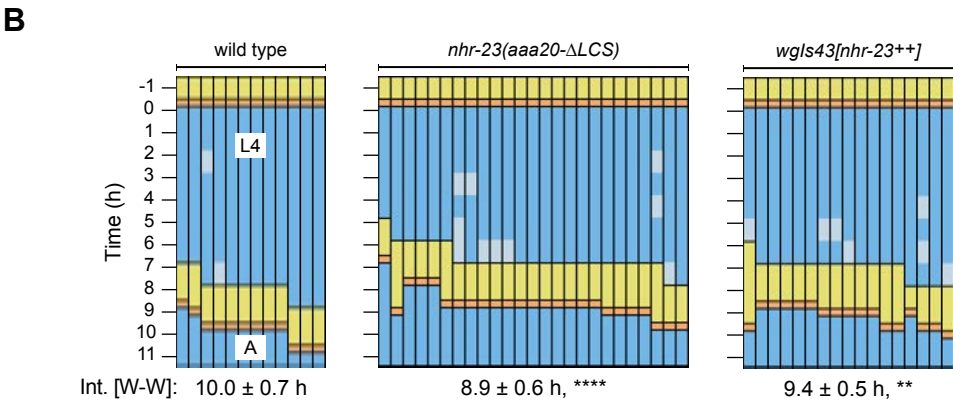


Figure 7

Patel, Galagali et al.

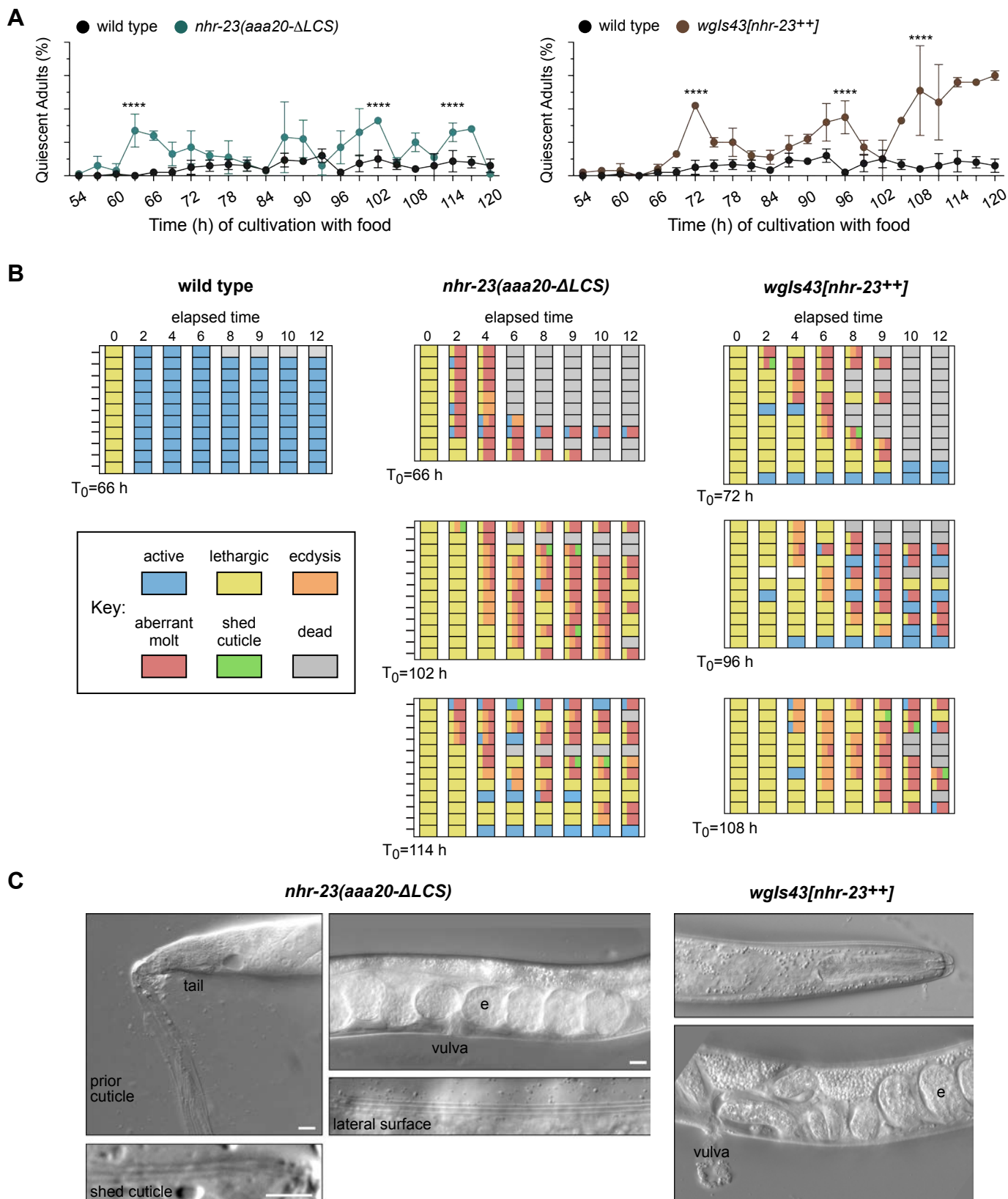
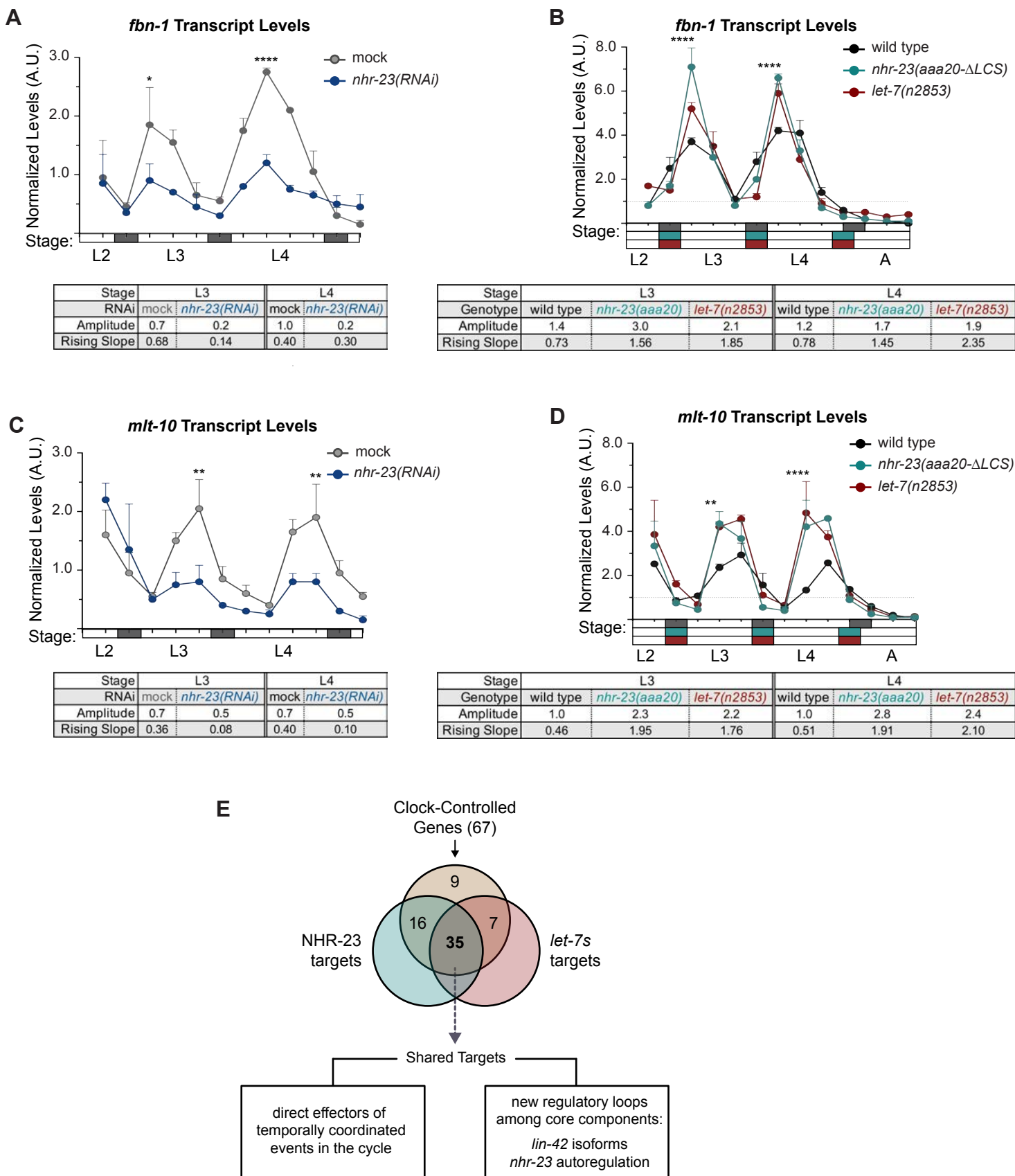


Figure 8



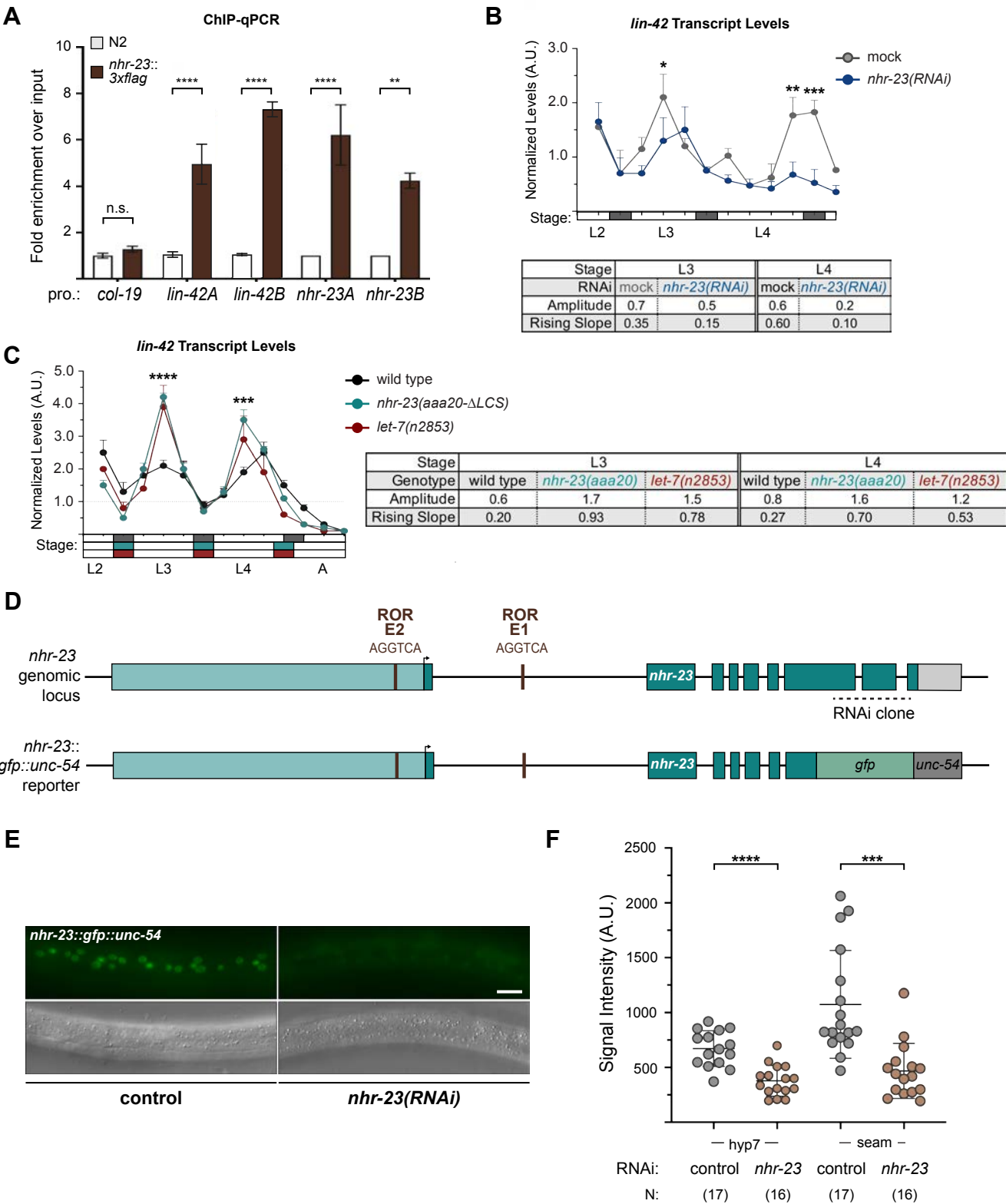
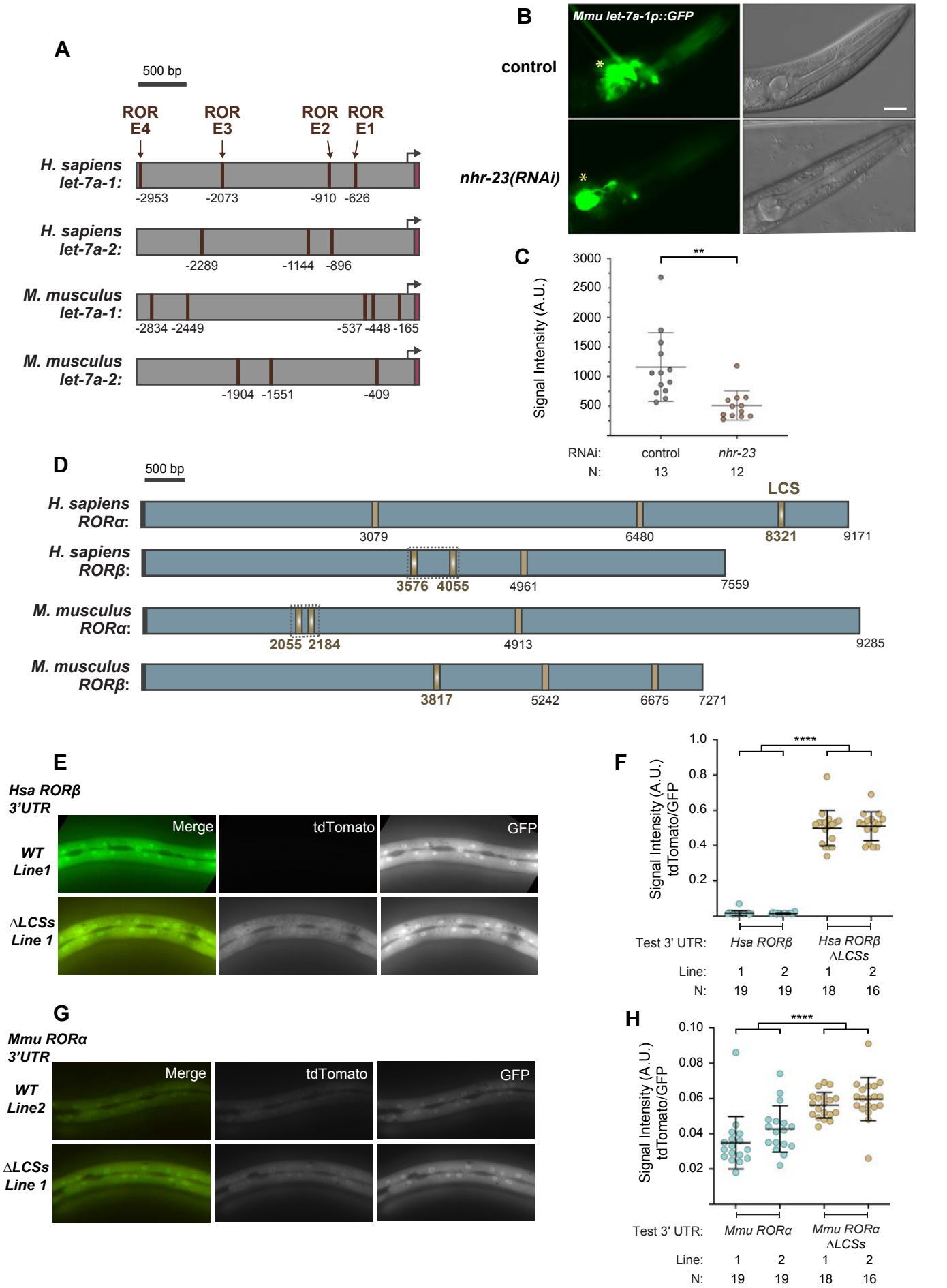
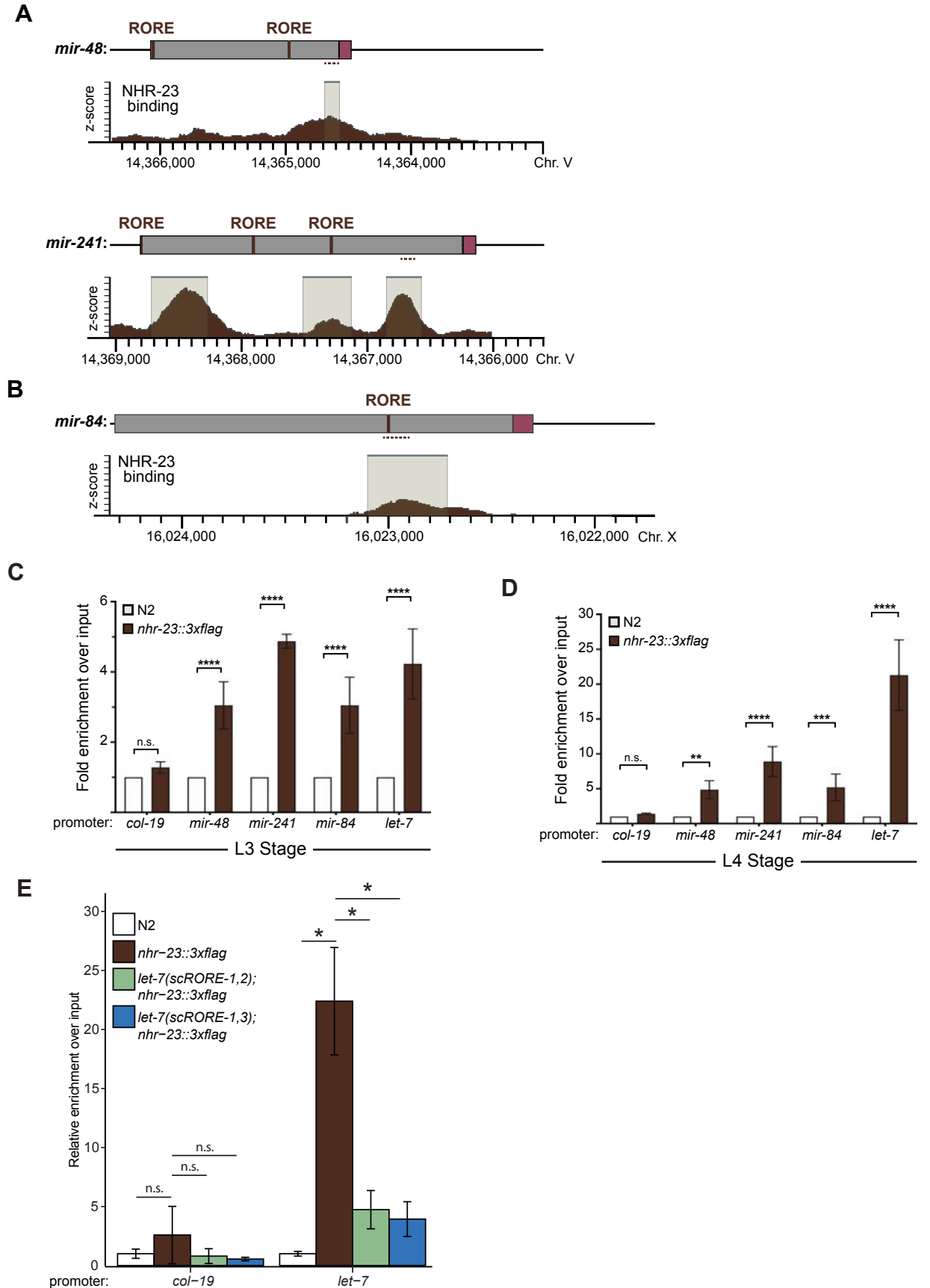
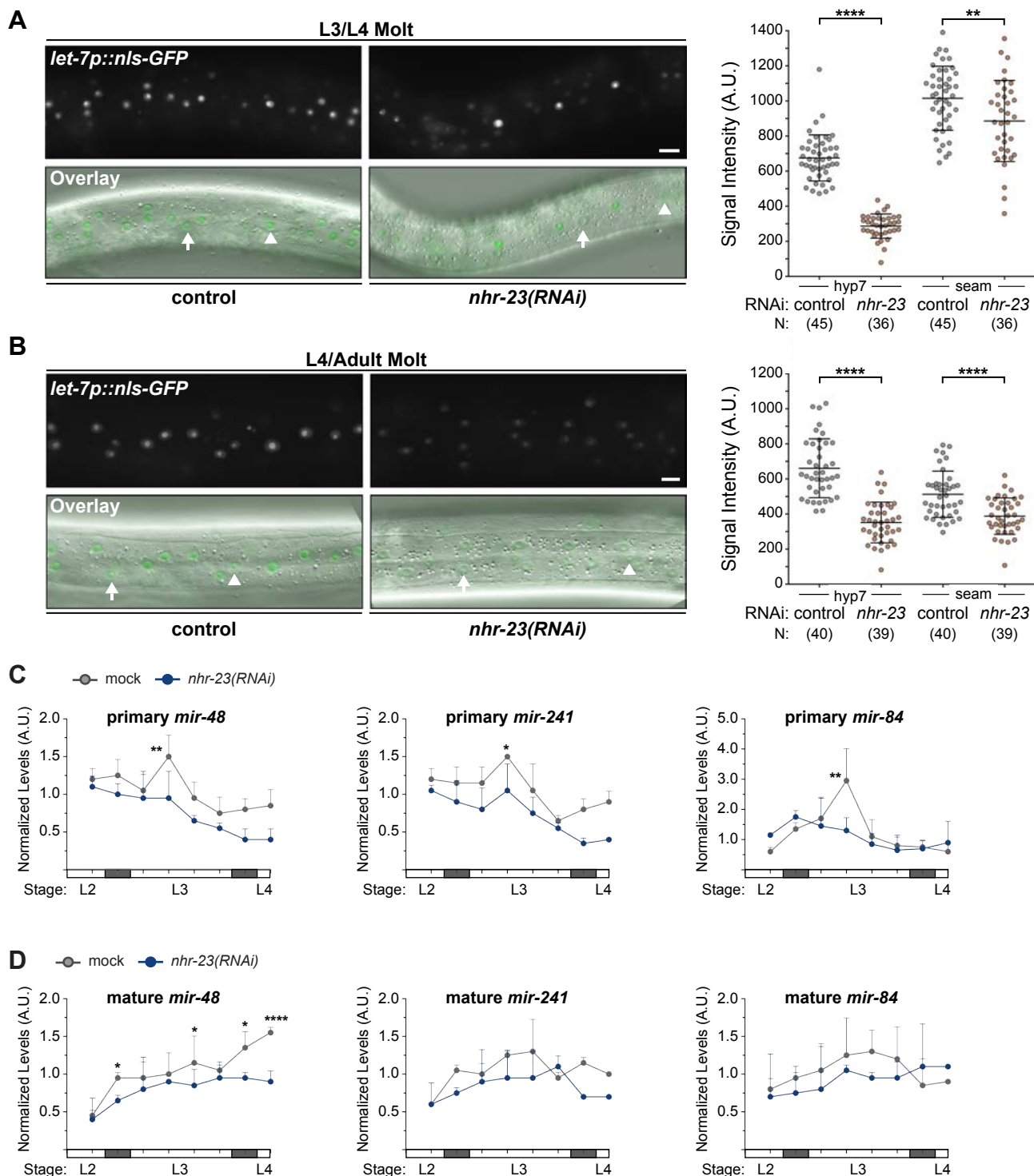
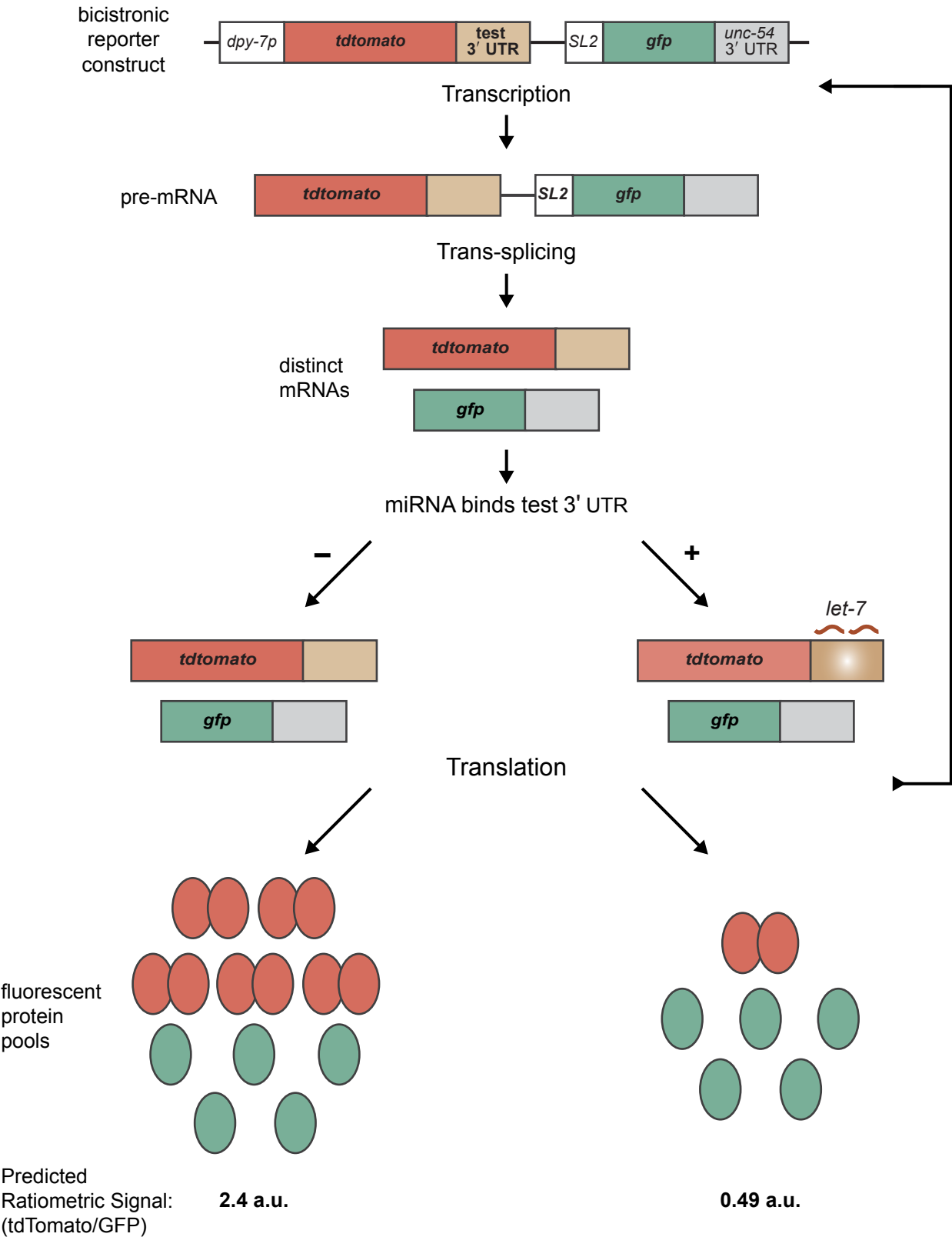


Figure 10



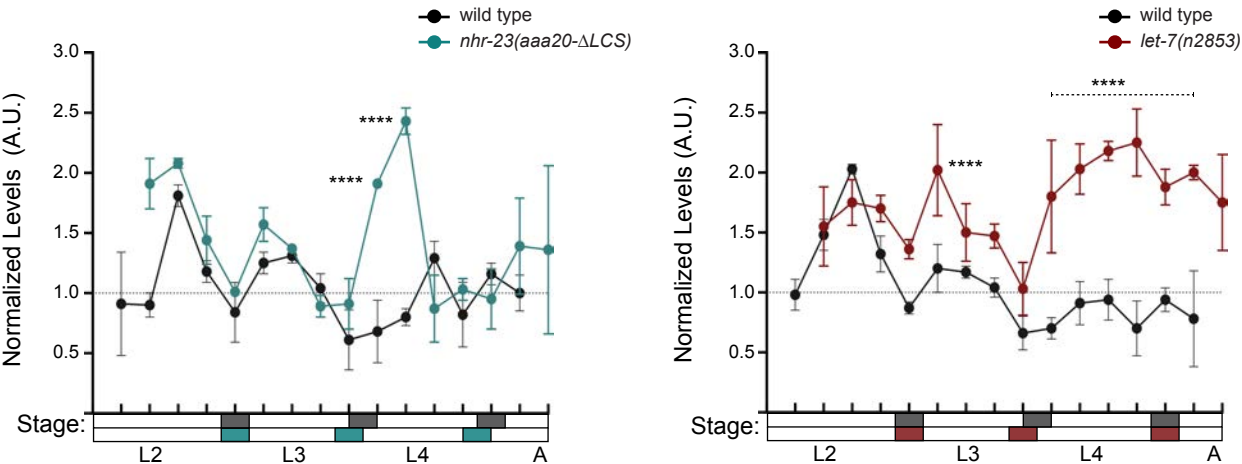






A

Oscillation of *nhr-23* Transcripts

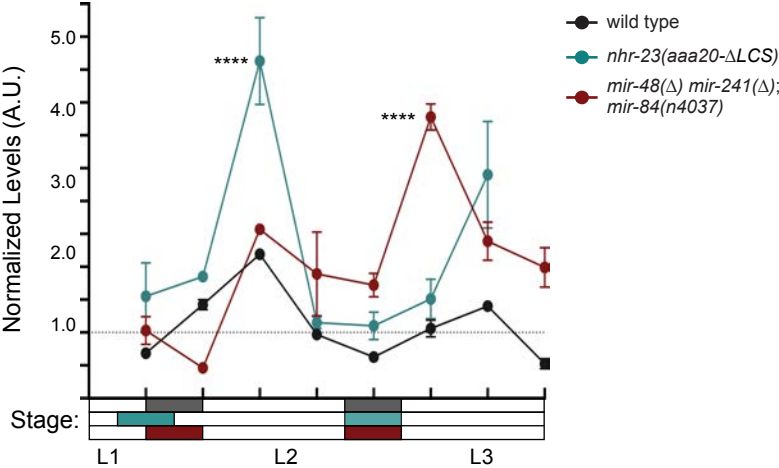


A'

Stage	L3				L4			
Genotype	wild type	<i>nhr-23(aaa20)</i>	wild type	<i>let-7(n2853)</i>	wild type	<i>nhr-23(aaa20)</i>	wild type	<i>let-7(n2853)</i>
Amplitude	0.3	0.4	0.2	0.3	0.2	0.7	0.1	0.3
Rising Slope	0.12	0.30	0.17	0.33	0.11	0.40	0.05	0.25

B

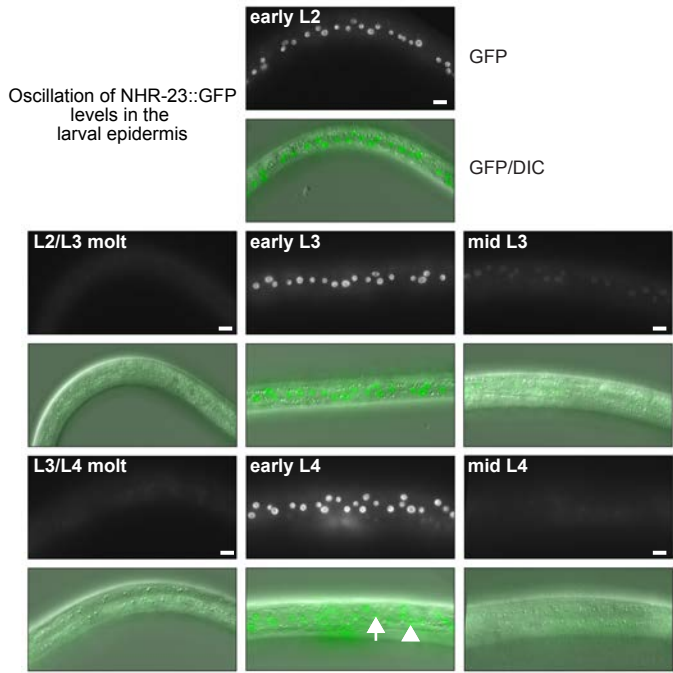
Oscillation of *nhr-23* Transcripts



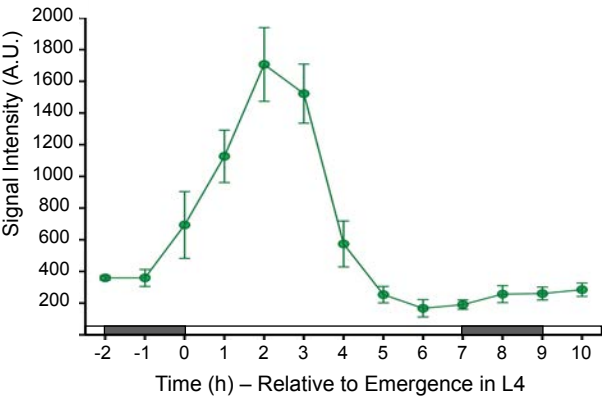
B'

Stage	L2		
Genotype	wild type	<i>nhr-23(aaa20)</i>	<i>mir-48(Δ) mir-241(Δ); mir-84(n4037)</i>
Amplitude	0.7	1.6	0.6
Rising Slope	0.38	1.64	1.10

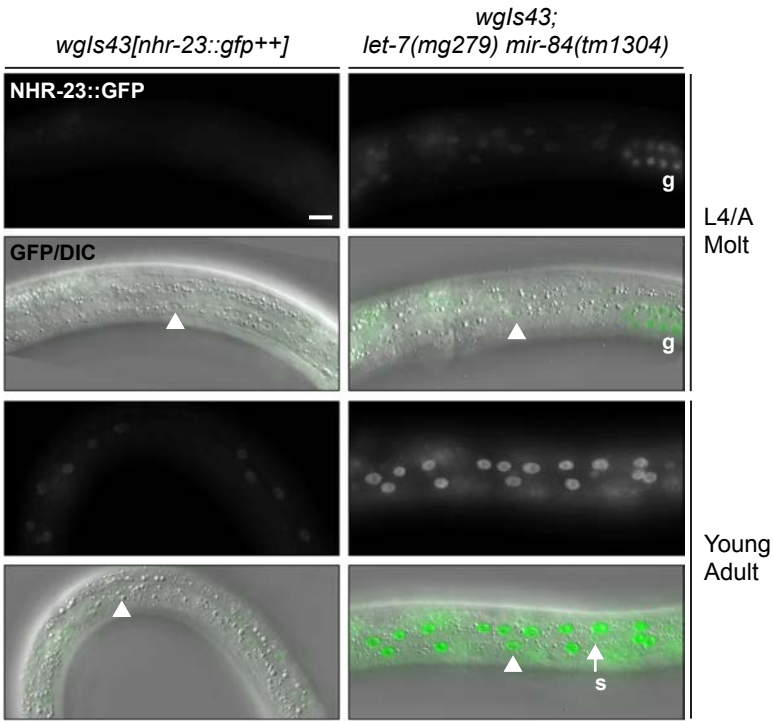
A



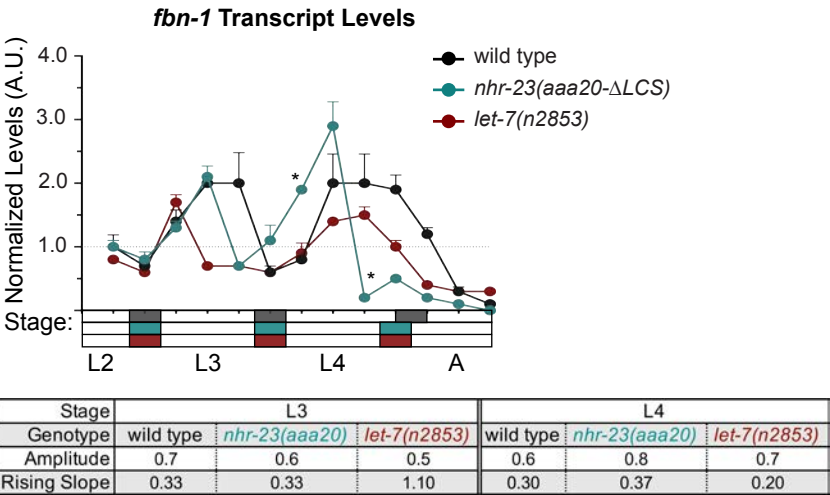
B



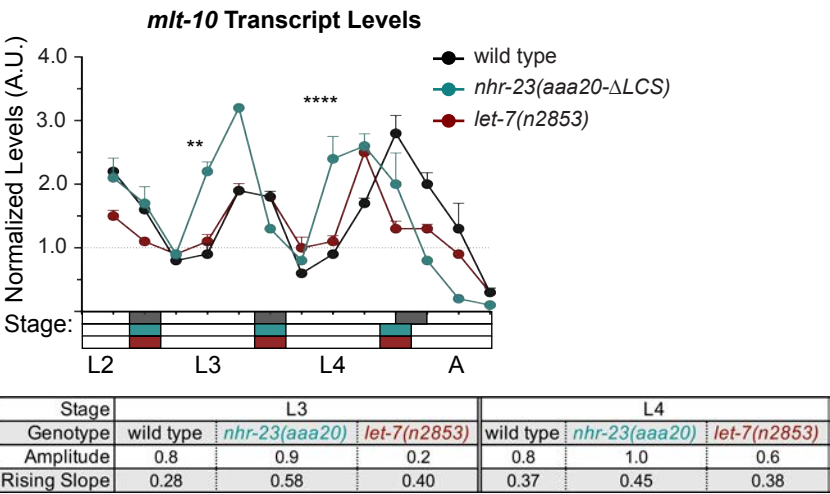
C

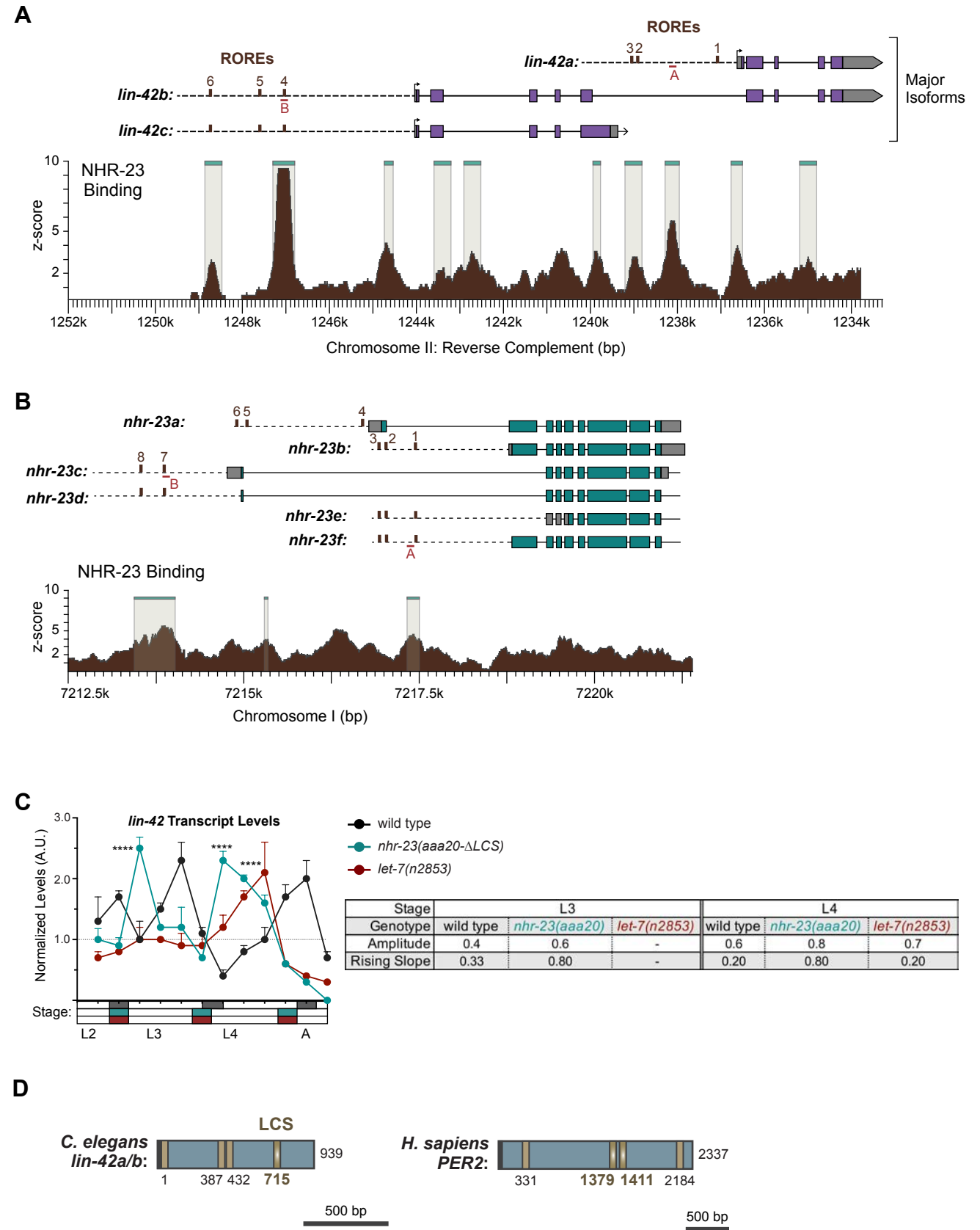


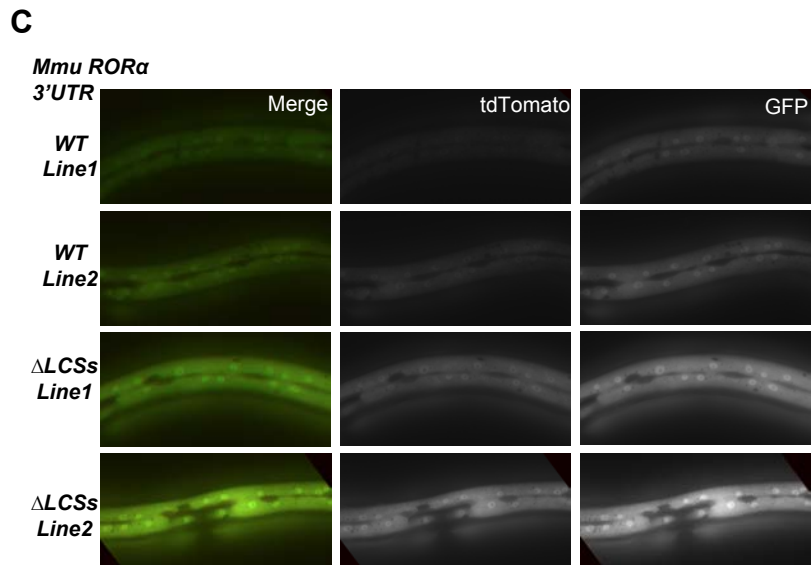
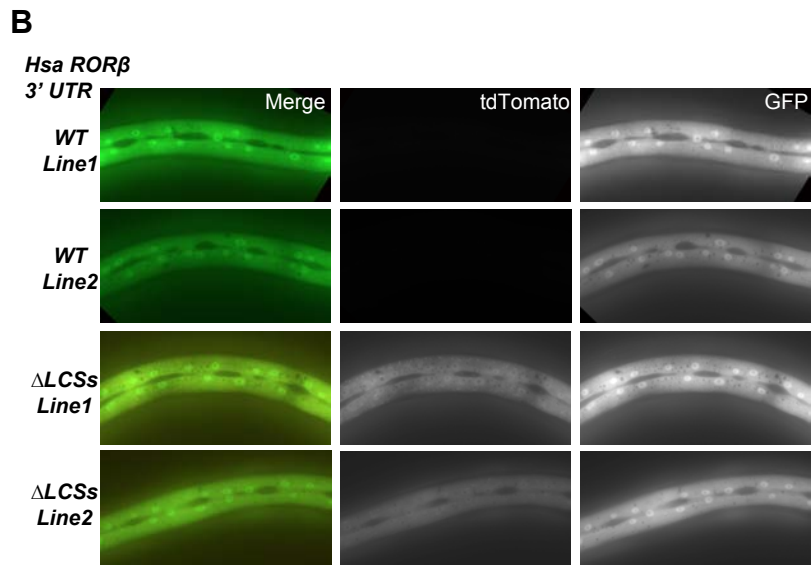
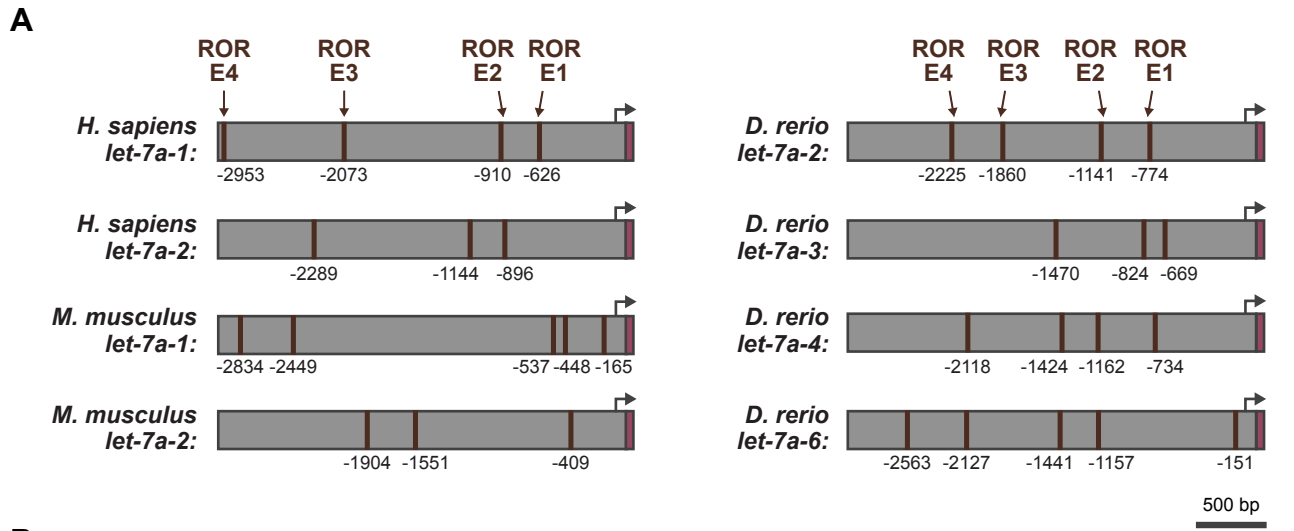
A



B







1988
1989

Supplemental Table 1 – Relates to Figures 2, 4 and 6

Metrics of the Molting Biorhythm Associated with Specific Genotypes														
			Interval (h)											
L4 stage cohort			Active				Lethargic				Wake-to-Wake			
Strain	RNAi	N	mean	sd	cv	p	mean	sd	cv	p	mean	sd	cv	p
wild type (N2)	—	16	8.1	0.5	0.06	—	2.2	0.4	0.18	—	10.3	0.4	0.05	—
wild type	<i>nhr-23</i>	17	8.4	0.8	0.09	n.s.	4.6	0.7	0.16	****	13.0	1.1	0.08	****
<i>let-7(n2853)</i>	—	15	6.3	0.4	0.08	****	1.5	0.5	0.33	*	7.9	0.6	0.08	****
<i>let-7(n2853)</i>	<i>nhr-23</i>	19	6.7	0.6	0.10	****	3.9	0.6	0.16	****	10.6	0.8	0.07	n.s.
<i>let-7(n2853)†</i>	—	17	6.7	0.6	0.09	****	1.6	0.5	0.30	**	8.4	0.6	0.07	****
wild type (GR1395)	—	20	7.8	0.5	0.07	—	2.2	0.6	0.18	—	10.0	0.5	0.05	—
<i>let-7(mg279)</i>	—	20	7.2	0.6	0.08	**	2.2	0.4	0.17	n.s.	9.3	0.6	0.06	**
<i>let-7(mg279)</i> <i>mir-84(tm1304)</i>	—	18	6.1	0.9	0.15	****	2.4	0.6	0.25	n.s.	8.5	0.9	0.15	****
wild type (N2)	—	17	7.7	0.5	0.07	—	2.0	0.0	0.00	—	9.7	0.5	0.05	—§
<i>let-7(xk41-scRORE1,2)</i>	—	12	6.9	0.7	0.10	*	1.8	0.6	0.36	n.s.	8.7	0.9	0.10	***
<i>let-7(xk44-scRORE1,2)</i>	—	8	6.6	0.5	0.08	**	2.3	0.5	0.21	n.s.	8.9	0.4	0.04	*
<i>let-7(xk39-scRORE1,3)</i>	—	17	6.5	0.6	0.10	****	2.4	0.6	0.26	n.s.	8.7	0.6	0.07	****

<i>let-7(xk42-scRORE1,3)</i>	—	14	6.6	1.1	0.17	***	2.1	0.6	0.30	n.s.	8.6	0.7	0.09	****	****
wild type (N2)	—	12	8.1	0.7	0.08	—	2.0	0.0	0.0	—	10.0	0.7	0.07	—	
<i>wgls43</i> <i>[nhr-23++]</i>	—	17	7.2	0.5	0.07	***	2.2	0.6	0.29	n.s.	9.4	0.5	0.05	**	
<i>nhr-23</i> <i>(aaa20-ΔLCS)</i>	—	25	6.8	0.7	0.1	****	2.1	0.3	0.16	n.s.	8.9	0.6	0.07	****	
L3 stage cohort			Active				Lethargic				Wake-to-Wake				
Strain	RNAi	N	mean	sd	cv	p	mean	sd	cv	p	mean	sd	cv	p	
wild type (N2)	—	17	6.3	0.4	0.07	—	1.6	0.5	0.31	—	7.9	0.7	0.08	—	
wild type	<i>nhr-23</i>	12	7.7	1.2	0.15	****	3.8	1.9	0.49	****	11.0±	1.3	0.12	****	
<i>let-7(n2853)</i>	—	18	5.6	0.6	0.11	*	1.3	0.4	0.36	n.s.	6.8	0.5	0.07	*	
<i>let-7(n2853)</i>	<i>nhr-23</i>	18	5.8	0.8	0.13	n.s.	3.8	0.6	0.17	****	9.6	0.9	0.09	****	
wild type (N2)	—	13	6.4	0.7	0.11	—	1.4	0.5	0.37	—	7.8	0.6	0.08	—	
<i>wgls43</i> <i>[nhr-23++]</i>	—	15	5.2	0.9	0.18	***	1.7	0.6	0.34	n.s.	6.9	0.6	0.09	**	
<i>nhr-23</i> <i>(aaa20-ΔLCS)</i>	—	19	5.1	0.7	0.14	***	1.2	0.5	0.44	n.s.	6.3	0.7	0.11	****	
L2 stage cohort			Active				Lethargic				Wake-to-Wake				
Strain	RNAi	N	mean	sd	cv	p	mean	sd	cv	p	mean	sd	cv	p	
wild type (N2)	—	18	5.9	0.3	0.05	—	1.3	0.5	0.36	—	7.2	0.4	0.06	—	
wild type	<i>nhr-23</i>	19	6.1	0.6	0.10	n.s.	3.9	1.1	0.28	****	9.9	1.0	0.10	****	

<i>mir-48 mir-241</i> (<i>nDf51</i>); <i>mir-84(n4037)</i>	—	17	6.3	0.7	0.11	n.s.	1.3	0.5	0.36	n.s.	7.6	0.7	0.10	n.s.
<i>mir-48 mir-241</i> (<i>nDf51</i>); <i>mir-84(n4037)</i>	<i>nhr-23</i>	15	6.4	0.8	0.13	n.s.	3.0	0.4	0.13	****	9.4	0.8	0.09	****

†Entry for the L3 cohort fortuitously observed throughout L4 and depicted by the penultimate actogram in Figure 2C.

‡Value excludes the one and only *nhr-23(RNAi)* larvae that remained lethargic at the final time-sample.

§ p-values of wake-to-wake interval by Mann-Whitney Test

Supplemental Table 2 – Relates to Figures 5 and 10

<i>let-7</i> Consensus Sites (LCSs) Identified in 3' UTRs of Selected Nematode and Vertebrate Homologs of <i>ROR</i>						
Species	Gene	Identifier	3' UTR Length (nt.)	LCS Position (3' nt.)	TS (kcal/mol)	Alignment of LCS (5' to 3') with <i>let-7</i> (3' to 5')
<i>C. elegans</i>	<i>nhr-23</i>	NM_001025806	868	42	-21.8	5' UU C UG — — C 3' UUAU CA CU CU CCUU GAUA GU GA GA GGAG 3' UU U UG U U 5'
				249	-15.2	5' U U GAG G U 3' G CUG UGCAG A U CCUCA U GAU AUGUU U A GGAGU 3' U — GGA G U 5'
				594	-17.0	5' UUAA CU CCAUU U 3' AUAU CC UAUGCCUU UAUG GG AUGAUGGAG 3' UUGA UU ——— U 5'
				646	-17.6	5' C UUAAU — UC — U 3' GCU UAC GCCU UUACC CA UGA AUG UGGA GAUGG GU 3' U ——— U — A 5'
<i>C. briggsae</i>	<i>nhr-23</i>	WBGene 00040598	866	629	-20.7	5' UU C CGCU U C 3' C AUACAACU CUGC CUC G UAUGUUGG GAUG GAG 3' UU A AU — U 5'
				835	-21.8	5' UUAC CUUUUUU C 3' AUUAUAUCU CUGCCUC UAUGUUGGA GAUGGAG 3' UUGA U ——— U 5'
<i>H. sapiens</i>	<i>RORβ</i>	NM_006914	7559	3576	-25.9	5' GGCU CGC UGCAAUCU CUGCCUC C 3' UUGA U — AUGUUGGA GAUGGAG 3' U — U — U 5'
				4055	-23.1	5' U A UUU AUCAUA G 3' G C GUACA CCU GCUGCCUU U G UAUGU GGA UGAUGGAG 3' U A U ——— U 5'
				4961	-23.1	5' C — A U 3' GAU GU CAGCUUGC GCCUC UUG UA GUUGGAUG UGGAG 3' A U A U 5'
<i>M. musculus</i>	<i>RORβ</i>	NM_146095	7271	3817	-23.8	5' A GC CU U 3' GG UG CAACU UACUGCCUC UU AU GUUGG AUGAUGGAG 3' G AU — U 5'
				5242	-22.7	5' AACUA GUCACA GAUGCUUC G 3' UUGAU A ——— AU ——— GAUGGA 3' A ——— U ——— GU 5'
				6675	-26.7	5' AG — C 3' GA GUACAGCUUGC CCUC UU UAUGUUGGAUGA GGAG 3' GA U U 5'
<i>D. rerio</i>	<i>RORβ</i>	NM_001082856	5431	949	-21.8	5' AA C U — U 3' U AUAU UCUGCUGCCUU G UAUG GGAUGAUGGAG 3' UU A UU U 5'
				4318	-23.8	5' U UUGUACA AAAAAUAAA G 3' U GAUAUGU ——— UGG ACUACUUA 3' U ——— A UGAUGGAGU 5'
				4421	-23.3	5'U ACACAGGCAAAACA AUCA U 3' GCUAUUU GAC UACUGCCUU UGAUAUG UUG AUGAUGGAG 3'U ——— G ——— U 5'
<i>H. sapiens</i>	<i>RORα</i>	NM_134261	9171	3079	-23.7	5' C — CC A 3' ACUGU CAGCC GCUGCU CA UGAUA GUUGG UGAUGG GU 3' U U A — A 5'
				3142	-22.8	5' UU AA AA C 3' UUGUACA GCCUG UACCUU GAUAUGU UGGAU AUGGAG 3' UU — G — U 5'
				6480	-24.0	5' C UGUCU — U 3' A CUGUAU GCCUGCU CCUU U GAUAUG UGGAUGA GGAG 3' U U ——— U 5'
				8321	-22.2	5' U AAUC UCAUU UA U 3' A ACA CCU ACUGCCUC U UGU GGA UGAUGGAG 3' U GAUA U ——— — 5'

<i>M. musculus</i>	<i>RORα</i>	NM_013646	9285	2055	-23.9	5' CC CJ AUGUA C A GCUGCCUC C 3' 3' UU GAUAUGU U GG UGAUGGAG U 5'
				2184	-23.7	5' AACU UAC GACUU CUGCCUUA 3' 3' UUGA U UUGGA GAUGGAGU 5'
				4913	-22.6	5' C A GUGCAGCC CAUC G C 3' 3' U A UAUUUUGG ---- AUGAU GAG U 5'

Supplemental Table 3 – Relates to Figures 5, 7, 8 and Supplemental Figures 6 and 7

Comparisons among wild type, <i>nhr-23(aaa20)</i> and <i>let-7(n2853)</i>								
Transcript: <i>nhr-23</i>								
Stage	Replicate 1							
	L3				L4			
Genotype	wild type	<i>nhr-23 (aaa20)</i>	wild type	<i>let-7 (n2853)</i>	wild type	<i>nhr-23 (aaa20)</i>	wild type	<i>let-7 (n2853)</i>
Amplitude	0.4	1.1	0.5	0.9	0.3	0.4	0.1	0.8
Phase	3.2	2.4	3.2	3.0	0.4	3.2	0.04	3.8
Rising Slope	0.19	0.46	0.15	0.71	0.19	0.21	0.11	0.26
Falling Slope	0.50	0.49	0.36	0.45	0.21	0.19	0.20	0.38
Peak Value	1.78	2.93	1.69	2.84	1.14	1.81	1.18	2.65
Stage	Replicate 2							
	L3				L4			
Genotype	wild type	<i>nhr-23 (aaa20)</i>	wild type	<i>let-7 (n2853)</i>	wild type	<i>nhr-23 (aaa20)</i>	wild type	<i>let-7 (n2853)</i>
Amplitude	0.3	0.4	0.2	0.3	0.2	0.7	0.1	0.3
Phase	3.1	2.1	4.5	2.0	5.3	4.0	4.5	4.8
Rising Slope	0.12	0.30	0.17	0.33	0.11	0.40	0.05	0.25
Falling Slope	0.14	0.17	0.10	0.14	0.24	0.39	0.12	0.19
Peak Value	1.31	1.57	1.17	2.02	1.30	2.43	0.94	2.25
Transcript: <i>fbn-1</i>								
Stage	Replicate 1							
	L3			L4				
Genotype	wild type	<i>nhr-23 (aaa20)</i>	<i>let-7 (n2853)</i>	wild type	<i>nhr-23 (aaa20)</i>	<i>let-7 (n2853)</i>		
Amplitude	1.4	3.0	2.1	1.2	1.7	1.9		
Phase	2.1	2.4	2.8	3.6	2.9	2.9		
Rising Slope	0.73	1.56	1.85	0.78	1.45	2.35		
Falling Slope	0.64	1.59	1.02	0.60	1.00	0.91		
Peak Value	3.65	7.15	5.19	4.24	6.63	5.94		
Stage	Replicate 2							
	L3			L4				

Genotype	wild type	<i>nhr-23</i> (<i>aaa20</i>)	<i>let-7</i> (<i>n2853</i>)	wild type	<i>nhr-23</i> (<i>aaa20</i>)	<i>let-7</i> (<i>n2853</i>)
Amplitude	0.7	0.6	0.5	0.6	0.8	0.7
Phase	2.2	1.5	1.6	6.3	4.6	5.2
Rising Slope	0.33	0.33	1.10	0.30	0.37	0.20
Falling Slope	0.70	0.70	0.50	0.40	1.35	0.28
Peak Value	1.90	2.10	1.70	2.00	2.90	1.50

Transcript: *mlt-10*

Replicate 1						
Stage	L3			L4		
	wild type	<i>nhr-23</i> (<i>aaa20</i>)	<i>let-7</i> (<i>n2853</i>)	wild type	<i>nhr-23</i> (<i>aaa20</i>)	<i>let-7</i> (<i>n2853</i>)
Genotype	wild type	<i>nhr-23</i> (<i>aaa20</i>)	<i>let-7</i> (<i>n2853</i>)	wild type	<i>nhr-23</i> (<i>aaa20</i>)	<i>let-7</i> (<i>n2853</i>)
Amplitude	1.0	2.3	2.2	1.0	2.8	2.4
Phase	5.4	4.9	5.1	6.2	5.0	4.9
Rising Slope	0.46	1.95	1.76	0.51	1.91	2.10
Falling Slope	0.88	0.95	0.65	0.30	0.69	0.63
Peak Value	3.95	4.36	4.56	1.92	4.31	5.17

Replicate 2						
Stage	L3			L4		
	wild type	<i>nhr-23</i> (<i>aaa20</i>)	<i>let-7</i> (<i>n2853</i>)	wild type	<i>nhr-23</i> (<i>aaa20</i>)	<i>let-7</i> (<i>n2853</i>)
Genotype	wild type	<i>nhr-23</i> (<i>aaa20</i>)	<i>let-7</i> (<i>n2853</i>)	wild type	<i>nhr-23</i> (<i>aaa20</i>)	<i>let-7</i> (<i>n2853</i>)
Amplitude	0.8	0.9	0.2	0.8	1.0	0.6
Phase	2.7	1.5	2.8	8.6	6.6	6.3
Rising Slope	0.28	0.58	0.40	0.37	0.45	0.38
Falling Slope	0.60	0.60	0.23	0.38	0.40	0.35
Peak Value	1.80	3.20	1.90	2.80	2.60	2.50

Transcript: *lin-42*

Replicate 1						
Stage	L3			L4		
	wild type	<i>nhr-23</i> (<i>aaa20</i>)	<i>let-7</i> (<i>n2853</i>)	wild type	<i>nhr-23</i> (<i>aaa20</i>)	<i>let-7</i> (<i>n2853</i>)
Genotype	wild type	<i>nhr-23</i> (<i>aaa20</i>)	<i>let-7</i> (<i>n2853</i>)	wild type	<i>nhr-23</i> (<i>aaa20</i>)	<i>let-7</i> (<i>n2853</i>)
Amplitude	0.6	1.7	1.5	0.8	1.6	1.2
Phase	4.5	3.9	4.2	5.4	4.8	4.7















Rising Slope	0.20	0.93	0.78	0.27	0.70	0.53	
Falling Slope	0.30	0.86	0.78	0.37	0.52	0.44	
Peak Value	2.12	4.15	3.88	2.50	3.48	2.94	
Stage	Replicate 2						
	L3			L4			
	wild type	<i>nhr-23</i> (<i>aaa20</i>)	<i>let-7</i> (<i>n2853</i>)	wild type	<i>nhr-23</i> (<i>aaa20</i>)	<i>let-7</i> (<i>n2853</i>)	
	Amplitude	0.4	0.6	-	0.6	0.8	0.7
	Phase	1.9	0.3	-	6.20	4.10	5.00
	Rising Slope	0.33	0.80	-	0.20	0.80	0.20
	Falling Slope	0.48	0.30	-	0.65	0.28	0.30
	Peak Value	2.30	2.50	-	2.00	2.30	2.10
Comparisons between vector and <i>nhr-23</i> (RNAi)							
Transcript: <i>fbn-1</i>							
Stage	L3		L4				
	RNAi	mock	<i>nhr-23</i> (RNAi)	mock	<i>nhr-23</i> (RNAi)		
	Amplitude	0.7	0.2	1.0	0.2		
	Phase	2.0	2.0	1.9	2.1		
	Rising Slope	0.68	0.14	0.40	0.30		
	Falling Slope	0.21	0.15	0.42	0.12		
	Peak Value	1.85	0.90	2.80	1.20		
Transcript: <i>mlt-10</i>							
Stage	L3		L4				
	RNAi	mock	<i>nhr-23</i> (RNAi)	mock	<i>nhr-23</i> (RNAi)		
	Amplitude	0.7	0.5	0.7	0.5		
	Phase	5.9	6.1	4.9	4.9		
	Rising Slope	0.36	0.08	0.40	0.10		
	Falling Slope	0.58	0.20	0.33	0.15		
	Peak Value	2.10	0.80	1.90	0.80		
Transcript: <i>lin-42</i>							

























Stage	L3		L4	
RNAi	mock	<i>nhr-23</i> (RNAi)	mock	<i>nhr-23</i> (RNAi)
Amplitude	0.7	0.5	0.6	0.2
Phase	3.2	5.3	4.8	4.1
Rising Slope	0.35	0.15	0.60	0.10
Falling Slope	0.33	0.25	0.50	0.15
Peak Value	2.10	1.30	1.80	0.70

















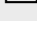






Comparisons among wild type, <i>nhr-23(aaa20)</i> and <i>mir-48 mir-241(nDf51); mir-84(n4037)</i>			
Transcript: <i>nhr-23</i>			
Stage	L2		
Genotype	wild type	<i>nhr-23</i> (<i>aaa20</i>)	<i>mir-48</i> <i>mir-241</i> (<i>nDf51</i>); <i>mir-84</i> (<i>n4037</i>)
Amplitude	0.7	1.6	0.6
Phase	1.8	2.0	1.6
Rising Slope	0.38	1.64	1.10
Falling Slope	0.39	2.00	0.21
Peak Value	2.20	5.10	2.60








Supplemental Table 4 – relates to Figures 8 and 9

Supplemental Table 1. Related to Figures 6 and 7

Classification of Clock-Controlled Genes (CCGs) as Direct Targets of NHR-23, <i>let-7s</i> , neither or both.														
Gene Name	Sequence	Criteria for targets of NHR-23:					NHR-23 target (Y/N)	Criteria for targets of <i>let-7s</i> :				<i>let-7s</i> target (Y/N)	Target class	Cyclic mRNA levels ()
		Size of upstream regulatory region & first intron (kb)	ROREs		mRNA levels after <i>nhr-23</i> RNAi	NHR-23 ChIP-Seq Peaks (#)		Size of 3' UTR (nt.)	LCSs		ALG-1 iCLIP Peaks (+/-)			
			#	# Obs. / # Exp.					#	# Obs. / # Exp.				
Potential Key Clock Components														
<i>let-7</i>	C05G5.6	1.5	3	5.8	↓	1	Y	N/A	–	–	–	N/A	NHR-23	
<i>lin-42a</i>	F47F6.1	3.7	3	2.3	↓	4	Y	939	4	3.2	+	Y	Shared	
<i>lin-42b</i>	F47F6.1	5.5	3	1.6	↓	3	Y	939	4	3.2	+	Y	Shared	
<i>lin-42c</i>	F47F6.1	5.5	3	1.6	↓	3	Y	156	0	0.0	–	N	NHR-23	
<i>mir-48</i>	F56A12.3	1.7	2	3.4	–	1	Y	N/A	–	–	–	N/A	NHR-23	
<i>mir-241</i>	F56A12.4	2.0	2	2.9	–	2	Y	N/A	–	–	–	N/A	NHR-23	
<i>mir-84</i>	B0395.4	2.8	1	1.1	–	2	Y	N/A	–	–	–	N/A	NHR-23	
<i>nhr-23</i>	C01H6.5	6.1	8	3.8	↓	3	Y	868	4	2.6	+	Y	Shared	
<i>nhr-25</i>	F11C1.6	6.9	3	1.3	–	3	Y	749	1	1.0	+	Y	Shared	
Other Gene Regulatory Factors														
<i>alg-1</i>	F48F7.1	9.9	1 / 1	3.2	–	3	Y	400	1	1.9	+	Y	Shared	
<i>bed-3</i>	F25H8.6	1.7	2	3.4	–	1	Y	459	1	1.6	+	Y	Shared	
<i>blmp-1</i>	F25D7.3	6.7	7	3.0	–	4	Y	861	3	2.6	+	Y	Shared	
<i>bro-1</i>	F56A3.5	1.2	0	0.0	–	1	N	379	1	2.0	–	N	–	

<i>dre-1</i>	K04A8.6	7.5	8	3.1	–	4	Y	376	2	4.0	+	Y	Shared	
<i>mab-10</i>	R166.1	6.0	8	3.9	–	2	Y	374	1	2.0	–	N	NHR-23	
<i>nhr-41</i>	Y104H12A.1	11.1	2 3	6.0	–	2	Y	332	1	2.3	–	N	NHR-23	
<i>pqn-47</i>	F59B10.1	5.9	7	3.4	–	5	Y	804	2	1.9	+	Y	Shared	
<i>rnt-1</i>	B0414.2	9.2	4	1.3	–	0	N	221	0	0.0	–	N	–	
Signaling Pathway Components														
<i>acn-1</i>	C42D8.5	4.0	4	2.9	↓	3	Y	384	1	2.0	+	Y	Shared	
<i>apl-1</i>	C42D8.8	4.9	4	2.4	–	5	Y	678	1	1.1	+	Y	Shared	
<i>calu-1</i>	M03F4.7	1.7	3	5.1	–	3	Y	256	1	3.0	+	Y	Shared	
<i>cki-1</i>	T05A6.1	1.9	2	3.1	–	1	Y	235	2	6.5	+	Y	Shared	
<i>glf-1</i>	H04M03.4	2.4	1	1.2	↓	1	Y	247	2	6.2	–	N	NHR-23	
<i>lon-1</i>	F48E8.1	4.8	3	1.8	–	5	Y	185	2	8.3	+	Y	Shared	
<i>lrp-1</i>	F29D11.1	7.9	3	1.1	–	6	Y	346	2	4.4	+	Y	Shared	
<i>mlt-8</i>	W08F4.6	3.5	2	1.7	↓	1	Y	270	2	5.6	+	Y	Shared	
<i>nekl-2</i>	ZC581.1	1.1	1	2.6	–	0	N	73	0	0.0	–	N	–	
<i>nlp-22</i>	T24D8.3	0.8	0	0.0	–	0	N	1000	2	1.5	–	N	–	
<i>osm-7</i>	T05D4.4	3.5	1	0.8	–	0	N	121	1	6.5	+	Y	<i>let-7s</i>	
<i>osm-11</i>	F11C7.5	2.8	1	1.1	–	3	Y	545	4	5.5	+	Y	Shared	
<i>phi-59</i>	T19B10.2	1.5	0	0.0	↓	1	Y	121	1	6.5	+	Y	Shared	
<i>pod-2a</i>	W09B6.1	3.0	4	3.9	–	2	Y	324	1	2.3	–	N	NHR-23	
<i>ptr-4</i>	C45B2.7	4.5	4	2.6	↓	2	Y	221	2	6.9	–	N	NHR-23	
<i>ptr-23</i>	ZK270.1	2.0	0	0.0	–	2	N	311	3	7.3	+	Y	<i>let-7s</i>	
<i>qua-1</i>	T05C12.10	5.7	3	1.5	↓	4	Y	340	1	2.2	+	Y	Shared	
	E03H4.8	3.4	1	0.9	–	0	N	307	1	2.5	–	N	–	
	T19A5.3	4.9	2	1.2	↓	2	Y	347	1	2.2	+	Y	Shared	

	Y47D3B.1	4.9	3	1.8	–	1	Y	98	1	8.1	–	N	NHR-23	
Extracellular Matrix Proteins and Receptors														
<i>adt-2</i>	F08C6.1	7.6	7	2.7	–	6	Y	621	1	1.2	+	Y	Shared	
<i>bli-5</i>	F45G2.5	1.4	0	0.0	–	0	N	300	1	2.5	+	Y	<i>let-7s</i>	
<i>bus-8</i>	T23F2.1	3.6	0	0.0	↓	0	N	453	2	3.3	–	N	–	
<i>clc-1</i>	C09F12.1	5.4	0	0.0	–	0	N	101	1	7.8	–	N	–	
<i>col-12</i>	F15H10.1	0.7	0	0.0	–	0	N	101	1	7.8	+	Y	<i>let-7s</i>	
<i>dpy-13</i>	F30B5.1	3.8	5	3.8	–	4	Y	63	2	26.1	+	Y	Shared	
<i>dpy-17</i>	F54D8.1	0.4	1	7.3	–	0	N	54	1	15.5	–	N	–	
<i>dpy-4</i>	Y41E3.2	2.4	0	0.0	–	1	N	102	1	7.8	+	Y	<i>let-7s</i>	
<i>dpy-5</i>	F27C1.8	0.8	1	3.6	↓	1	Y	39	0	0.0	–	N	NHR-23	
<i>dpy-7</i>	F46C8.6	0.7	2	8.3	↓	1	Y	236	1	3.2	–	N	NHR-23	
<i>fbn-1</i>	ZK783.1	8.3	1 2	4.2	↓	6	Y	457	1	1.7	+	Y	Shared	
<i>ina-1</i>	Y116A8A.9	8.0	8	2.9	–	2	Y	261	1	2.9	+	Y	Shared	
<i>mam-1</i>	ZC13.3	3.8	3	2.3	–	0	N	243	0	0.0	–	N	–	
<i>mlt-10</i>	C09E8.3	8.6	4	1.3	↓	1	Y	139	2	11.2	+	Y	Shared	
<i>mlt-11</i>	W01F3.3	5.2	1 1	6.1	↓	4	Y	353	1	2.1	+	Y	Shared	
<i>mlt-7</i>	ZK430.8	11.5	1 5	3.8	–	1	Y	317	2	4.8	+	Y	Shared	
<i>mlt-9</i>	F09B12.1	3.5	1	0.8	↓	5	Y	313	1	2.4	–	N	NHR-23	
<i>mup-4</i>	K07D8.1	5.8	5	2.5	–	2	Y	394	0	0.0	–	N	NHR-23	
<i>nas-36</i>	C26C6.3	1.1	1	2.6	↓	0	Y	327	5	11.6	+	Y	Shared	
<i>nas-37</i>	C17G1.6	3.6	7	5.6	↓	2	Y	240	4	12.7	–	N	NHR-23	
<i>noah-1</i>	C34G6.6	7.9	9	3.3	↓	5	Y	550	1	1.4	+	Y	Shared	
<i>noah-2</i>	F52B11.3	8.9	3	1.0	↓	6	Y	316	2	4.8	+	Y	Shared	

<i>pan-1</i>	M88.6	2.5	2	2.3	–	2	Y	393	2	3.8	+	Y	Shared	
<i>pat-2</i>	F54F2.1	4.0	4	2.9	–	2	Y	292	2	5.2	+	Y	Shared	
<i>rol-6</i>	T01B7.7	3.4	2	1.7	↓	4	Y	117	1	6.7	+	Y	Shared	
<i>pat-3</i>	ZK1058.2	5.0	0	0.0	–	2	N	400	1	1.9	+	Y	<i>let-7s</i>	
Cytoskeletal Components														
<i>ifa-2</i>	W10G6.3	1.7	1	1.7	–	1	Y	186	2	8.3	–	N	Shared	
<i>ifc-2</i>	M6.1	3.0	0	0.0	–	0	N	536	2	2.8	+	Y	<i>let-7s</i>	
<i>nmy-2</i>	F20G4.3	1.8	6	9.7	–	1	Y	448	2	3.4	+	Y	Shared	
Genes linked to the molting cycle whose expression is not known to oscillate														
<i>daf-9</i>	T13C5.1	1.1	0	0.0	↓	1	Y	214	2	7.2	+	Y	Shared	–
<i>daf-12</i>	F11A1.3	17.0	1 2	2.0	–	7	Y	1393	5	2.7	+	Y	Shared	–
<i>gei-8</i>	C14B9.6	1.8	1	1.6	–	3	Y	449	4	6.7	+	Y	Shared	–
<i>let-767</i>	C56G2.6	0.6	1	4.8	–	1	Y	87	1	9.2	+	Y	Shared	–
<i>lin-3</i>	F36H1.4	5.5	5	1.9	–	0	N	442	5	8.5	+	Y	<i>let-7s</i>	–
<i>nhr-67</i>	C08F8.8	5.5	5	2.6	–	0	N	241	3	9.5	–	N	–	–
<i>skn-1</i>	T19E7.2	5.1	2	1.1	–	2	Y	677	1	1.1	+	Y	Shared	–
Non-CCGs (Randomly Selected)														
<i>acs-13</i>	Y65B4BL.5	4.9	3	1.8	–	2	Y	424	1	1.8	+	Y	Shared	–
<i>ced-8</i>	F08F1.5	0.7	0	0.0	–	0	N	85	0	0.0	–	N	–	–
<i>cyp-33C12</i>	Y5H2B.6	1.5	0	0.0	–	0	N	148	0	0.0	–	N	–	–
<i>ech-5</i>	F56B3.5	0.5	0	0.0	–	1	N	602	1	1.2	–	N	–	–
<i>map-2</i>	Y116A8A.9	1.5	1	1.9	–	0	N	274	2	5.6	–	N	–	–
<i>mpst-7</i>	R186.6	1.0	0	0.0	–	1	N	84	0	0.0	+	N	–	–
<i>nhr-176</i>	F14H3.11	0.2	0	0.0	–	0	N	54	1	15.5	–	N	–	–

<i>nlp-37</i>	F48B9.4	2.9	3	3.0	–	0	N	302	2	5.0	–	N	–	–
<i>nuo-2</i>	T10E9.7	0.2	0	0.0	–	1	N	109	1	14.5	–	N	–	–
<i>srz-10</i>	ZK1037.11	1.1	1	2.6	–	0	N	16	0	0.0	–	N	–	–
<i>ttl-12</i>	D2013.9	0.1	0	0.0	–	0	N	175	1	4.4	+	Y	<i>let-7s</i>	–
<i>unc-112</i>	C47E8.7	2.8	1	1.1	–	1	Y	295	1	2.6	+	Y	Shared	–
<i>viln-1</i>	C10H11.1	7.0	3	1.1	–	0	N	119	2	13.2	–	N	–	–
	C01G6.9	0.1	0	0.0	–	0	N	76	1	10.6	–	N	–	–
	F44E5.5	0.4	0	0.0	–	1	N	39	0	0.0	–	N	–	–
	R10E8.6	1.3	0	0.0	–	0	N	31	0	0.0	–	N	–	–
	R12B2.2	0.5	0	0.0	–	0	N	115	0	0.0	–	N	–	–
	T06D4.1	2.3	3	3.8	–	0	N	234	0	0.0	–	N	–	–
	W02D7.3	2.0	1	1.3	–	0	N	78	0	0.0	–	N	–	–
	Y53C10A.6	6.3	0	0.0	–	0	N	201	2	7.6	–	N	–	–

Supplemental Table 5. Oligonucleotides used in this study

PCR Primer	Nucleotide Sequence (5' to 3')	Application
HM01	GAAGAACGCCTCACCGAAGGAAGGAAGCATGCGGGATTGGCCAAAGGACCCAAAGGTATGTTT CGAATGATACTAACATAACATAGAACATTTTCAGGAGGACCCTTGGAGGGTAGAAAAAATGGTG AGCAAGGGCGAGGAGGTCATCAAAG	Construction of the bicistronic reporter for <i>cis</i> -regulatory elements in the 3' UTR of <i>unc-54</i> (pHR011 and <i>aaaEx97</i>)
<i>SL2::GFP</i> :: <i>unc-54</i> cassette	GCTGTCTCATCCTACTtcacctagtttaactgcttgctttaaactctatgcttctcttagtatctaaaatttcctagaagcttacaagtatat aaatgggtctctctcaataaagggtgtatatttattcatcttattgaatctgccatttcctcgttttgtaggtttatataacctccaattttcttctattgtattt caacttctaattttaattcagggaaactgctgTACCGGTAGAAAAAATGAGTAAAGGAGAAGAACTTTTCACTGGA GTTGTCCCAATTCTTGTTGAATTAGATGGTGATGTTAATGGGCACAAATTTTCTGTCAGTGGAGA GGGTGAAGGTGATGCAACATACGGAAAACTTACCCTTAAATTTATTTGCACTACTGGAAAACTAC CTGTTCCATGGGTAAAGTTTAAACATATATATACTAACTAACCCTGATTATTTAAATTTTCAGCCAA CACTTGTCACTACTTTCTGTTATGGTGTTCAATGCTTCTCGAGATACCCAGATCATATGAAACGG CATGACTTTTTCAAGAGTGCCATGCCCGAAGGTTATGTACAGGAAAGAACTATATTTTTCAAAGA TGACGGGAACCTACAAGACACGTAAGTTTAAACAGTTCGGTACTAACTAACCATACATATTTAAAT TTTCAGGTGCTGAAGTCAAGTTTGAAGGTGATACCCTTGTTAATAGAATCGAGTTAAAAGGTATT GATTTTAAAGAAGATGGAACATTCTTGACACAAATTGGAATACAACCTATAACTCACACAATGTA TACATCATGGCAGACAAACAAAAGAATGGAATCAAAGTTGTAAGTTTAAACATGATTTTACTAACT AACTAATCTGATTTAAATTTTCAGAACTTCAAATTAGACACAACATTGAAGATGGAAGCGTTCAA CTAGCAGACCATTATCAACAAAATACTCCAATTGGCGATGGCCCTGTCCTTTTACCAGACAACCA TTACCTGTCCACACAATCTGCCCTTTCGAAAGATCCCAACGAAAAGAGAGACCACATGGTCCTT CTTGAGTTTGTAACAGCTGCTGGGATTACACATGGCATGGATGAACTATACAAATAGgagctcCGC ATCGGCCGCTGTCATCAGATCGCCATCTCGCGCCCGTGCCTCTGACTTCTAAGTCCAATTACTC TTCAACATCCCTACATGCTCTTCTCCCTGTGCTCCCACCCCTATTTTTGTTATTATCAAAAAA CTTCTTCTTAATTTCTTTGTTTTTTAGCTTCTTTTAAAGTCACCTCTAACAATGAAATTGTGTAGATT CAAAAATAGAATTAATTCGTAATAAAAAAGTCGAAAAAATTGTGCTCCCTCCCCCATTAATAATA ATTCTATCCCAAAATCTACACAATGTTCTGTGTACACTTCTTATGTTTTTTTTACTTCTGATAAATT TTTTTTGAAACATCATAGAAAAAACCGCACACAAAATACCTTATCATATGTTACGTTTCAGTTTAT GACCGCAATTTTTATTTCTTCGCACGTCTGGGCCTCTCATGACGTCAAATCATGCTCATCGTGAA AAAGTTTTGGAGTATTTTTGGAATTTTCAATCAAGTGAAAGTTTATGAAATTAATTTTCCTGCTTT TGCTTTTTGGGGGTTTCCCCTATTGTTTGTCAAGAGTTTCGAGGACGGCGTTTTTCTTGCTAAAA TCACAAGTATTGATGAGCACGATGCAAGAAAGATCGGAAGAAGTTTGGGTTTGAGGCTCAGTG GAAGGTGAGTAGAAGTTGATAATTTGAAAGTGGAGTAGTGTCTATGGGGTTTTTGCCTTAAATGA CAGAATACATTCCCAATATACCAAACATAACTGTTTCC	Construction of the bicistronic reporter for <i>cis</i> -regulatory elements in the 3' UTR of <i>unc-54</i> (pHR011 and <i>aaaEx97</i>)

HM04	ATGGTGAGCAAGGGCGAGG	
HM27	GCGGCCGCTTACTTGTACAGCTCGTCC	
HM28	GGACGAGCTGTACAAGTAAGCGGCCGCGTCCAATTACTCTTCAACATCCC	
HM37	GGTACCATGGTATTGAGCTGTCTCATCC	
HM29	CCGCGCACATTTCCCCGAAAAGTGCCACGGTACCCAAAAAAATTTATCAGAAG	Construction of pHR011 and <i>aaaEx97</i>
HM32	GTGGCACTTTTCGGGGAAATG	
HM34	CCTTTTCTGTACATGTCCTGGCCGGCCGGCCAGCAAAGGCCAGGAACC	
RA31	GATGGCCGGCCTGATCGAAAGTCTCTCCGG	
RA32	CTAGTGATATCCATTTATCTGGAACAAAATGTAAG	
RA101	GGATCCCTGAATCCATATATCATC	Construction of <i>nhr-23</i> 3' UTR reporter (pHR017 and <i>aaaEx129</i>)
RA102	GGTACCGAGACGTTTTATCACTG	
RA190	GGATCCACACTTTCTTCTTGCTCTTTACC	Construction of <i>lin-41</i> 3' UTR reporter (pHR023 and <i>aaaEx146</i>)
RA191	GGTACCAATTTTCGCAGTGAAATTTGCG	
RA169	TTAAAACTCGTATCATTCCAGTGTCTGC	Deletion of LCS from <i>nhr-23</i> 3' UTR reporter (pHR021 and <i>aaaEx131</i>)
RA170	TTAATAAAATAAAAATTAGTGCGCCTAGAAATCC	
RA171	TTTGATCCAACCATTTTCTCGTTTATGG	Deletion of nucleotides 623-646 from <i>nhr-23</i> 3' UTR reporter (pHR022 and <i>aaaEx165</i>)
RA172	GCAGACACTGGAATGATACGAGTTTTAA	
RA184	TTCTTTCTCTCCTTTTCCTGTTTTTAAAG	Deletion of nucleotides 227-249 from <i>nhr-23</i> 3' UTR reporter (pHR026 and <i>aaaEx166</i>)
RA185	GACTACAATTATTTTCTATTAATTTTCTG	
RA168	AACTATTGATGATATATGGATTCAGGGATCC	Deletion of nucleotides 26-42 from <i>nhr-23</i> 3' UTR reporter (pHR020 and <i>aaaEx130</i>)
RA167	CCCTATCCCCGTCCATGAATC	
RA227	CACGGGTACAAAACCACAAATTTCC	Genotype <i>nhr-23(aaa20)</i> /

RA228	GCGACCACTACACCATAAACG	
RA272	AGATGAGATGACTAATGAAAGTCCTCG	Genotype <i>dpy-10 II</i>
RA273	AGTGAAGAAAGTCCTGCCTTATCC	
RA202	GGTGACAGCCCACTTGGTGCC	Genotype <i>let-7(n2853) X</i>
RA203	TCCTTCTAAATTCGTCTAGGCGTCG	
RA277	GGGATAAATGATAAAATGATAACG	Genotype <i>nDf51 V</i>
RA278	GGCCGAAAGGCTTCTTACAC	
RA246	GCTCAATTCTTGGAGCCAGC	Genotype <i>mir-84(n4037) X</i>
RA247	GATTTTCTGCTCCGACAGATTAACATG	
RA173	TGCCAGACGGCATTCCCTAG	Genotype <i>let-7(mg279) X</i>
RA174	AATCAAGTGTGCACTGACCACTC	
RA109	GCAACGGGAAGCTCTGTTACAGG	Genotype <i>mir-84(tm1304) X</i>
RA110	GTTCTCCATTTCGACCATAAAGCC	
oHG206	GCTCTTCAAACTTCCGAATGTCTG	Genotype <i>nhr-23(xk22) I</i>
oHG207	AATAACCGGAGGAAACGAGATTCAT	
oHG280	CACTGCGTGACACCCGATTAA	Genotype <i>let-7(xk39) X, let-7(xk41) X, let-7(xk42) X, let-7(xk43) X, let-7(xk44) X</i>
oHG281	TACATGCCCATTTCAAATGTTTCTT	
oHG290	CTCGAAGAACAACATGTTATTTAC	Sanger sequencing of <i>let-7(xk39) X, let-7(xk41) X, let-7(xk42) X, let-7(xk43) X, let-7(xk44) X</i>
oHG281	TACATGCCCATTTCAAATGTTTCTT	
oHG227	ACTGCGTGACACCCGATTAAA	ChIP-qPCR for <i>let-7</i> promoter
oHG228	CAAAATCCAGGTCACCGCAA	
oHG235	TCCATCTCTCTTGGAACACAT	

oHG236	ACACCTTCAAACCTAACCAGTGT	ChIP-qPCR for <i>col-19</i> promoter
oHG294	GCCTGACTCAGACTTCTCCATAGAT	ChIP-qPCR for <i>mir-84</i> promoter
oHG295	AGAAGAGGAAAGGAAAAAACAAGTTA	
oHG298	GCTCGGTGCCGTGTACTTTTATA	
oHG299	CCAACCTTCCATCTCTGTCTCT	ChIP-qPCR for <i>mir-241</i> promoter
oHG300	AAGCGGATCGAGGGAAAAGA	ChIP-qPCR for <i>mir-48</i> promoter
oHG301	CCTCTCTAGTTCCTTCTGACTCTCTTG	
oHG373	GGACAGACTGTGGACATCCGA	ChIP-qPCR for <i>let-7</i> promoter in the <i>let-7(scRORE)</i> mutants
oHG374	GCACGGAACCAACTTGCACT	
oHG251	CACCACCATCATCGCAAACC	ChIP-qPCR for <i>nhr-23</i> promoter, amplicon A
oHG252	AACGGTACGGTATGCCTCC	
oHG253	CTGAGGGTCAGTGGTGTGAAA	ChIP-qPCR for <i>nhr-23</i> promoter, amplicon B
oHG254	ACACAAAACACCTGCGTTCTC	
oHG306	CCCTTTCATGCACTATTCCGAGA	ChIP-qPCR for <i>lin-42</i> promoter, amplicon A
oHG307	CCACCACCGCTAAACCTTTTG	
oHG304	GCGGAGACGCAGAGTACAG	ChIP-qPCR for <i>lin-42</i> promoter, amplicon B
oHG305	TGCGAGACATGCCTACAGC	
oHG193	CAAGCAGGCGATTGGTGGA	qPCR primers for <i>pri-let-7</i>
oHG194	GACGCAGCTTCGAAGAGTTCTGTC	
oTH1269	acgctcgtgatgagttcaag	qPCR primers for <i>eft-2</i>
oTH1270	atttggtccagttccgtctg	
CRISPR	Nucleotide Sequence (5' to 3')	Application
<i>dpy-10</i> crRNA	GCUACCAUAGGCACCACGAGGUUUUAGAGCUAUGCUGUUUUG	Edit the <i>dpy-10</i> locus

RA226	CACTTGAAC TTCAATACGGCAAGATGAGAATGACTGGAACCGTACCGCATGCGGTGCCTATGG TAGCGGAGCTTCACATGGCTTCAGACCAACAGCCTAT	<i>dpy-10</i> ssODN
<i>nhr-23</i> crRNA	GAGUUUUAAAAGGCAAUAAAGUUUUAGAGCUAUGCUGUUUUUG	Edit the 3' UTR of <i>nhr-23</i>
tracrRNA	AACAGCAUAGCAAGUUAAAUAAGGCUAGUCCGUUAUCAACUUGAAAAAGUGGCACCGAGUC GGUGCUUUUUUU	Trans-activation of CAS9
RA225	CTGGATTTCTAGGCGCACTAATTTTTATTTTATTAATTA AAACTCGTATCATTCCAGTGTCTGCGC TTTAA	Repair template (ssODN) for excision of the LCS from 3' UTR of <i>nhr-23</i>
oHG202 crRNA	AUGAUUAUGGAUUCAGUCA	Edit the final exon of <i>nhr-23</i>
oHG257	TAGGGAAGGAGAGCATGGATAAACTATTGATGATATATGGATTCAGTCATCCCTTGTCGTCGT CGTCCTTG TAGTCGATATCATGGTCCTTGTAATCTCCGTCGTGATCTTTATAGTCCGATCCCGAT CCTCCTGAGCCTCCAGGCCGATCTGCAGTGAATAGCTCTTTGTAGAGGGCAGGAAGCTTTTCA G	Repair template (ssODN) for insertion of the coding sequence for 3xFLAG between the last coding codon and the stop codon of <i>nhr-23</i>
oHG278 crRNA	GGTATTTTATTGCGGTGACC	Edit RORE3 in the promoter of <i>let-7</i>
oHG291	CTTTTGTTCCACTTTTGATGGTATTTTATTGCGGgtctacGGATTTTGCAACATGTGCATTGAGGG TAAAGGAAG	Repair template (ssODN) for scrambling RORE3 in the promoter of <i>let-7</i>
oHG282 crRNA	CGCAGTGCTAGCCGTTGCAC	Edit RORE2 in the promoter of <i>let-7</i>
oHG292	CAAAAAACAGTGCAAGTTGGTTCCGTGCAAACAgtctacGTGCAACGGCTAGCACTGCGTGACA CCCGATTAAA	Repair template (ssODN) for scrambling RORE2 in the promoter of <i>let-7</i>
oHG287 crRNA	AAACTATCTAGGAGGGA ACT	Edit RORE1 in the promoter of <i>let-7</i>
oHG293	AGGAATTGAAAGTGGACAGACTGTGGACATCCGAGgcctaCAGTTCCCTCCTAGATAGTTTTTTTT CGCTTTCAA	Repair template (ssODN) for scrambling RORE1 in the promoter of <i>let-7</i>
oHG3	TCCGAGgcctaCAGTTCCCTCCTAGATAGTTTTTTTTCGCTTTCAACTCCGCCCACAAAAAACAGT GCAAGTTGGTTCCGTGCAAACAgtctacGTGCAACGGCTAGCACTGCGTGACACCCGATTAAA	Repair template (ssODN) for scrambling RORE1 and RORE2 in the promoter of <i>let-7</i>